7.06 Temperatures, Heat and Energy in the Mantle of the Earth

C. Jaupart and S. Labrosse, Institut de Physique du Globe, Paris, France

J.-C. Mareschal, GEOTOP-UQAM-McGill, Montreal, QC, Canada

7.06.1 Introduction

Earth's heat engine works in ways which still elude us after many years of research, both on the fundamental physical aspects of convection in the mantle and on securing new and precise observations. In this context, it is worth remembering that we pursue two different goals in studies of mantle convection. One is to account for specific phenomena, such as hot spots or back-arc spreading centers. The other goal is to go back in time in order to evaluate how the rates of geological processes have changed with time and to decipher processes which are no longer active today. Both goals require a thorough understanding of dynamics but each relies on a different set of constraints. The former can be attained using present-day observations, such as the distributions of seismic velocities and density at depth. The latter goal relies on a global energy balance, which specifies how the convective regime evolved as the Earth cooled down and its energy sources got depleted. From another standpoint, the present-day energy budget of the planet and the distribution of heat flux at the surface are constraints that mantle models must satisfy.

The present-day energy budget reflects how Earth's convective engine has evolved through geological time and hence provides clues on the past. The power of this constraint has motivated a large number of studies. With hind-sight, one may note that the emergence of convection models coincided with the failure of conductive (and radiative) thermal history models to account for the mantle temperature regime and the Earth energy budget (Jacobs and Allan, 1956; Jacobs, 1961; MacDonald, 1959). Convection in the Earth's mantle had become an inescapable conclusion of that failure and was required to explain the observation that the mantle is not molten. The difficulty in running fully consistent dynamical calculations of convection over the whole history of our planet led to so-called 'parametrized' models such that the heat flux out of the Earth is written directly as a function of dimensionless numbers describing the bulk convective system, such as the Rayleigh number (Schubert *et al.*, 2001). For a given set of initial conditions, the model results were required to match the present-day energy budget, or more precisely the ratio of heat production to heat loss (the Urey ratio). The earliest study of this kind was probably that of McKenzie and Weiss (1975) and was followed by countless others. This approach was used to argue against whole-layer mantle convection (McKenzie and Richter, 1981), to date the emergence of plate tectonics [Peltier and Jarvis, 1982], to derive constraints on the distribution of radiogenic heat sources in the mantle (Schubert *et al.*, 1980), and even to determine the amount of radioactive sources in the Earth's core (Davies, 1980; Breuer and Spohn, 1993). The difficulty in accounting for the wealth of processes that characterize the Earth, such as continental growth as well as degassing and the implied changes of rheological properties, however, has led to disenchantment. Yet, it is clear that the present-day thermal and tectonic regime of the Earth results from several billions of years of convective processes and is best understood within a time-dependent framework.

Determination of Earth's rate of heat loss requires a very large number of heat flux measurements in a variety of geological settings. Local surveys as well as global analyses of large data sets have shown that heat flux varies on a wide range of spatial scales and, in the continents, is not a function of a single variable such as geological age, for example. Heat flux data exhibit large scatter, which has had unfortunate consequences. One has been that few scientists have invested time and energy to sort out the large number of variables and physical processes which come into play. The 1980s saw a rapid decrease in the number of research teams active in that field as well as in the number of measurements carried out at sea and on land. Another consequence has been that, with few notable exceptions (e.g., Pari and Peltier, 1995), the distribution of heat flux is rarely used as a constraint that mantle models must satisfy. Many evolutionary models for convection in the Earth's mantle have thus abandoned the energy budget as a viable constraint and have turned to geochemical

data. Here, we will assess the reliability of heat flux measurements and shall demonstrate that the spatial distribution of heat flux provides a key constraint for understanding convection in the Earth.

The last two decades have seen notable advances in the interpretation of heat flux. In the oceans, these include a thorough understanding of hydrothermal circulation through oceanic crust and sediments, as well as detailed and precise heat flux measurements through both very young and very old seafloor. In the continents, sampling of old cratons is now adequate in several areas, heat production of lower-crustal assemblages is better understood, and systematic studies of heat flux and heat production allow strong constraints on the crustal contribution to the surface heat flux. Today, we have a better understanding of the energy sources in the Earth than we did 20 years ago and know how large some of the uncertainties are.

In this chapter, we shall focus on two different, but closely related, problems. One is to evaluate the present-day energy budget of the mantle with emphasis on the associated uncertainties. The other is to evaluate how thermal evolution models must be developed in order to account for this budget. We shall establish the gross thermodynamics of the Earth and shall explain how estimates of heat loss and heat production have been obtained, drawing from recent advances. We shall emphasize the peculiarities of heat loss mechanisms of our planet and in particular the spatial distribution of heat flux. We shall then rely on the heat budget to infer the present-day secular cooling rate of our planet. We shall also evaluate independent constraints on temperature in the Earth's mantle and present a reference temperature profile through the convective mantle. Finally, we shall discuss the thermal evolution of our planet, from the standpoint of both observations and theoretical models. In order to facilitate the reader's task, we give a short summary of major points at the end of each section.

7.06.2 Basic Thermodynamics

7.06.2.1 Breakdown of the Energy Budget

The integral form of the energy balance for the whole planet takes the form

$$\frac{\mathrm{d}\left(U+E_{\mathrm{c}}+E_{\mathrm{g}}\right)}{\mathrm{d}t}=-\int_{A}\mathbf{q}\cdot\mathbf{n}\,\mathrm{d}A+\int_{V}H\,\mathrm{d}V+\int_{V}\psi\,\mathrm{d}V-p_{\mathrm{a}}\frac{\mathrm{d}V}{\mathrm{d}t} \quad [1]$$

where U is internal energy, E_{c} is kinetic energy, and E_{g} is gravitational potential energy. $\mathbf{q}$ is the surface heat flux, $\mathbf{n}$ is the unit normal vector, A is the Earth's outer surface, H is internal heat production per unit volume, p_{a} is atmospheric pressure, V is the Earth's total volume, and ψ stands for energy transfers to or from external systems, such as tidal dissipation. Table 1 provides a list of the main symbols used in this chapter. Equation [1] states that the Earth's total energy changes due to heat loss, internal heat generation, energy transfer between our planet interior and its surroundings (atmosphere as well as other celestial bodies), and finally the work of atmospheric pressure as the planet contracts. We have assumed that Earth's surface is stress-free, such that there is no work due to external shear stresses. Dissipation induced by internal convective motions is not included because it is due to internal transfers of energy and does not act to change the total energy of the system. We explain below how these internal energy transfers operate and show that changes of gravitational energy are compensated by changes of strain energy E_{S}, which is the energy required to compress matter to its actual local pressure p.

Our main purpose in this chapter is to evaluate the different terms in the energy balance, including changes of strain energy and gravitational energy, and to derive an equation for the average temperature of the Earth. The dominant terms on the right of eqn [1] are the Earth's rate of heat loss and internal heat generation, which are inferred from field measurements and chemical Earth models. The other terms are evaluated theoretically and are shown to be negligible.

The gravitational energy of the Earth is defined as the energy required to bring matter from infinity and, assuming spherical symmetry, can be written as

$$E_{\mathrm{g}}=\int_{0}^{R}\rho(r)g(r)r4\pi r^{2}\,\mathrm{d}r \quad [2]$$

with ρ and g the spatially varying density and gravity. This energy is negative because the accretion process releases energy. This energy can be computed for the present Earth and an upper limit can be obtained for a sphere with uniform density:

$$E_{\mathrm{g}}=-\frac{3}{5}\frac{GM^{2}}{R} \quad [3]$$

where G is the gravitational constant and M is the mass of the Earth.

Kinetic energy may be broken down into three different components:

$$E_{\mathrm{c}}=E_{\mathrm{rot}}+E_{\mathrm{contr}}+E_{\mathrm{conv}} \quad [4]$$

Table 1 Symbols used

Symbol	Definition	Units (commonly used units/or value)
C_p	Heat capacity	$J\,kg^{-1}\,K^{-1}$
C_Q	Heat flux/age$^{1/2}$	$470–510\,mW\,m^{-2}/(My)^{1/2}$
C_A	Seafloor accretion rate	$3.34\,km^2\,My^{-1}$
D	Thickness of convecting layer	m
E_c	Kinetic energy	J
E_g	Gravitational potential energy	J
E_{rot}	Rotational energy	J
E_s	Strain energy	J
F_b	Buoyancy flux	$W\,m^{-1}$
g	Acceleration of gravity	$m\,s^{-2}$
G	Gravitational constant	$6.67 \times 10^{-11}\,kg\,m^3\,s^{-2}$
H	(volumetric) Heat production	$W\,m^{-3}$ ($\mu W\,m^{-3}$)
I	Moment of inertia	$kg\,m^2$
K	Bulk modulus	Pa
k	Thermal conductivity	$W\,m^{-1}\,K^{-1}$
L	Length of oceanic plate (length-scale)	m
M	Mass of Earth	$5.973 \times 10^{24}\,kg$
Q, q	Heat flux	$W\,m^{-2}$ ($mW\,m^{-2}$)
p	Pressure	Pa (MPa, GPa)
R	Radius of Earth	6378 km
Ra	Rayleigh number	/
s	Entropy per unit mass	$J\,kg^{-1}\,K^{-1}$
T	Temperature	K (°C)
u	Internal energy per unit-mass (also used for horizontal velocity component)	$J\,kg^{-1}$
U	Internal energy (also used for horizontal velocity component)	J
Ur	Urey ratio	/
V	Volume	m^3
v_c	Contraction velocity	$m\,s^{-1}$
w	Convective velocity	
α	Coefficient of thermal expansion	K^{-1}
γ	Grüneisen parameter	/
κ	Thermal diffusivity	$m^2\,s^{-1}$
μ	Viscosity	Pa s
Ω	Angular velocity	$rad\,s^{-1}$
ϕ	Heat dissipated by friction	$W\,m^{-3}$
ψ	External energy sources	$W\,m^{-3}$
ρ	Density	$kg\,m^{-3}$
ΔS_{cond}	Entropy production	$J\,K^{-1}$
σ	Deviatoric stress tensor	Pa (MPa)

corresponding to the bulk rotation of our planet, radial contraction induced by secular cooling, and internal convective motions, respectively. One may easily show that the latter two are small compared to the first one.

Table 2 lists estimates for gravitational, kinetic, and internal energy components and makes it clear that kinetic energy is very small compared to the other two. A striking result is that the largest component by far is gravitational energy, which is larger than internal energy by at least one order of magnitude. In a constant mass planet, gravitational energy changes are due to thermal contraction, chemical differentiation, and vertical movements of Earth's surface (tectonic processes and erosion–deposition). These various processes work in different ways and are associated with different energy transport mechanisms, and hence must be dealt with separately.

7.06.2.2 Changes in Gravitational Energy: Contraction due to Secular Cooling

Gravitational energy is the largest component of the budget (Table 2) and special care is warranted to evaluate how it gets converted to other forms of energy when the planet contracts. This has been discussed in a series of papers (Lapwood, 1952;

Table 2 Numbers – order of magnitude

	Value	Units
Rotational energy	2.1×10^{29}	J
Internal energy (for 2500 K average temperature)	1.7×10^{31}	J
Gravitational energy (uniform sphere)	2.2×10^{32}	J
Rotation angular velocity	7.292×10^{-5}	rad s^{-1}
Polar moment of inertia	8.0363×10^{37}	kg m^2
Total mass	5.9737×10^{24}	kg
Total Volume	1.08×10^{21}	m^3
Mass mantle	$\approx 4.0 \times 10^{24}$	kg
Mass crust	$\approx 2.8 \times 10^{22}$	kg

Flasar and Birch, 1973). Here, we avoid detailed calculations and throw light on some interesting thermodynamical aspects.

The gravitational energy changes when the planet contracts:

$$\frac{\Delta E_g}{E_g} = -\frac{\Delta R}{R} \quad [5]$$

For uniform cooling by an amount ΔT, we show in Appendix 1 that

$$\frac{\Delta R}{R} \approx \frac{\langle\alpha\rangle \Delta T}{3} \quad [6]$$

where $\langle\alpha\rangle$ is an average value for the coefficient of thermal expansion and ΔT is negative. Assuming $\langle\alpha\rangle \approx 2 \times 10^{-5}\,\mathrm{K}^{-1}$ and a secular cooling rate of $100\,\mathrm{K\,Gy}^{-1}$, the contraction velocity is $\mathrm{d}R/\mathrm{d}t \approx -10^{-13}\,\mathrm{m\,s}^{-1}$, a very small value compared to the typical convective velocity of $\approx 10^{-9}\,\mathrm{m\,s}^{-1}$. The induced change of gravitational energy, however, is far from being negligible. For the same choice of parameter values, it is $\approx 4\,\mathrm{TW}$, which, as we shall see, corresponds to 10% of the total energy loss of our planet. We shall demonstrate, however, that such changes of gravitational energy are not converted to heat.

Thermal contraction affects the planet's rotation. The moment of inertia I changes:

$$\Delta I/I = 2\Delta R/R \quad [7]$$

and hence

$$\Delta E_{\mathrm{rot}}/E_{\mathrm{rot}} = \Delta\Omega/\Omega = -2\Delta R/R \quad [8]$$

where Ω is the Earth rotation velocity. Thus, some of the gravitational potential energy goes into the energy of rotation. Rotational energy is much less (three orders of magnitude) than gravitational energy, however, and hence may be neglected in the analysis of energy changes.

To elucidate energy transfer processes, we now consider thermodynamics at the local scale. We focus on a few specific aspects of interest and refer the reader to the study by Braginsky and Roberts (1995) for a comprehensive analysis. All energies are now written per unit mass with small letters, that is, e_c and u stand for the kinetic energy and internal energy per unit mass, respectively. We begin with the standard form of the first law of thermodynamics (Bird *et al.*, 1960; Schubert *et al.*, 2001, *see also* Chapter 7.08):

$$\rho\frac{\mathrm{D}(u+e_c)}{\mathrm{D}t} = -\nabla\cdot\mathbf{q} - \nabla\cdot(p\mathbf{v}) - \nabla\cdot[\boldsymbol{\sigma}\cdot\mathbf{v}] + H + \psi + \rho\mathbf{g}\cdot\mathbf{v} \quad [9]$$

where $\boldsymbol{\sigma}$ is the deviatoric stress tensor, $\mathbf{v}$ velocity, and ψ collects external source terms such as tidal dissipation. From the momentum equation, we get

$$\rho\frac{\mathrm{D}e_c}{\mathrm{D}t} = \rho\frac{\mathrm{D}(v^2/2)}{\mathrm{D}t} = -\mathbf{v}\cdot\nabla p - \mathbf{v}\cdot\nabla\cdot\boldsymbol{\sigma} + \rho\mathbf{g}\cdot\mathbf{v} \quad [10]$$

Subtracting this from the bulk energy balance leads to an equation for the internal energy:

$$\rho\frac{\mathrm{D}u}{\mathrm{D}t} = -\nabla\cdot\mathbf{q} + H + \psi + \phi - p\nabla\cdot\mathbf{v} \quad [11]$$

where ϕ stands for viscous dissipation:

$$\phi = -\nabla\cdot[\sigma\cdot\mathbf{v}] + \mathbf{v}\cdot\nabla\cdot\sigma = -\sigma:\nabla\mathbf{v} \quad [12]$$

Equation [11] is thus the usual statement that changes of internal energy u are due to heat gains or losses (which are broken into four contributions) and to the work of pressure (the last term on the right-hand side).

All the equations above stem from standard thermodynamics theory. We now introduce gravitational energy and strain energy. We decompose variables into the sum of the azimuthal average and a perturbation, for example, such as

$$T = \bar{T} + \theta \quad [13]$$

for temperature. The velocity field is decomposed into a component due to contraction, $\mathbf{v}_c$, and a convective

component, **w**. One key difference between these two is that the azimuthal average of the radial convective velocity, $\bar{w}_r$, is zero, in contrast to that of contraction. We may assume that contraction proceeds in conditions close to hydrostatic equilibrium, such that it involves no deviatoric stress and no dissipation. In this case, the azimuthal average of the momentum equation reduces to a hydrostatic balance:

$$0 = -\nabla\bar{p} + \bar{\rho}\mathbf{g} \qquad [14]$$

We now consider separately the effects of contraction, which act on the average density and pressure, and the effects of convection, which involve departures from these averages. We focus on the contraction process with velocity $\mathbf{v}_c$. In the internal energy equation [11], we identify the work done by pressure as a change of strain energy:

$$-\bar{p}\nabla\cdot\mathbf{v}_c = \bar{\rho}\frac{De_s}{Dt} \qquad [15]$$

and break internal energy down into heat content e_T and strain energy e_s:

$$\bar{\rho}\frac{Du}{Dt} = \bar{\rho}\left(\frac{De_T}{Dt} + \frac{De_s}{Dt}\right) \qquad [16]$$

In the total energy balance [9], the last term on the right-hand side is the work done by the gravity force. By definition, this term can be written as the change of gravitational potential energy when it is carried over to the left-hand side of the balance:

$$\bar{\rho}\frac{De_g}{Dt} = -\bar{\rho}\mathbf{g}\cdot\mathbf{v}_c \qquad [17]$$

This relationship is demonstrated in integral form in Appendix 2.

Collecting all terms, the energy balance [9] is written as

$$\bar{\rho}\frac{D\left[e_T + e_s + e_g + e_c\right]}{Dt} = -\nabla\cdot\mathbf{q} + H + \psi - \nabla\cdot(\bar{p}\mathbf{v}_c) + (\cdots) \qquad [18]$$

In this equation, terms associated with convective motions are not written explicitly and will be dealt with later. Kinetic energy is also negligible and, by inspection, one may deduce from eqn [18] that

$$\bar{\rho}\frac{D\left[e_s + e_g\right]}{Dt} = -\nabla\cdot(\bar{p}\mathbf{v}_c) \qquad [19]$$

This can be demonstrated by recalling the identity

$$\nabla\cdot(\bar{p}\mathbf{v}_c) = \bar{p}\nabla\cdot\mathbf{v}_c + \mathbf{v}_c\cdot\nabla\bar{p} \qquad [20]$$

Using the hydrostatic balance and eqn [17] the right-hand side of this equation can be recast as

$$\bar{p}\nabla\cdot\mathbf{v}_c + \mathbf{v}_c\cdot\nabla\bar{p} = -\bar{\rho}\frac{De_s}{Dt} - \bar{\rho}\frac{De_g}{Dt} \qquad [21]$$

which is indeed eqn [19].

Integrating eqn [19] over the whole-planet volume, we finally obtain

$$\frac{dE_g}{dt} + \frac{dE_s}{dt} = -p_a\frac{dV}{dt} \qquad [22]$$

where E_s is the total strain energy of the planet. The term on the right-hand side is very small and this equation therefore states that the change of gravitational energy is compensated by one of strain energy, so that no heat is generated.

7.06.2.3 Secular Cooling Equation

To derive an equation for temperature, we return to local variables. Introducing variables of state, we write

$$\rho\frac{De_T}{Dt} = \rho T\frac{Ds}{Dt} = \rho C_p\frac{DT}{Dt} - \alpha T\frac{Dp}{Dt} \qquad [23]$$

where s, the entropy per unit mass, has been expressed as a function of temperature and pressure and α is the coefficient of thermal expansion. From [11], we deduce that

$$\rho C_p\frac{DT}{Dt} = \alpha T\frac{Dp}{Dt} - \nabla\cdot\mathbf{q} + H + \psi + \phi \qquad [24]$$

By definition,

$$\frac{Dp}{Dt} = \frac{\partial p}{\partial t} + \mathbf{v}\cdot\nabla p = \frac{\partial p}{\partial t} + \mathbf{v}_c\cdot\nabla p + \mathbf{w}\cdot\nabla p \qquad [25]$$

Thus, the first two terms on the right of this equation are responsible for the so-called 'adiabatic heating', which is the only remaining contribution of contraction in eqn [24]. It may be safely neglected because of the small contraction velocity. As we shall see below, the last term on the right is not negligible and, even though $\bar{w}_r = 0$, contributes a key term in the energy budget, the buoyancy flux.

We now focus on the contribution of convective motions to the energy budget and no longer deal with contraction. Thus, time variations of the average density and pressure are neglected. Averaging eqn [24] over a spherical shell of radius r and neglecting second-order terms gives

$$\rho C_p\frac{D\bar{T}}{Dt} = -\rho\alpha g\overline{w_r\theta} - \frac{\partial\bar{q}_r}{\partial r} + H + \psi + \bar{\phi} \qquad [26]$$

where the first term on the right is the buoyancy flux and where w_r is the radial convective velocity component such that $\bar{w}_r = 0$. Integrating over the planet, we finally obtain

$$\int_V \rho C_p \frac{D\bar{T}}{Dt}\,dV = M\langle C_p\rangle \frac{d\langle T\rangle}{dt} = -\int_V \rho\alpha g\overline{w_r\theta}\,dV - \int_A \bar{q}_r\,dA + \int_V H\,dV + \int_V \psi\,dV + \int_V \bar{\phi}\,dV \quad [27]$$

where M is the mass of the Earth and $\langle C_p\rangle$ and $\langle T\rangle$ are its average heat capacity and average temperature, respectively. This equation involves viscous dissipation and may be simplified because, as shown in Appendix 3,

$$-\int_V \rho\alpha g\overline{w_r\theta}\,dV + \int_V \bar{\phi}\,dV = 0 \quad [28]$$

This equation states that viscous dissipation is balanced by the bulk buoyancy flux and explains why it does not enter the bulk energy balance (*see also* Chapter 7.08). This equation is very useful because it allows one to include all the dissipative processes that are active simultaneously. We shall refer to it in Section 7.06.7, where we discuss the controls on convective motions on Earth.

Subtracting this equation from the bulk energy balance [27], we finally obtain

$$M\langle C_p\rangle \frac{d\langle T\rangle}{dt} = -\int_A \bar{q}_r\,dA + \int_V H\,dV + \int_V \psi\,dV \quad [29]$$

which is the secular cooling equation.

7.06.2.4 Summary

The thermodynamics of the cooling Earth requires to separate slow contraction from the convective velocities. The gravitational energy from thermal contraction does not enter in the global heat budget because it is stored as strain energy. Similarly, the viscous dissipation can be important but is balanced by the bulk buoyancy flux. The secular cooling is dominated by the imbalance between radiogenic heat production and total heat flow.

7.06.3 Heat Loss through the Seafloor

For the purposes of calculating the rate at which the Earth is losing heat, the most direct and unbiased method is to integrate individual measurements of heat flux over the surface. As we shall see this method fails in the oceans and one has to use theory in order to obtain a reasonable estimate (*see* Chapter 6.05). This approach has drawn a lot of criticisms on the grounds that the procedure is a theoretical one and hence leads to a biased result. We shall discuss this point in detail. Our present understanding of the global thermal budget of the Earth can be summarized in the spherical harmonic representation of the surface heat flux (**Figure 1**). It is important to note that the spherical harmonic coefficients are not simply determined as the best fit to the observations but are adjusted to fit our best model of energy loss by the oceanic lithosphere.

7.06.3.1 Oceanic Heat Flux Data

Heat flow through permeable rock and sediment involves two mechanisms: conduction through the solid, and static, matrix and water flow through pores and fractures into the sea. Measuring the latter directly would be very costly and would require continuous recording over long timescales in order to determine a representative flow rate. It is clear that hydrothermal circulation is a highly efficient heat transport mechanism. It involves large volumes of oceanic rocks as shown by the extent of alteration in ophiolitic massifs (Davis and Elderfield, 2004).

Available measurement methods account only for heat conduction. The vast majority of marine heat flux determinations rely on the probe technique, such that a rigid rod carrying a thermistor chain is shoved into sediments. Obviously, this requires thick sedimentary cover, a systematic bias in the measurement environment that has important consequences discussed below. Another technique is to measure temperatures in deep-sea drillholes. This is clearly the best technique because it relies on measurements over a large depth range through poorly permeable crystalline basement, but it is particularly time consuming. Drilling operations perturb the thermal environment greatly, implying that measurements cannot be done just after drilling is completed and require hole reentry. In addition, the number of deep-sea drillholes is too small to provide a good sampling of the seafloor. The few comparisons that have been made between the two techniques show that the shallow probe technique provides reliable results (Erickson *et al.*, 1975).

High heat flux values near oceanic ridges were one of the decisive observations confirming seafloor spreading and thermal convection as a key geological mechanism (von Herzen, 1959; Langseth *et al.*, 1966).

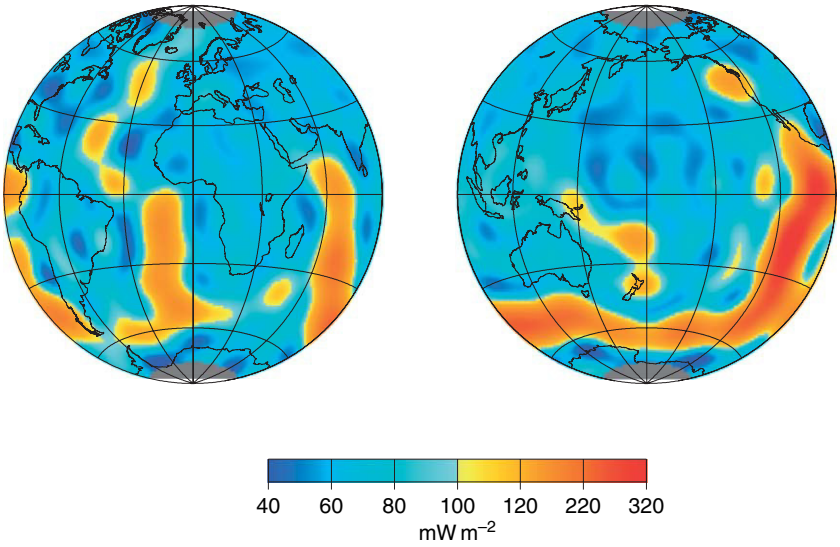

Figure 1 Global heat flux of the Earth obtained from the spherical harmonic representation to degree and order 18 (Pollack *et al.*, 1993).

Yet, these early surveys made it very clear that heat flux data exhibit enormous scatter and that heat conduction cannot account for all the observations. Heat flux data from the compilation by Stein and Stein (1992) have been binned in 2 My age intervals and are shown as a function of age in **Figure 2**. It is immediately apparent that there is a lot of scatter, particularly at young ages. Binning data for all oceans by age group is done for statistical reasons, in the hope that measurement errors cancel each other in a large data set. This is not valid if measurement errors are not random, which is the case here. Data reliability depends in part on environmental factors, such as basement roughness and sediment thickness. A rough basement/sediment interface leads to heat refraction effects and focussing of hydrothermal flows. At young ages, seafloor roughness depends in part on spreading velocity and hence varies from ocean to ocean. Also, the thin sedimentary cover implies severe environmental problems. Such effects explain why the data scatter is larger for young ages than for old ages. The first age bin presents a specific problem. It is characterized by the largest heat flux values (as well as the most conspicuous signs of hydrothermal activity) and hence deserves special consideration. Clearly, a proper average for this age bin requires data at very young ages, less than 1 My, say, which are virtually nonexistent. A final issue is that the global data set includes measurements made with different techniques and care. Some early data are associated with larger errors than in recent surveys due to small probe lengths and because thermal conductivity determinations were not made *in situ*.

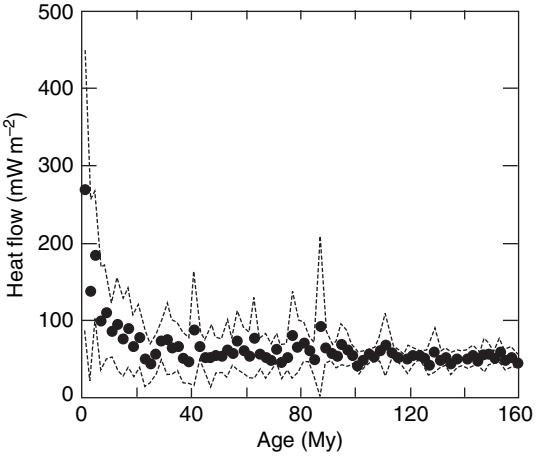

Figure 2 Distribution of heat flux data as a function of age from the compilation by Stein and Stein (1992). Dots represent averaged heat flux values in 2 My bins. Dash lines indicate the envelope at one standard deviation.

Accounting for the cooling of oceanic lithosphere at young ages requires detailed understanding of oceanic hydrothermal flows, which have been recently described in Davis and Elderfield (2004). In areas of hydrothermal circulation, sediment ponds are frequently zones of recharge, such that downward advection of cold water lowers the temperature. Recharge tends to occur over wide regions in contrast

to discharge, which is usually focussed through basement outcrops. By design, heat flux measurements require sedimentary cover and hence are systematically biased toward anomalously low heat flux areas. This error is systematic and hence cannot be eliminated by a large number of measurements. We shall give a specific example below. Far from oceanic ridges, sediment cover is much thicker, which alleviates most of the measurement problems. With thick hydraulically resistive sediment, hydrothermal circulation occurs in a closed system confined to the crystalline crust. In such conditions, heat flux varies spatially but the integrated value is equal to the heat extracted from the lithosphere. A reliable heat flux determination therefore requires closely spaced stations.

To summarize this description of oceanic heat flux data, we emphasize that systematic errors arise from the measurement environment. In such conditions, error analysis can only be achieved by small-scale local studies. There are very sound reasons that explain why heat flux data underestimates the total heat flux out of the seafloor (Harris and Chapman, 2004). Using the raw data average turns a blind eye to the problem of measuring heat flux through young lithosphere. Furthermore, it pays no attention to the systematics of the scatter. For the purposes of calculating heat loss through the oceans, it is therefore necessary to resort to other methods. We shall rely on detailed heat flux surveys in specific environments to obtain accurate estimates. We shall also show how the topography of the seafloor records the amount of heat that is lost by the oceanic lithosphere.

7.06.3.2 Cooling of the Oceanic Lithosphere

The basic framework for determining the temperature in the oceanic lithosphere is the heat equation:

$$\rho C_p\left(\frac{\partial T}{\partial t}+\mathbf{v}\cdot\nabla T\right)=\nabla\cdot(k\nabla T) \qquad [30]$$

where C_p is the heat capacity, ρ is the density of the lithosphere, k is thermal conductivity, and $\mathbf{v}$ is the velocity of the plate. We have neglected radiogenic heat production, which is very small in the oceanic crust and in mantle rocks (see below) and viscous heat dissipation. Over the temperature range of interest here, variations of heat capacity amount to $\pm 20\%$. Such subtleties will be neglected here for the sake of clarity and simplicity. They must be taken into account, however, for accurate calculations of the thermal structure of oceanic plates (McKenzie *et al.*, 2005). In the upper boundary layer of a convection cell (*see* Chapter 7.03), vertical advective heat transport is negligible. Over the large horizontal distances involved, vertical temperature gradients are much larger than horizontal ones, even in the vicinity of the ridge axis, and hence one may neglect horizontal diffusion of heat. The validity of this standard boundary-layer approximation is easily verified *a posteriori*. One final simplification is to assume steady-state. A detailed study of oceanic tholeiitic basalts demonstrates that their composition, and hence the temperature of the mantle from which they were derived, remains constant for about 80 My (Humler *et al.*, 1999). Over the lifetime of an oceanic plate, secular cooling may be safely neglected and the plate is in quasi-steady state. We shall neglect temperature variations in the direction parallel to the ridge axis. With these simplifications, the heat equation reduces to

$$\rho C_p u\frac{\partial T}{\partial x}=k\frac{\partial^2 T}{\partial z^2} \qquad [31]$$

where x is the distance from the ridge, z is depth, and u is the plate velocity relative to the ridge (i.e., half the spreading rate). Defining age τ for a constant spreading rate

$$u\tau=x \qquad [32]$$

leads to

$$\frac{\partial T}{\partial \tau}=\kappa\frac{\partial^2 T}{\partial z^2} \qquad [33]$$

where κ is thermal diffusivity. This is the one-dimensional (1-D) heat diffusion equation, whose solution requires a set of initial and boundary conditions. The upper boundary condition is straightforward and robust: a fixed temperature of about 4°C (in practice 0°C for convenience), due to the high efficiency of heat transport in water. All the discussion deals with the validity of the other two. The initial condition requires specification of the thermal structure of an oceanic spreading center. The bottom boundary condition may not account for the complex dynamics of the Earth's upper thermal boundary layer.

7.06.3.2.1 Initial condition: Temperature distribution at the ridge axis

As mantle rises toward the oceanic ridge, it undergoes pressure release and partial melting, which affects temperature. Furthermore, the upwelling is hotter than surrounding mantle and hence loses heat laterally by diffusion. During isentropic ascent

of dry mantle, temperature decreases by about 200 K (McKenzie and Bickle, 1988), which is small relative to the temperature drop at the surface of the ridge. Thus, it is commonly assumed that the axial temperature does not vary with depth and is equal to a constant value noted T_M. The validity of this assumption can be assessed by a comparison between model predictions and observations. Recent calculations by McKenzie *et al.* (2005), however, rely on a realistic axial temperature profile.

7.06.3.2.2 Bottom boundary condition

The simplest model has the lower boundary at infinite depth and assumes that temperature remains finite, such that cooling proceeds unhampered over the entire age span of oceanic lithosphere, and has been called the 'half-space' model. The temperature distribution is then

$$T(z,\tau) = T_M \operatorname{erf}\left(\frac{z}{2\sqrt{\kappa\tau}}\right) = \frac{2T_M}{\sqrt{\pi}}\int_0^{z/2\sqrt{\kappa\tau}} \exp\left(-\eta^2\right)\mathrm{d}\eta \qquad [34]$$

for which the surface heat flux is

$$Q(\tau) = \frac{T_M}{\sqrt{\pi\kappa\tau}} = C_Q\,\tau^{-1/2} \qquad [35]$$

where C_Q is a constant. One remarkable feature is that the surface heat flux follows the $\tau^{-1/2}$ relationship for arbitrary temperature-dependent physical properties (Carslaw and Jaeger, 1959; Lister, 1977) (Appendix 4). This equation makes the very simple prediction that heat flux varies as $\tau^{-1/2}$. Lord Kelvin used this property in his attempt to derive the age of the Earth from the present heat loss (Thomson, 1862). Numerical models of mantle convection which are in a plate-like regime conform very well to this relationship. **Figure 3** displays a snapshot of the temperature field and surface observables in such a model, from the study of Grigné *et al.* (2005). One sees clearly that the horizontal velocity at the surface is piece-wise constant, defining plates, and that the heat flux decreases with distance x from ridges as $1/\sqrt{x}$, that is to say $1/\sqrt{\tau}$ for a constant velocity. We shall see that the value for the mantle temperature T_M remains subject to some uncertainty. The value of the constant C_Q, however, may be determined empirically from the data, as shown below.

In the other class of models, a boundary condition is applied at some depth, which marks the base of the 'plate'. In principle, one should solve for heat supply from the underlying mantle. However, this requires elaborate physical models of mantle convection relying on specific choices of material properties and simplifying assumptions. For the sake of simplicity, one may consider two simple end-member cases, such that temperature or heat flux is constant at the base of the plate. Both these boundary conditions are approximations. For example, the fixed-temperature boundary condition requires infinite thermal efficiency for heat exchange between the plate and the mantle below.

The choice of the proper basal boundary condition is important because it determines the

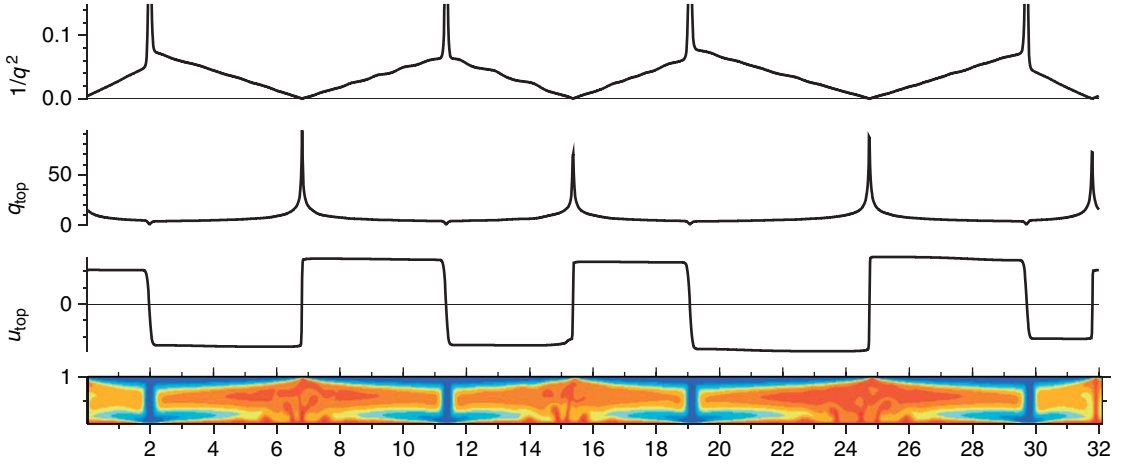

Figure 3 Snapshot of temperature, surface velocity (u_{top}), heat flux (q), and pseudoage ($1/q^2$) in a numerical convection model with self-consistent plate tectonics (Grigné *et al.*, 2005). See Appendix 8 for details. Note that the pseudoage varies linearly as function of distance to the ridge, which is consistent with the $\tau^{-1/2}$ heat flux law for young oceanic lithosphere.

relationship between the relaxation time and the plate thickness. Specifically, the thermal relaxation time of the plate is four times as long for fixed heat flux at the base than it is for fixed temperature. Alternatively, with fixed temperature at the base the plate must be twice as thick as the plate with fixed heat flux to have the same relaxation time. For very short time, the cooling rate (i.e., the surface heat flux) does not depend on the lower boundary condition and is the same for a plate with fixed heat flux or with fixed temperature at the base: it is the same as the heat flux for the cooling half-space. The details are provided in Appendix 5. Thus, it is better to use a half-space model for young ages because it relies on a reduced set of hypotheses. It does fit the oceanic data, as shown below. Furthermore, it has been tested over and over again and forms the basis for scaling laws of convective heat flux in many different configurations (Howard, 1964; Turcotte and Oxburgh, 1967; Olson, 1987). This simple model breaks down at ages larger than about 80 My for reasons that are still debated. For this reason, it may be wise not to rely on a specific physical model, such as the plate model with fixed basal temperature. At old ages, heat flux data exhibit small scatter and may be used directly.

7.06.3.2.3 Check: Heat flux data

A very detailed heat flux survey on young seafloor near the Juan de Fuca ridge was conducted by Davis *et al.* (1999) with three specific goals: evaluate the intensity and characteristics of hydrothermal circulation, assess local thermal perturbations due to basement irregular topography, and test cooling models for the lithosphere. **Figure 4** shows the salient results. Data between 1 and 3 My conform to the expected $\tau^{-1/2}$ relationship and suggest that constant C_Q in eqn [35] is between 470 and 510 (with heat flux in mW m^{-2} and age in My).

This value can be corroborated independently using heat flux data over a larger age range. To this aim, we use the 'reliable' heat flux data of Sclater *et al.* (1976) in well-sedimented areas younger than 80 My. For those sites, thick sedimentary cover is hydraulically resistive and seals off hydrothermal circulation which may still be effective in the igneous basement. Thus, there are no localized discharge zones and the average heat flux is equal to the rate at which the basement loses energy. Adding the constraint that, according to the half-space model, heat flux tends to zero as age tends to infinity tightens the estimate (Harris and Chapman, 2004). **Figure 5** shows that values for C_Q are between 475 and 500 with the same units as above, in remarkable agreement with the value deduced from the local Juan de Fuca survey. Combining these two independent determinations, we conclude that $C_Q = 490 \pm 20$, corresponding to an uncertainty of $\pm 4\%$. **Table 3** compares the various estimates that have been used in the past. The heat loss estimate of Pollack *et al.* (1993) was based on $C_Q = 510$, which is clearly an upper bound. This specific value was taken from the analysis of Stein and Stein (1992), which itself was

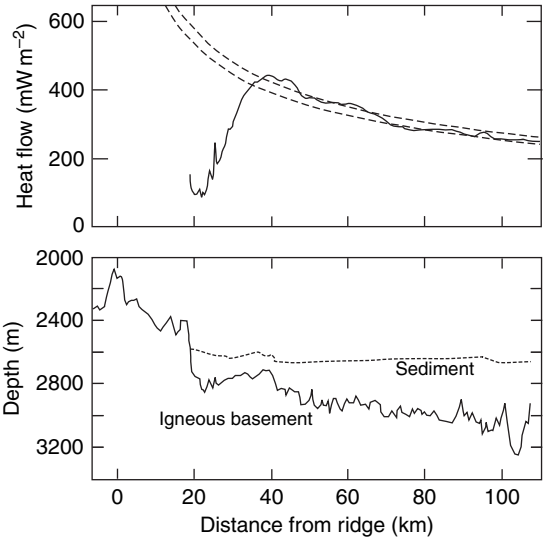

Figure 4 High-resolution heat flux profile near the Juan de Fuca ridge from Davis *et al.* (1999). Dashed lines stand for two predictions of the half-space cooling model with constant C_Q in the $\tau^{-1/2}$ heat flux–age relationship equal to 470 and 510 (with heat flux in mW m^{-2} and age in My).

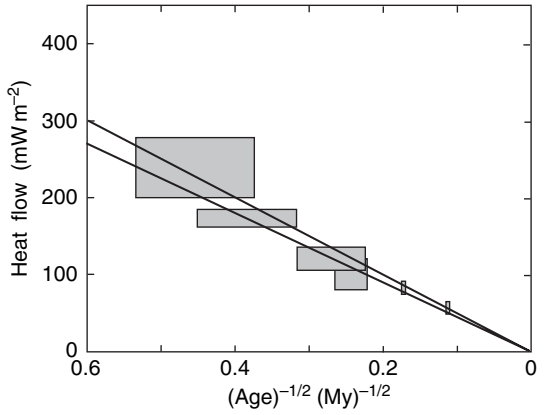

Figure 5 Averaged heat flux over well-sedimented areas excluding ocean floor older than 80 My. Data through very young ocean floor with very large scatter provide no useful constraints and have been omitted for clarity. Solid lines correspond to values of 475 and 500 for constant C_Q.

Table 3 Estimates of the continental and oceanic heat flux and global heat loss

	Continental ($mW\,m^{-2}$)	Oceanic ($mW\,m^{-2}$)	Total (TW)
Williams and von Herzen (1974)	61	93	43
Davies (1980)	55	95	41
Sclater *et al.* (1980)	57	99	42
Pollack *et al.* (1993)	65	101	44
This study[a]	65	94	46

[a]The average oceanic heat flux does not include the contribution of hot spots. The total heat loss estimate does include 3 TW from oceanic hot spots.

based on the plate model with constant basal temperature. One feature of this model is that $T_M = 1725$ K, a high value that is not consistent with the average ridge-axis temperature derived from the compositions of mid-ocean ridge basalts (MORBs) (Kinzler and Grove, 1992) (**Table 4**).

7.06.3.2.4 Depth of the seafloor

An isostatic balance condition leads to a very simple equation for subsidence with respect to the ridge axis (Sclater and Francheteau, 1970):

$$\Delta b(\tau) = b(\tau) - b(0) = \frac{1}{\rho_m - \rho_w}\int_0^d (\rho[T(z,\ \tau)] - \rho[T(z,\ 0)])\mathrm{d}z \quad [36]$$

where $b(\tau)$ and $\Delta b(\tau)$ are the depth of the ocean floor and subsidence at age τ and where ρ_m and ρ_ω denote the densities of mantle rocks at temperature T_M and water, respectively. In this equation, d is some reference depth in the mantle below the thermal boundary layer. This equation neglects the vertical normal stress at depth d, which may be significant only above the mantle upwelling structure, that is, near the ridge axis. We are interested in the heat flux out of the seafloor, $q(0, \tau)$. Assuming for simplicity that the coefficient of thermal expansion α is constant, the equation of state for near-surface conditions is

$$\rho(T) = \rho_m[1 - \alpha(T - T_M)] \quad [37]$$

From the isostatic balance [36], we obtain

$$\frac{\mathrm{d}b}{\mathrm{d}\tau} = \frac{-\alpha\rho_m}{\rho_m - \rho_w}\frac{\mathrm{d}}{\mathrm{d}\tau}\left[\int_0^d T(z,\ \tau)\mathrm{d}z\right] = \frac{-\alpha}{C_p(\rho_m - \rho_w)}\frac{\mathrm{d}}{\mathrm{d}\tau}\left[\int_0^d \rho_m C_p T(z,\ \tau)\mathrm{d}z\right] \quad [38]$$

where we have also assumed that C_p is constant. Heat balance over a vertical column of mantle between $z = 0$ and $z = d$ implies that

$$\frac{\mathrm{d}b}{\mathrm{d}\tau} = \frac{\alpha}{C_p(\rho_m - \rho_w)}[q(0,\ \tau) - q(d,\ \tau)] \quad [39]$$

which states that thermal contraction reflects the net heat loss between the surface and depth d. Because $q(0, \tau)$ depends on T_M, the subsidence rate also depends on the initial temperature at the ridge axis. This equation states that the surface heat flux is the sum of heat flux at depth d and the amount of cooling over vertical extent d. Using only the latter therefore leads to an underestimate of the surface heat flux.

Carlson and Johnson (1994) investigated these theoretical predictions using the best data set, basement depths from deep-sea drillholes, which require no correction for sediment thickness. They reached three important conclusions. One is that "no simple plate model has an acceptable degree of systematic misfit over the entire range of ages". They further found that the plate model underestimates depth for ages less than 80 My. Their third conclusion was that the half-space cooling model was consistent with the depth data. Using the best-fit parameters deduced from subsidence data and estimates for the various physical properties of mantle rocks in eqn [39] (i.e., for α, C_p, and the densities), they predicted heat flux

Table 4 Potential temperature of the oceanic upper mantle

	Reference	Method
1333°C[a]	Parsons and Sclater (1977)	Average depth + heat flux
1450°C[a]	Stein and Stein (1992)	Average depth + heat flux
1300–1370°C[a]	Carlson and Johnson (1994)	True basement depth (DSDP)
1315°C	McKenzie *et al.* (2005)	Depth + heat flux with $k(T)$, $C_p(T)$ and $\alpha(T)$
1280°C	McKenzie and Bickle (1988)	Average basalt composition
1315–1475°C	Kinzler and Grove (1992)	Basalt composition
1275–1375°C	Katsura *et al.* (2004)	Isentropic profile through Ol–Wa phase-change

[a]Temperature estimate for a cooling model with constant temperature below the ridge axis (i.e., which does not account for isentropic decompression melting).

values that were consistent with reliable heat flux data. For ages less than 80 My, the best-fit depth versus age relationship is

$$b(\tau) = (2600 \pm 20) + (345 \pm 3)\tau^{-1/2} \quad [40]$$

with b in meters and τ in My. From this relationship, the predicted heat flux over the same age range is

$$q(0,\ \tau) = (480\ \pm\ 4)\tau^{-1/2} \quad [41]$$

with q in mW m^{-2} and τ in My. We shall return to these estimates below. Using the same physical properties, Carlson and Johnson (1994) find that fitting the depth data with the plate model and half-space model lead to different values for the average ridge-axis temperature T_M: 1470°C and 1370°C, respectively. The former value is inconsistent with phase diagram constraints for mantle melting (Kinzler and Grove, 1992) (**Table 4**).

7.06.3.3 Heat Loss through the Ocean Floor

These simple physical considerations demonstrate that seafloor topography and surface heat flux record the same phenomenon, and furthermore that, within uncertainty, the subsidence rate is proportional to surface heat flux. In contrast, the raw oceanic heat flux data set records the conductive heat flux through a thin and heterogeneous superficial permeable layer. Using this data set leaves the seafloor topography unexplained.

The simple plate model with fixed basal temperature leads to an overestimate of the temperature at the ridge axis and hence leads to an overestimate of the oceanic heat flux. No such problem is encountered with the half-space model. To calculate the total rate of oceanic heat loss with as few hypotheses as possible, we break down the data into two different age intervals: 0–80 My, where the simple $t^{-1/2}$ law holds, and older seafloor where heat flux data depart from the half-space model. For seafloor older than 80 My, the heat flux is approximately constant $q_{80} \approx 48$ mW m^{-2} (Lister *et al.*, 1990) (**Figure 6**). Deviations from this value are ±3m W m^{-2} and exhibit no systematic trend as a function of age. The mean is determined with an uncertainty of 1 mW m^{-2}, which represents 1% of the average oceanic heat flux. This has no impact on the total heat loss estimate which is dominated by the young seafloor contribution. We also use depth data for the first time interval but not for the second one, because intrinsic basement roughness and volcanic

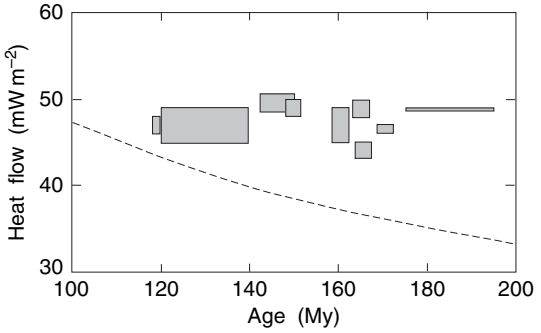

Figure 6 Heat flux data and prediction of the half-space cooling model for ages larger than 100 My. From Lister CRB, Sclater JG, Davis EE, Villinger H, and Nagahira S (1990) Heat flow maintained in ocean basins of great age: Investigations in the north equatorial west Pacific. *Geophysical Journal International* 102: 603–630.

constructions obscure age variations. We also add the contribution of marginal basins, whose heat flux conforms to the standard oceanic heat flux model, as demonstrated by Sclater *et al.* (1980).

Heat loss through the ocean floor is equal to

$$Q_0 = \int_0^{\tau_{max}} q(0,\ \tau)\frac{dA}{d\tau}d\tau \quad [42]$$

where $A(\tau)$ is the distribution of seafloor with age, which can be deduced from maps of the ocean floor (Sclater *et al.*, 1980; Müller *et al.*, 1997; Royer *et al.*, 1992). Using the most recent global data set of Royer *et al.* (1992), Rowley (2002), and Cogné and Humler (2004) found that a simple linear relationship provides a good fit to the data (**Figure 7**), confirming the earlier result of Sclater *et al.* (1980):

$$\frac{dA}{d\tau} = C_A(1 - \tau/\tau_m) \quad [43]$$

These three different groups of authors agree that $\tau_m = 180$ My but quote slightly different values of the coefficient C_A: 3.45 km^2 yr^{-1} for Sclater *et al.* (1980), 2.96 km^2 yr^{-1} for Rowley (2002) and 2.85 km^2 yr^{-1} for Cogné and Humler (2004). The larger estimate of Sclater *et al.* (1980) is due to the inclusion of marginal basins, which contribute ≈0.38 km^2 yr^{-1} to the global accretion rate. The small difference of about 0.12 km^2 yr^{-1} (4%) between the more recent estimates of Rowley (2002) and Cogné and Humler (2004) arises from the different methods used to fit the data. One independent constraint is brought by the total area of ocean floor, which is sensitive to the exact location of the continent–ocean boundary. A detailed analysis of continental margins leads to a

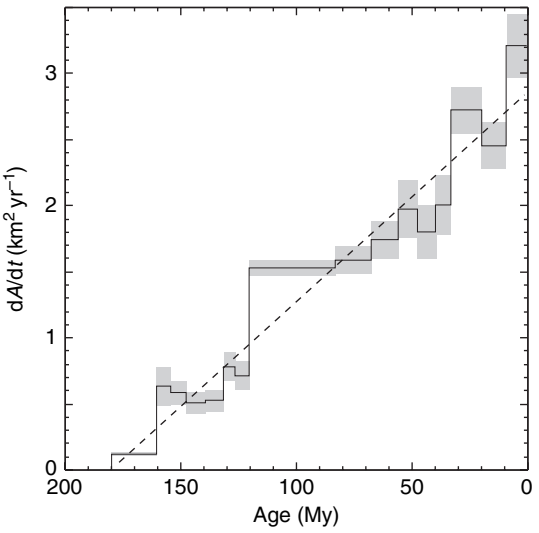

Figure 7 Distribution of seafloor ages. The dashed line is the best-fit linear function. Modified from Cogné JP and Humler E (2004). Temporal variation of oceanic spreading and crustal production rates during the last 180 My. *Earth and Planetary Science Letters* 227: 427–439.

total continental area of $210 \times 10^6\,\mathrm{km}^2$ (Cogley, 1984). From this, the total seafloor surface is $300 \times 10^6\,\mathrm{km}^2$, slightly less than the value used by Sclater *et al.* (1980). For a triangular age distribution with a maximum age $\tau_m = 180\,\mathrm{My}$, this implies that $C_A = 3.34\,\mathrm{km}^2\,\mathrm{yr}^{-1}$. Subtracting the contribution of marginal basins, this corresponds exactly to the Rowley (2002) estimate. Thus, for our purposes, we shall use $C_A = 3.34\,\mathrm{km}^2\,\mathrm{yr}^{-1}$. This discussion illustrates that uncertainties may come from unexpected variables, the area of the sea floor in this particular instance. The continental heat flux budget must account for the remaining $210 \times 10^6\,\mathrm{km}^2$.

Uncertainties come from estimates of the total area of ocean floor, or, more precisely, the total area of continental shelves as well as departures from the simple triangular age distribution. The former is less than 3% and implies a much smaller uncertainty on the global heat loss estimate because the total surface of the Earth is known very precisely: a change in the area of oceans is compensated by an opposite change in the area of continents. Considering the difference between the average oceanic and continental heat flux values, the resulting uncertainty on the global heat loss estimate is only 1%. The impact of departures from the triangular age distribution is best assessed by comparing the heat loss estimate derived from eqn [42] and that obtained by adding the individual contribution of each age group. Parsons (1982) showed that this difference amounts to about 0.3% of the total, which may be considered negligible. As we shall see later on, however, evaluating the uncertainty on the age distribution must be done over a large timescale and involves consideration of the stability of the convective planform.

Integrating separately seafloor younger and older than 80 My gives

$$\underline{Q}_{80-} = \int_0^{80} \underline{C_Q}\,\tau^{-1/2} C_A (1 - \tau/180)\mathrm{d}\tau = 24.3\,\mathrm{TW} \quad [44]$$

$$\underline{Q}_{80+} = q_{80} \int_{80}^{180} C_A (1 - \tau/180)\mathrm{d}t' = 4.4\,\mathrm{TW} \quad [45]$$

$$\underline{Q}_{\mathrm{oceans}} = 29 \pm 1\,\mathrm{TW} \quad [46]$$

where the uncertainty comes mostly from that on coefficient $\underline{C_Q}$. The present estimate is slightly less than earlier estimates because of the slightly lower ridge temperature (or equivalently, the slightly smaller value of coefficient $\underline{C_Q}$ in the heat flux vs age relationship) and because of the revised estimate for the mean accretion rate at zero age C_A. For $\underline{C_Q} = 510\,\mathrm{mW\,m}^{-2}\,\mathrm{My}^{-1/2}$ and $C_A = 3.45\,\mathrm{km}^2\,\mathrm{yr}^{-1}$, the heat loss would be 31 TW.

For small ages, the bathymetry provides a direct measure of the heat lost by the cooling plate. We obtain another heat loss estimate with the following equation:

$$\underline{Q}\,(80-) = \frac{C_p}{\alpha}(\rho_m - \rho_w) \times \int_0^{80} \frac{\mathrm{d}b}{\mathrm{d}\tau}\frac{\mathrm{d}A(\tau)}{\mathrm{d}\tau}\mathrm{d}\tau \quad [47]$$

$$\approx 24\,\mathrm{TW} \quad [48]$$

which is formally identical to the heat flux equation above and where $\rho_m = 3300\,\mathrm{kg\,m}^{-3}$, $C_p = 10^3\,\mathrm{J\,kg}^{-1}\,\mathrm{K}^{-1}$, $\alpha = 3 \times 10^{-5}\,\mathrm{K}^{-1}$. In old basins, where heat flux $\approx 48\,\mathrm{mW\,m}^{-2}$, the bathymetry is almost flat and hence cannot be used to estimate the rate of heat loss.

These estimates of oceanic heat loss do not account for the contribution of hot spots which are areas of enhanced heat flux (Bonneville *et al.*, 1997). The heat flux from hot spots can be estimated from the buoyancy of bathymetric swells (Davies, 1988; Sleep, 1990, *see also* Chapter 1.13). These estimates are in the range 2–4 TW and must be added to the heat loss due to plate cooling. We discuss below the relationship between the hot-spot component and the core heat loss.

7.06.3.4 Summary

Heat loss through the ocean floor cannot be determined using the raw heat flux data set which includes many measurements that are affected by

hydrothermal circulation and irregularities of the sediment cover. Predictions of the 'half-space' theoretical model for the cooling of the lithosphere can be compared successfully to measurements in selected environments where the effects of hydrothermal circulation can be assessed and accounted for. This model also implies values for the mantle temperature beneath mid-ocean ridges that are consistent with independent petrological models for basalt genesis. Finally, it is consistent with the evolution of seafloor bathymetry. Relying on the raw heat flux data would leave bathymetry data unaccounted for. The heat loss estimate requires accurate values for the areal distribution of seafloor ages. Uncertainty in the end result is essentially due to errors on the extent of continental margins. Accounting for the various uncertainties involved, the present-day rate of heat loss through the ocean floor is 32 ± 2 TW. This estimate includes the enhanced heat flux over hot spots.

Table 5 Continental heat flux statistics

	$\mu(Q)$[a] (mW m^{-2})	$\sigma(Q)$[b] (mW m^{-2})	N(Q)[c]
World			
All values	79.7	162	14123
Averages $1° \times 1°$	65.3	82.4	3024
Averages $2° \times 2°$	64.0	57.5	1562
Averages $3° \times 3°$	63.3	35.2	979
USA			
All values	112.4	288	4243
Averages $1° \times 1°$	84	183	532
Averages $2° \times 2°$	78.3	131.0	221
Averages $3° \times 3°$	73.5	51.7	128
Without USA			
All values	65.7	40.4	9880
Averages $1° \times 1°$	61.1	30.6	2516
Averages $2° \times 2°$	61.6	31.6	1359
Averages $3° \times 3°$	61.3	31.3	889

[a]Mean of the window-averaged heat flux values.
[b]Standard deviation of the window-averaged heat flux values.
[c]Number of windows with heat flux data.

7.06.4 Heat Loss through Continents

7.06.4.1 Average Continental Heat Flux and Heat Loss through Continental Areas

There are more than 10 000 heat flux measurements over the continents and their margins. The raw average of all the continental heat flux values is 80 mW m^{-2} (Pollack *et al.*, 1993). However, there is a strong bias to high heat flux values because many measurements were made in geothermal areas (e.g., western US, Baikal Rift) and large areas (Antarctica, Greenland, parts of the shields in Brazil and Africa) have almost no data. In the United States, a large fraction of the more than 2000 heat flux measurements belong to the Basin and Range Province. Excluding the values from the United States, the mean continental heat flux is only 66 mW m^{-2}.

Bias in the sampling can be removed by area-weighting the average as demonstrated in **Table 5**. Averaging over $1° \times 1°$ windows yields a mean heat flux of 65.3 mW m^{-2}. Using wider windows does not change this mean value significantly. The histograms of heat flux values or averages over $1° \times 1°$ windows have identical shapes, except for the extremely high values (>200 mW m^{-2}). Pollack *et al.* (1993) have obtained a mean continental heat flux of 66 mW m^{-2} by binning heat flux values by tectonic age and weighting by the area. Different methods to estimate the mean continental heat flux consistently yield 63–66 mW m^{-2} (*see* Chapter 6.05). Here, uncertainty is due to poor data coverage in several regions (Greenland, Antarctica, large areas in Africa). Those undersampled regions account for about 20% of the total continental surface and it would take large departures from the continental heat flux trends to affect the end result significantly.

For a mean continental heat flux value of 65 mW m^{-2}, the contribution of all the continental areas (i.e., 210×10^6 km^2) to the energy loss of the Earth represents ≈14 TW. This number includes the submerged margins and continental areas with active tectonics, where higher than normal heat flux values are associated with thick radiogenic crust and shallow magmatic activity. Uncertainty in this number is due to lack of adequate data coverage in Greenland, Antarctica, and large parts of Africa. To estimate the induced uncertainty, we assume that heat flux in those areas is equal to either the lowest or the highest average heat flux recorded in well-sampled geological provinces (36 and 100 mW m^{-2}, respectively). This procedure allows departures of ±1.5 TW from the estimate of 14 TW. This uncertainty is certainly overestimated because the poorly sampled regions are vast and must encompass geological provinces of various ages and geological histories; for instance, both Antarctica and Greenland are known to include high and low heat flux regions. For the sake of simplicity, we shall retain a final uncertainty estimate of 1 TW only.

7.06.4.2 Various Contributions to the Surface Heat Flux in Continental Areas

Determining the heat loss from the mantle through the continental lithosphere requires accounting for the crustal heat production. In stable continents, for ages greater than about 500 My, continents are near thermal steady-state such that surface heat flux is the sum of heat production in the lithosphere and of the heat supply at the base of the lithosphere. We shall focus on estimating the crustal heat production and shall discuss briefly the contribution of the lithospheric mantle. The average heat flux does not vary significantly for provinces older than 500 My (Sclater *et al.*, 1980) and, only in Archean (i.e. older than 2.5 Gy) provinces, it might be lower than in younger terranes (Morgan, 1985). The number of heat flux determinations in Archean and Pre-Cambrian provinces has increased during the past 20 years. With adequate sampling of heat flux and heat production, and detailed information on geology and crustal structure, the crustal and mantle components of the heat flux can now be determined. It will be shown that, for stable regions, the crustal heat production makes the dominant contribution and the heat flux from the mantle is low.

Recently active regions are in a transient thermal regime and the high surface heat flux reflects cooling of the continental lithosphere. After removing the crustal heat production (which has been determined in stable provinces), it is possible to estimate the transient component of the heat flux, which originates in mantle cooling.

7.06.4.3 Estimating Moho Heat Flux

7.06.4.3.1 Direct estimates of Moho heat flux

Early attempts to calculate mantle heat flux relied on an empirical relationship between heat flux and heat production rate, the so-called 'linear heat flow–heat production relationship' (Birch *et al.*, 1968; Roy *et al.*, 1968):

$$Q = Q_r + D \times H \qquad [49]$$

where Q is the local surface heat flux, H is the local surface heat production, and D is a length scale related to the thickness of a shallow layer enriched in radiogenic elements. The intercept Q_r is called the reduced heat flux and represents the contribution of the mantle and crust below the enriched shallow layer. It was suggested that crustal heat production decreases exponentially as a function of depth down to the Moho (Lachenbruch, 1970). If this were true, values for D ($\approx$10 km) would imply that the mantle heat flux is equal to Q_r. Although it was soon realized than it cannot be so, many studies still rely on heat production that it cannot decrease exponentially with depth.

The significance of the empirical heat flow relationship has been questioned on theoretical grounds (England *et al.*, 1980; Jaupart, 1983). It was shown that, for the rather small wavelengths involved, surface heat flux is only sensitive to shallow heat production contrasts (Jaupart, 1983; Vasseur and Singh, 1986). With more data available, it was found that for many provinces such a linear relationship is not verified (Jaupart *et al.*, 1982; Jaupart and Mareschal, 1999). Secondly, the crustal component of the heat flux can now be estimated from systematic investigations of lower crustal rocks, from both large granulite facies terrains (Fountain and Salisbury, 1981; Ashwal *et al.*, 1987; Fountain *et al.*, 1987) and xenoliths suites (Rudnick and Fountain, 1995). The heat production values, obtained on samples from large exposure of granulite facies terranes in different areas of the Superior Province, are very consistent ($\approx$0.4 μW m^{-3}). They appear to be representative of all granulite facies terranes worldwide, including the Ivrea Zone (Pinet and Jaupart, 1987; Joeleht and Kukkonen, 1998). Thirdly, sampling in superdeep holes (Kola, Russia, and KTB, Germany) demonstrates that heat production shows no systematic variation with depth as would be required by the linear relationship. At Kola, the Proterozoic supracrustal rocks (above 4 km depth) have lower heat production (0.4 μW m^{-3}) than the Archean basement (1.47 μW m^{-3}) (Kremenentsky *et al.*, 1989). At KTB, heat production decreases with depth at shallow levels, reaches a minimum between 3 and 8 km and increases again in the deepest parts of the borehole (Clauser *et al.*, 1997). Over a larger depth extent, studies of exposed crustal sections suggest a general trend of decreasing heat production with depth, but this trend is not a monotonic function (Ashwal *et al.*, 1987; Fountain *et al.*, 1987; Ketcham, 1996). Even for the Sierra Nevada batholith where the exponential model had initially been proposed, a recent compilation has shown that the heat production does not decrease exponentially with depth (Brady *et al.*, 2006). In the Sierra Nevada, heat production first increases, then decreases and remains constant in the lower crust beneath 15 km.

Many authors have assumed that the mantle heat flux is $\approx$25 mW m^{-2} in stable continental regions,

because this was the lowest measured value (Pollack and Chapman, 1977a; Cermak and Bodri, 1986). New heat flux values ≈20 mW m^{-2} have been obtained at several locations (Chapman and Pollack, 1974; Swanberg *et al.*, 1974; Duchkov, 1991; Mareschal *et al.*, 2000; Mareschal *et al.*, 2005) and the average heat flux over wide areas (500×500 km^2) of the Baltic and Siberian Shields is <18 mW m^{-2}. The mantle heat flux cannot be higher than these values. For the mantle heat flux to be equal to such values, the whole crust below specific measurement sites must be completely devoid of heat-producing elements over a large area.

Another approach was to assume that the mantle heat flux is roughly proportional to the average surface heat flux. Pollack and Chapman (1977b) have argued that mantle heat flux is ≈40% of the regional average surface heat flux. Their analysis, however, was based on a small data set. In order to detect changes of basal heat flux, small-scale heat flux variations are of little use because they record shallow heat production contrasts and one must work at a minimum scale of about 300 km (Mareschal and Jaupart, 2004). This places stringent constraints on data coverage because heat flux and heat production vary on a typical scale of 10 km due to the heterogeneity of the crust. In North America, there are sufficient heat flux data to sample five well-defined provinces or subprovinces with different geological structures on a scale of about 500 km. For these five large provinces, average values of heat flux and surface heat production are statistically correlated (**Figure 8**). The data are close to a relationship of the form

$$\bar{Q} = Q_i + D\bar{H} \qquad [50]$$

where $\bar{Q}$ and $\bar{H}$ are province-wide-averaged heat flux and heat production. That this relationship takes the same form as the 'local' relationship (eqn [49]) is fortuitous. In northern America, the latter is only valid for relatively small-scale variations (typically 10–50 km) of heat flux and heat production over Appalachian plutons and does not hold in the Pre-Cambrian provinces (Grenville, Trans-Hudson Orogen, Superior Province). The new relationship (eqn [50]) reflects variations of average heat flux on a much larger scale (>500 km) and relies on a very large data set. It implies that the average heat flux takes the same value Q_i at some intermediate crustal depth in all provinces. Formally, it is not possible to rule out variations of mantle heat flux between the five provinces but the data require that such variations are exactly compensated by opposite variations of lower-crustal heat production. It is hard to explain how this may be achieved in practice and the most sensible hypothesis is that the mantle heat flux is approximately the same beneath the five provinces. For these provinces, independent geophysical and petrological constraints on crustal structure show indeed that changes of crustal heat production account for the observed heat flux variations (Pinet *et al.*, 1991; Mareschal *et al.*, 1999).

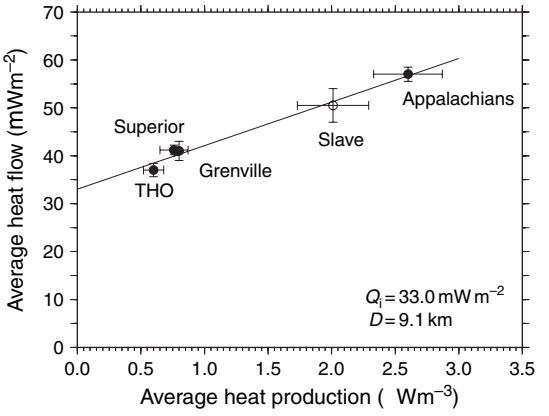

Figure 8 Averaged heat flux versus average surface heat production for five major geological provinces of North America. The solid line is the best-fit linear relationship of eqn [50].

We shall explain how we calculated the crustal heat production by various methods and obtained for the mantle heat flux values that are consistently ≤18 mW m^{-2}.

7.06.4.3.2 Crustal heat production and Moho heat flux

Regions of low surface heat flux provide a strong constraint on the Moho heat flux. In several parts of the Canadian Shield, heat flux values as low as 22 mW m^{-2} have been measured (Jaupart and Mareschal, 1999; Mareschal *et al.*, 2000). Similar values have also been reported for the Siberian Shield (Duchkov, 1991), the Norwegian Shield (Swanberg *et al.*, 1974), and western Australia (Cull, 1991). These correspond to areas where the crustal contribution is smallest and hence provide an upper bound to the mantle heat flux. One may refine this estimate further by subtracting some lower bound for crustal heat production. Surface heat flux records a large-scale average of heat production, and hence one should consider a representative crustal

assemblage, and not a single rock type, such as gabbro, for example. For no crustal material are heat production estimates lower than $0.1\,\mu W\,m^{-3}$ (Pinet and Jaupart, 1987; Joeleht and Kukkonen, 1998; Rudnick and Fountain, 1995). Over the average thickness of ≈40 km, the contribution of the crust must be at least $4\,mW\,m^{-2}$, and hence the mantle heat flux must be $<18\,mW\,m^{-2}$. In Norway, Swanberg *et al.* (1974) obtained a heat flux value of $21\,mW\,m^{-2}$ over an anorthosite body, after estimating the crustal heat production, they concluded that mantle heat flux is about $11\,mW\,m^{-2}$. The same value of mantle heat flux was obtained from the analysis of all the heat flux and radiogenic heat production data in the Norwegian Shield (Pinet and Jaupart, 1987).

A lower bound on mantle heat flux can be obtained by requiring that melting conditions are not attained in the crust in the absence of tectonic events and magmatic intrusions (Rolandone *et al.*, 2002). In high heat flux areas of the Canadian Shield, crustal rocks are at high temperatures today and were still hotter in the past when radiogenic heat production was higher. The condition of thermal stability provides a lower bound of $11\,mW\,m^{-2}$ on the mantle heat flux. Combining this result with the independent constraints derived from present-day heat flux values leads to a range of $11–18\,mW\,m^{-2}$ for the mantle heat flux beneath the Canadian Shield. Arguments different from these have led to the same range of values in other Pre-Cambrian areas (Jones, 1988; Guillou-Frottier *et al.*, 1995; Gupta *et al.*, 1991).

In several regions of the world, a large fraction of the crustal column has been exposed by tectonic processes. Sampling of such exposed cross-sections allows the determination of the vertical distribution of radiogenic elements. If heat flux and seismic data are also available, it is possible to determine the total crustal heat production. For the Kapuskasing structure in the Canadian Shield where the crustal contribution could be determined, the Moho heat flux was calculated to be $13\,mW\,m^{-2}$ (Ashwal *et al.*, 1987; Pinet *et al.*, 1991). The average crustal heat production can also be estimated in provinces where all crustal levels can be found at the surface. In these provinces, systematic sampling will yield an estimate of the average bulk crustal heat production. In the Grenville Province of the Canadian Shield, the average crustal heat production was determined to be $0.65\,\mu W\,m^{-3}$ for an average surface heat flux of $41\,mW\,m^{-2}$. This yields a Moho heat flux of $15\,mW\,m^{-2}$ (Pinet *et al.*, 1991). Similar results have been reported for other shields in the world, including South Africa (Nicolaysen *et al.*, 1981) and India (Roy and Rao, 2000), and are listed in **Table 6**.

Other methods have combined heat flux with other geophysical data, mainly long-wavelength Bouguer gravity, to estimate changes in crustal composition. A search for all models consistent with all the available data, including gravity data and bounds on heat production rates for the various rock types involved, leads to a range of $7–15\,mW\,m^{-2}$ for the mantle heat flux (Guillou *et al.*, 1994).

The above estimates were derived using local geophysical and heat production data in several provinces and rely on knowledge of crustal structure. Independent determinations of the mantle heat flux may be obtained by considering the lithospheric thickness determined by seismic and xenolith studies. Pressure and temperature estimates from mantle xenoliths may be combined to determine a best-fit geotherm consistent with heat transport by conduction. Mantle heat flux estimates obtained in this manner depend on the value assumed for thermal conductivity. Available estimates are consistent with those deduced from crustal models and are listed in **Table 6**.

The estimates of **Table 6** come from Archean and Proterozoic cratons where heat flux values are generally low. Heat flux values tend to be larger in younger stable continental regions. For example, heat flux is higher ($57\,mW\,m^{-2}$) in the Appalachians than in the Canadian Shield. The crust of the Appalachians contains many young granite intrusions with very high heat production ($>3\,\mu W\,m^{-3}$). The elevated heat flux can be accounted for by the contribution of these granites and does not require mantle heat flux to be higher than in the Shield (Pinet *et al.*, 1991; Mareschal *et al.*, 2000). Throughout stable North America, including the Appalachians, variations of the mantle heat flux may not be exactly zero but must be less than departures from the best-fitting relationship (**Figure 8**), or about $\pm 2\,mW\,m^{-2}$. This estimate is close to the intrinsic uncertainty of heat flux measurements (Jaupart and Mareschal, 1999).

Allowing for the uncertainties and requiring consistency with low heat flux measurements, we retain the range of $15 \pm 3\,mW\,m^{-2}$ for the mantle heat flux in stable continents. For this range, the differences of average heat flux values between geological provinces cannot be accounted for by changes of mantle heat flux and hence must be attributed to changes of crustal heat production. The ranges of

Table 6 Various estimates of the heat flux at Moho in stable continental regions

Location	Heat flux (mW m^2)	Reference
Norwegian Shield	11[a]	Swanberg *et al.* (1974), Pinet and Jaupart (1987)
Vredefort (South Africa)	18[a]	Nicolaysen *et al.* (1981)
Kapuskasing (Canadian Shield)	11–13[a]	Ashwal *et al.* (1987), Pinet *et al.* (1991)
Grenville (Canadian Shield)	13[a]	Pinet *et al.* (1991)
Abitibi (Canadian Shield)	10–14[a]	Guillou *et al.* (1994)
Siberian craton	10–12[a]	Duchkov (1991)
Dharwar craton (India)	11[a]	Roy and Rao (2000)
Trans-Hudson Orogen (Canadian Shield)	11–16[a, b]	Rolandone *et al.* (2002)
Slave Province (Canada)	12–24[c]	Russell *et al.* (2001)
Baltic Shield	7–15[c]	Kukkonen and Peltonen (1999)
Kalahari craton (South Africa)	17–25[c]	Rudnick and Nyblade (1999)

[a]Estimated from surface heat flux and crustal heat production.
[b]Estimated from condition of no-melting in the lower crust at the time of stabilization.
[c]Estimated from geothermobarometry on mantle xenoliths.

Table 7 Estimates of bulk continental crust heat production from heat flux data (Jaupart and Mareschal, 2003)

Age group	Heat production (μW m^{-3})	Total (40 km crust) (mW m^{-2})	%Area[a]
Archean	0.56–0.73	23–30	9
Proterozoic	0.73–0.90	30–37	56
Phanerozoic	0.95–1.21	37–47	35
Total continents	0.79–0.95	32–40	

[a]Fraction of total continental surface, from Model 2 in Rudnick and Fountain (1995).

heat flux and heat production values are the same for all provinces between 200 My and 2.5 Gy, with a weak trend of decreasing average heat flux and heat production with age (Perry *et al.*, 2006). The range is narrower in Archean provinces where high heat flux values are not found, possibly because a very radioactive crust would have been too hot to be stabilized (Morgan, 1985). Averaging the heat production of the crust of different ages yields a range of 0.79–0.95 μW m^{-3} (**Table 7**; Jaupart and Mareschal, 2003).

7.06.4.4 Recently Active Regions and Continental Margins

Submerged and recently active (i.e., during the past 200 My) continental areas cover 92×10^6 km^2, ≈45% of the total continental surface (**Table 8**). These regions are not in thermal steady-state and are characterized by higher heat flux than the continental average. Because of the long thermal relaxation time of the continental lithosphere, present surface heat flux samples the inputs of heat from the mantle of the past 100–200 My. The crustal component can now be calculated from crustal thickness and average heat production. After accounting for crustal heat production, the heat from the mantle (some of which is included in the transient component) can be estimated.

7.06.4.4.1 Compressional orogens

In compressional orogens, crustal and lithospheric thickening result in reduced temperature gradients and heat flux, but the total heat production in the thick crust is high. These two competing effects lead to a complex transient thermal structure and few generalizations can be made on the surface heat flux. For instance, very high heat flux values (>100 mW m^{-2}) have been measured on the Tibetan Plateau (Francheteau *et al.*, 1984; Jaupart *et al.*, 1985; Hu *et al.*, 2000). They have been attributed to shallow magma intrusions and yield little information on the mantle heat flux. In contrast, present surface heat flux remains low in the Alps, and after removing the crustal heat production, heat flux at the Moho is estimated to be as low as 5 mW m^{-2} (Vosteen *et al.*, 2003). After removing the crustal contribution, heat flux from the mantle is also low

Table 8 Surface area and heat flux in oceans and continents

	Area	Total heat flux
Oceans		
Oceanic	273×10^6 km^2	
Marginal basins	27×10^6 km^2	
Total oceans	300×10^6 km^2	32 TW
Continents		
Pre-Cambrian	95×10^6 km^2	
Paleozoic	23×10^6 km^2	
Stable continents	118×10^6 km^2	
Active continental	30×10^6 km^2	
Submerged (Margins and basins)	62×10^6 km^2	
Total continental	210×10^6 km^2	14 TW

beneath the North American Cordillera (Brady *et al.*, 2006), and beneath the South American Cordillera, at least where it has not been affected by back-arc extension (Henry and Pollack, 1988).

7.06.4.4.2 Zones of extension and continental margins

In rifts, recently extended regions, continental margins and basins, heat flux is higher than in stable areas because of a large transient component, which ultimately represents additional inputs of heat from the mantle. Crustal extension and lithospheric thinning will instantly result in steepening the temperature gradient and increasing the heat flux. Thermal relaxation from the initial conditions depends on the boundary condition at the base of the lithosphere.

The heat flux is high (75–125 mW m^{-2}) in zones of extension and in continental rifts, significantly more than in stable regions (Morgan, 1983). A striking feature of the zones of extension is that the transition between the region of elevated heat flux and the surrounding is as sharp as the sampling allows one to determine, that is, Colorado Plateau–Basin and Range in North America (Bodell and Chapman, 1982), East African Rift–Tanzanian craton (Nyblade, 1997), Baikal Rift–Siberian craton (Poort and Klerkx, 2004). The absence of lateral diffusion of heat suggests that the enhanced heat flux in the extended area is not due to conductive processes but is the direct result of extension and lithospheric thinning. Where the sampling is sufficient, heat flux also exhibits short-wavelength variations. These variations are partly due to the cooling of shallow magmatic intrusions and to groundwater movement. The actual heat loss is higher than the average conductive heat flux because of the heat transport by hot springs and volcanoes. Lachenbruch and Sass (1978) have estimated that the heat delivered by volcanoes in rifts and in the Basin and Range is negligible. They have also argued that the integrated effect of heat transport by groundwater is small for the Basin and Range, with the exception of the Yellowstone system, where locally the heat flux is >40 W m^{-2}. However, the total heat loss at Yellowstone remains modest: the conductive and convective heat loss for the entire Yellowstone system has been estimated to be ≈5 GW (Fournier, 1989). It would thus require 200 'Yellowstones' to increase the continental heat loss by 1 TW. The effect of continental hot spots on the budget seems presently negligible. Values for the total heat loss through geothermal systems in the East African Rift are comparable to those of Yellowstone (Crane and O'Connell, 1983). In continental as well as in oceanic rifts, the heat loss is underestimated because of hydrothermal heat transport. However, because continental rifts are narrow and their total surface area is small, the error will not significantly affect the continental heat flux budget. For instance, the total heat loss for the Gregory Rift, in Kenya, is ≈20 GW (Crane and O'Connell, 1983). Similar values have been inferred for Baikal (Poort and Klerkx, 2004). Large igneous provinces testify of periods of enhanced volcanic activity in the continents. Their effect on the heat flow budget is however negligible. In the Deccan, where 500 000 km^3 of basalts were deposited *c.* 60 My, there is no heat flow anomaly, suggesting that the lavas did not heat up the lithosphere. Assuming that the lavas were deposited in 1 My, the heat that they carried to the surface contributed less than 0.1 TW to the energy budget.

The contribution of wide regions of extension is more significant than that of rifts. In the Basin and Range Province in the southwestern US, high

average heat flux (105 mW m^{-2}) has been interpreted to imply an extension of 100% (Lachenbruch and Sass, 1978). This interpretation depends on assumptions on the pre-extensional heat flux and on crustal heat production. Early estimates of the mantle heat loss are probably too large because the crustal heat production was underestimated (Ketcham, 1996). It now appears that the average heat production of the crust is the same as in stable regions and yields a total crustal heat production of $\approx$33 mW m^{-2}. This implies that the transient component due to cooling and the mantle heat flux in the Basin and Range contribute a total heat flux of $\approx$70 mW m^{-2} (Ketcham, 1996). Detailed models to account for this heat loss assume either delamination of the lithospheric mantle or stretching and transport of heat into the lithosphere by intrusions (Lachenbruch and Sass, 1978). Regardless of the mechanism, at least two-thirds of the heat flux in regions of extension comes from the mantle.

Basins and continental margins account for an important fraction ($\approx$30%) of the continental surface. Margins are characterized by gradual crustal thinning towards oceanic basins, which implies a lateral variation of the crustal heat flux component. The average heat flux of the margins (78 mW m^{-2}) is higher than in stable regions despite the thinner crust. This higher heat flux is explained by the cooling of the stretched lithosphere and is reflected in the thermal subsidence (Vogt and Ostenso, 1967; Sleep, 1971). Where detailed information on crustal thickness is available, the input of heat from the mantle can be calculated.

7.06.4.5 Mantle Heat Loss through Continental Areas

There is a major difference in the thermal regime between stable and active continental regions. In stable continental regions, the mean heat flux is low ($\leq$55 mW m^{-2}) and mostly comes from crustal heat production. Heat flux from the mantle is $\approx$15 mW m^{-2}. In extensional regions, the high heat flux ($\geq$75 mW m^{-2}) includes a contribution from crustal radioactivity ($\approx$30 mW m^{-2}) and heat from the mantle in the transient component. Despite the thin crust, continental margins also have higher than average heat flux ($\approx$80 mW m^{-2}) because they are cooling after being extended.

Different methods lead to a value of 14 TW for the integrated heat flux from continental areas. Neglecting geothermal and volcanic transport has no significant impact on this value. The estimated average heat production of the continental crust ranges between 0.79 and 0.95 μW m^{-3} (Jaupart and Mareschal, 2003) and the total volume of continental crust is $\approx 0.73 \times 10^{10}$ km^3, which gives a total heat production in the crust between 6 and 7 TW.

Little is known about the amounts of radiogenic elements in the lithospheric mantle. Direct estimates rely on a few exposures of peridotite massifs, which are typically depleted (Rudnick *et al.*, 1998), and on mantle xenoliths from kimberlite pipes, which are usually enriched (Russell *et al.*, 2001). Considerations on the thermal stability of continental roots and consistency with heat flux measurements as well as with petrological temperature estimates lead to the conclusion that enrichment must be recent and associated with metasomatic infiltrations (Jaupart and Mareschal, 1999; Russell *et al.*, 2001). This enrichment process is probably limited in both area and volume and our best estimate of radiogenic heat production in the lithospheric mantle comes from peridotite massifs. For the sake of completeness, we take a value of 0.02 μW m^{-3} from (Rudnick *et al.*, 1998) and consider an average lithosphere thickness of 150 km. The total heat thus generated in the subcontinental lithospheric mantle is about 0.5 TW, which is only accurate within a factor of about two.

Subtracting the contribution of radioactive sources from the total heat loss out of continents, we thus arrive at an estimate of the heat input from the mantle of 6–7 TW, most of which is brought through the tectonically active regions and the continental margins.

7.06.4.6 Summary

Heat flux data are now available for provinces of all ages, including Archean cratons which were poorly sampled 20 years ago. About half of the heat loss through continents is accounted for by crustal radiogenic heat production. Stable continents allow a small heat flux of about 15 mW m^{-2} out of the convecting mantle and hence act as insulators at the surface of the Earth.

7.06.5 Heat Sources

7.06.5.1 Radiogenic Sources in the Mantle

The composition of our planet cannot be measured directly for lack of direct samples from the lower mantle and the core, and hence has been estimated

using various methods. It had been noted by Birch (1965) that if the Earth had a chondritic composition, its heat production would match what was then thought to be the heat loss (30 TW). This remarkable coincidence did not resist close scrutiny. It was soon noted that the Earth is depleted in K relative to chondrites and this reduces the heat production (Wasserburg *et al.*, 1964). With the same amount of U and Th as in the chondrites, and a terrestrial K/U ratio, the total heat production was estimated to be only 20 TW (Wasserburg *et al.*, 1964). On the other side of the balance, the heat loss is now believed to be much larger than it was then.

All attempts to construct a bulk Earth composition model rely on two different kinds of samples: meteorites, which represent the starting material, and samples of today's upper mantle. Both show rather extensive variations of composition due to their different histories. Processes in the early solar nebula at high temperature contribute one type of compositional variation. Processes within the Earth, which occur at lower temperatures, contribute another type of compositional variation. Stated schematically, one has a range of compositions from the early solar system and a range of compositions for the upper mantle of the Earth, and one must devise the procedure to correct for two different sets of processes.

Chondrites represent samples of undifferentiated silicate material from the solar system prior to melting and metallic core segregation. Their composition derives from the solar composition altered by processes in the early solar nebula which have generated different families of chondrites. Perturbations are essentially brought in the gas state and elemental behavior is classified according to volatility (or condensation temperature). For our present purposes, the important elements are uranium, thorium, and potassium. The first two are associated with very high condensation temperatures and called 'refractory lithophile' elements. That these two elements have the same behavior in the early solar system is demonstrated by the fact that they have the same ratio in all types of chondritic meteorites. Potassium is a 'moderately volatile' element with a lower condensation temperature. The best match with solar concentration ratios is achieved by CI carbonaceous chondrites, which explains why many Earth models have relied on them. However, we do know that CI chondrites have larger amounts of volatiles, including water and CO_2, than the Earth. As regards samples from the Earth's mantle, one may establish a systematic compositional trend through the samples available and identify the most primitive (and least-differentiated) material. With these problems in mind, we review the four main types of approaches that have been used and the resulting estimates of Earth composition.

The first method relies on direct samples from the mantle. Ringwood (1962) argued that basalts and peridotites are complementary rocks, such that the latter is the solid residue of the partial melting event which led to basalt genesis and extraction. Thus, mixing them back together with the appropriate proportions yields the starting material, which was named 'pyrolite'. Clearly, one has to choose the best samples which have not been affected by leaching and low-temperature alteration. Unfortunately, this procedure is not efficient for uranium, which is very mobile.

A second method relies on a choice for the starting material. Many authors (e.g., Hart and Zindler, 1986) used CI chondrites, a particular class of chondrites, and worked their way through the processes that turn these meteorites into Earth-like material: devolatization (loss of water, CO_2, and other volatile elements present in very small amounts in the Earth) followed by reduction (loss of oxygen). Errors associated with this obviously come from the mass loss estimates, but also from the starting CI chondrite composition since this group of meteorites is quite heterogeneous. Javoy (1999) argued in favor of a different type of meteorite. His line of reasoning focusses on the oxidation state of the solar nebula as it started to condense. The only meteorites with the right oxidation state are enstatite chondrites, which are therefore close to the material which went into the protoplanets. These chondrites are largely degassed, save for sulfur, so that the volatile loss correction is small.

A third method tries to avoid a specific choice for the starting composition and aims at determining it. Hart and Zindler (1986) defined the compositional trends of chondritic meteorites and peridotites, which are not parallel to one another. Each trend records the effects of the two different sets of processes operating in the primitive solar nebula and in the Earth, and hence the intersection can only be the starting Earth material. In this case, the error comes from the scatter around the two compositional trends.

A fourth method relies on elemental ratios. For refractory lithophile elements, such as uranium and thorium, the concentration ratio is independent of chondrite type and hence is a property of the starting Earth material. Once these ratios have been

determined, two procedures can be used to determine primitive abundances from measurements on peridotite samples. One procedure is to study the relationship between abundance and elemental ratios: the primitive abundance is that which corresponds to the chondritic ratio (McDonough and Sun, 1995). In the other procedure, one starts with one specific element for which one can determine a reliable value for the bulk Earth and work sequentially to all the others using elemental ratios. The element of choice is Mg because, although it is not the most refractory element, its behavior during melting and alteration is well understood (Palme and O'Neill, 2003). Uncertainties on the uranium, thorium, and potassium concentrations are large (≈15%, see **Table 9**) (McDonough and Sun, 1995; Palme and O'Neill, 2003). Lyubetskaya and Korenaga (2007) have recently revisited the procedure of McDonough and Sun (1995). The correlation between abundance and elemental ratio can be accounted for by variations in the degree of melting of a peridotite and McDonough and Sun (1995) carried out a linear regression through the data. Depletion effects due to melt extraction, however, are intrinsically nonlinear. With a realistic treatment of depletion effects and statistical analysis of the highly scattered data, Lyubetskaya and Korenaga (2007) have obtained a model for the bulk silicate Earth (BSE) that is more depleted than previous ones.

As regards the radioactive elements of interest here, the 'pyrolite' method is unreliable and hence was not used. **Table 9** lists estimates obtained by different authors using the other methods. One should note that concentration ratios are constrained more tightly than absolute concentrations. One cannot separate uncertainties due to the starting chemical data from those of the calculation algorithm, because each author uses his own data and method. Save for major modifications in our understanding of early planetary accretion, it may well prove impossible to reduce the spread of results.

Values for U, Th, and K concentrations yield estimates of the radiogenic heat production rate in the Earth. We have used the revised decay constants listed in **Table 10** (Rybach, 1988) (see also *Handbook of Constants*). Those differ slightly from the earlier estimates given by Birch (1965), which are commonly used in the geophysical literature. Heat production values vary within a restricted range, from 3.9 to 5.1 pW kg^{-1}. The BSE model of Palme and O'Neill (2003) leads to the highest value and may well be an overestimate. The EH chondrite model does not lead to a major difference for the present-day heat production rate but implies important changes at early

Table 9 Radioelement concentration and heat production in meteorites, in the bulk silicate Earth, in Earth mantle, and crust

	U (ppm)	Th (ppm)	K (ppm)	A (pW kg^{-1})
CI Chondrites				
Palme and O'Neill (2003)	0.0080	0.030	544	3.5
McDonough and Sun (1995)	0.0070	0.029	550	3.4
Bulk silicate Earth				
From CI chondrites				
Javoy (1999)	0.020	0.069	270	4.6
From EH Chondrites				
Javoy (1999)	0.013	0.0414	383	3.6
From chondrites and lherzolites trends				
Hart and Zindler (1986)	0.021	0.079	264	4.9
From elemental ratios and refractory lithophile elements abundances				
McDonough and Sun (1995)	0.020 ± 20%	0.079 ± 15%	240 ± 20%	4.8 ± 0.8
Palme and O'Neill (2003)	0.022 ± 15%	0.083 ± 15%	261 ± 15%	5.1 ± 0.8
Lyubetskaya and Korenaga (2007)	.017 ± 0.003	.063 ± 0.011	190 ± 40	3.9 ± 0.7
Depleted MORB source				
Workman and Hart (2005)	0.0032	0.0079	25	0.59
Average MORB mantle source				
Su (2000); Langmuir *et al.* (2005)	0.013	0.040	160	2.8
Continental crust				
Rudnick and Gao (2003)	1.3	5.6	1.5 10^4	330
Jaupart and Mareschal (2003)	/	/	/	293–352

Table 10 Heat production constants

Isotope/Element	Natural abundance (%)	Half-life (yr)	Energy per atom ($\times 10^{-12}$ J)	Heat production per unit mass of isotope/element (W kg^{-1})
^{238}U	99.27	4.46×10^{9}	7.41	9.17×10^{-5}
^{235}U	0.72	7.04×10^{8}	7.24	5.75×10^{-4}
U				9.52×10^{-5}
^{232}Th	100.	1.40×10^{10}	6.24	2.56×10^{-5}
Th				2.56×10^{-5}
^{40}K	0.0117	1.26×10^{9}	0.114	2.97×10^{-5}
K				3.48×10^{-9}

From Rybach (1988).

ages because its Th/U and K/U ratios differ strongly from the others. One important result is that the uncertainty on each estimate (≈15%) is consistent with the range spanned by the various estimates.

Independent constraints can be derived from the compositions of MORBs, which have been sampled comprehensively. MORBs span a rather large compositional range and common practice has been to define end members associated with different chemical reservoirs. According to this framework, depleted MORBs come from a depleted reservoir whose complement is enriched continental crust. Enriched basalts are attributed to primitive mantle tapped by deep mantle plumes or to secondary enrichment processes, for example, infiltrations of low-degree melts and metasomatic fluids in subduction zones (Donnelly *et al.*, 2004). The heat production rate of the depleted MORB mantle source is ≈0.6 pW kg^{-1} (i.e., at this rate, the entire mantle would generate only 2.4 TW). This source, however, does not provide an exact complement of average continental crust (Workman and Hart, 2005). An alternative approach avoids the separation of different mantle reservoirs and determines the average composition of all the mantle that gets tapped by mid-ocean ridges (Su, 2000; Langmuir *et al.*, 2005). Composition of the average MORB mantle source is then derived from a well-constrained melting model. This mantle reservoir is a mixture of different components and is the average mantle lying below oceanic ridges. It is depleted in incompatible elements and represents a complement of continental crust. Thus, it may be interpreted as the mantle reservoir that has been processed to form continents (Langmuir *et al.*, 2005). There may be a volume of primitive mantle lying at depth that has never been sampled by mid-oceanic ridges. Therefore, a lower bound on the total amount of radioelements in the mantle is obtained by assuming that the average MORB source extends through the whole mantle. From **Table 9**, this leads to a total mantle heat production of 11 TW. Adding radioelements from the continental crust and lithospheric mantle, which contribute 7–8 TW (**Table 11**), we obtain a lower bound of 18 TW for the total rate of heat production in the Earth. This is consistent with the BSE models and their uncertainties.

Various models for the bulk silicate Earth, which includes continental crust, lead to a total rate of heat production of 20 TW, with an uncertainty of 15%. After removing the contributions of the continental crust (6–7 TW) and the lithospheric mantle (≈1 TW), heat production in the mantle amounts to a total of 13 TW, with an uncertainty of 20%.

7.06.5.2 Heat Flux from the Core

The outer core is made of molten iron and hence has very low viscosity, contrary to the deep mantle which is much more viscous. Thus, the heat flux out of the core is controlled by the efficacy of mantle convection and cannot be considered as an independent input. Nevertheless, the thermal evolution of the core controls the energy sources available to drive the geodynamo and one may thus deduce constraints on the heat flux at the core–mantle boundary (CMB) using thermodynamics. This question is briefly covered here and the interested reader should consult the volume concerning the core and some standard references (Gubbins and Roberts, 1987; Braginsky and Roberts, 1995; Lister and Buffett, 1995; Labrosse, 2005a, 2005b, *see also* Chapter 8.02).

An energy balance can be written for the core, in much the same way as it is done above for the mantle. The main differences come from electromagnetic processes and chemical buoyancy due to inner-core crystallization. The low viscosity maintains the convective state very close to the reference (radially symmetric) state. The convective velocity at the

Table 11 Mantle energy budget: preferred value and range

	TW	TW
Oceanic heat loss (300×10^6 km^2)	32	30–34
Continental heat loss (210×10^6 km^2)	14	13–15
Total surface heat loss (510×10^6 km^2)	46	43–49
Radioactive sources (mantle + crust)	20	17–23
Continental heat production (crust + lith. mantle)	7	6–8
Heat flux from convecting mantle	39	35–43
Radioactive heat sources (convecting mantle)	13	9–17
Heat from core	8	5–10[a]
Tidal dissipation in solid earth	0.1	
Gravitational energy (differentiation of crust)	0.3	
Total input	21	14–27
Net loss (mantle cooling)	18	8–29
Present cooling rate, K Gy^{-1}	118	53–190
Present Urey ratio[b]	0.33	0.21–0.49

[a]This range includes estimates from core thermodynamics and inference from the perovskite–post-perovskite phase diagram.
[b]Urey ratio for the convecting mantle, leaving out crustal heat sources from both the heat loss and heat production.
The distribution in the range is barely known for most cases and the preferred value is simply the middle one. The cooling rate is computed assuming $C_P = 1200\,\mathrm{J\,K^{-1}\,kg^{-1}}$.

surface of the core, which is of the order of $10^{-4}\,\mathrm{m\,s^{-1}}$ (Hulot *et al.*, 2002, *see also* Chapter 5.05), suggests relative density fluctuations of order 10^{-9} (Braginsky and Roberts, 1995; Labrosse *et al.*, 1997). Such fluctuations correspond to temperature variations $\delta T \sim 10^{-4}\,\mathrm{K}$ in the absence of other effects. This is very small compared to the secular temperature decrease, implying a very good separation of scales between the upper boundary layer and the whole outer core. Thus, for the secular cooling of the core, it is sufficient to consider radial profiles of temperature and concentration, which are usually assumed to be isentropic and uniform, respectively. The very thin boundary layer of the outer core is not significant for the bulk energy budget, contrary to that of the mantle.

The energy balance of the core equates the heat flux at the CMB to the sum of secular cooling, Q_C, latent heat from inner-core crystallization, Q_L, compositional energy due to chemical separation of the inner core (often called gravitational energy, but see Braginsky and Roberts, 1995), E_ξ, and, possibly, radiogenic heat generation, Q_H. Secular cooling makes the inner core grow, which releases latent heat and compositional energy and the first three energy sources in the balance can be related to the size of the inner core and its growth rate (Braginsky and Roberts, 1995). The current growth rate of the inner core is small (about $300\,\mathrm{m\,Gy^{-1}}$) and cannot be determined by observation. Thus, one has to resort to indirect means. Energy requirements for the geodynamo do not appear directly in the bulk energy balance for the core because they are accounted for by internal energy transfers, just like viscous dissipation in the mantle. The entropy balance, however, depends explicitly on dissipation (Φ_c), which is achieved mostly in the form of Joule heating (ohmic dissipation). Combining the energy and the entropy balances, an efficiency equation can be written, which is to leading order (Braginsky and Roberts, 1995; Labrosse, 2003; Lister, 2003):

$$\Phi_c + T_\Phi \Delta S_{\mathrm{cond}} = \frac{T_\Phi}{T_{\mathrm{CMB}}}\left(1 - \frac{T_{\mathrm{CMB}}}{T_{\mathrm{ICB}}}\right) Q_L + \frac{T_\Phi}{T_{\mathrm{CMB}}}\left(1 - \frac{T_{\mathrm{CMB}}}{T_C}\right) Q_C + \frac{T_\Phi}{T_{\mathrm{CMB}}}\left(1 - \frac{T_{\mathrm{CMB}}}{T_H}\right) Q_H + \frac{T_\Phi}{T_{\mathrm{CMB}}} E_\xi \quad [51]$$

where T_i is the temperature at which heat due to process (i) is released and where

$$\Delta S_{\mathrm{cond}} \equiv \int k \left(\frac{\nabla T}{T}\right)^2 \mathrm{d}V \quad [52]$$

is the entropy production due to heat conduction (*see* Chapter 7.02). The efficiency eqn [51] shows that heat is less efficiently transformed into ohmic dissipation than compositional energy.

All the source terms on the right-hand side of the efficiency eqn [51], save for radiogenic heating, are linked to inner-core growth and are proportional to its growth rate. Therefore, if Ohmic dissipation Φ_c

and radiogenic heat production Q_H can be estimated, one can calculate the inner-core growth rate and the heat flux across the CMB. **Figure 9** shows the different contributions to the energy and entropy budgets as a function of Ohmic dissipation for zero radiogenic heat production from Labrosse (2003). $\Phi_c = 1$ TW implies a heat flux of about 6 TW at the CMB. In addition, about 1 TW is dissipated by conduction along the isentropic temperature gradient.

Ohmic dissipation in the core is dominated by small-scale components of the magnetic field, which cannot be determined directly because they are screened by crustal magnetic sources (Hulot *et al.*, 2002). Using high-resolution numerical models of the geodynamo, Christensen and Tilgner (2004) have recently claimed that $\Phi_c = 0.2$–0.5 TW, which implies a heat flux across the CMB of about 2–4 TW. These models rely on the Boussinesq approximation, and hence neglect the isentropic temperature gradient in both the heat and entropy balances. As a rough correction, one may add an estimate of the associated dissipation $\Delta S_{cond} \sim 1$ TW, which would bring the total dissipation estimate to $\Phi_c = 1$–2 TW, close to that of Roberts *et al.* (2003). From **Figure 9**, the corresponding heat flux across the CMB would thus be in the range 5–10 TW.

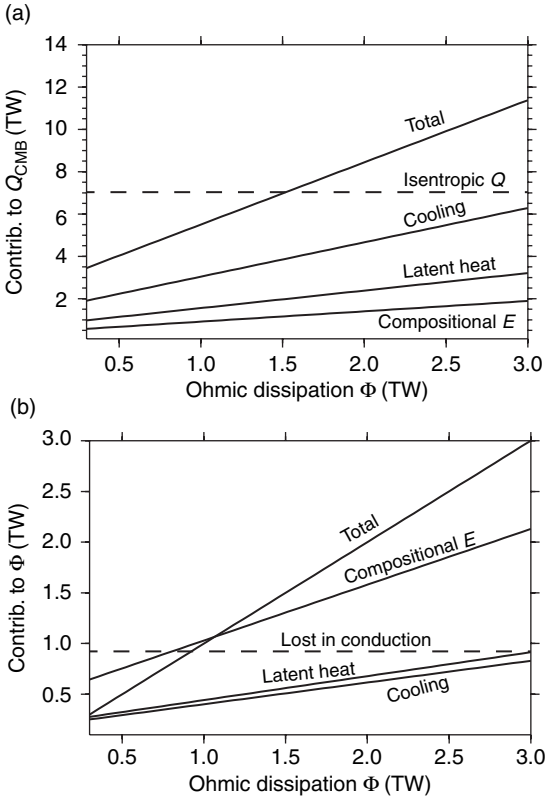

Figure 9 Contributions to the energy (a) and entropy (b) balance in the core, in the absence of internal heat production. Based on the model of Labrosse (2003).

Studies of hot-spot swells have led to estimates of ≈2–4 TW for the heat flux carried by mantle plumes (Sleep, 1990; Davies, 1988). The relevance of this heat flux to the cooling of the core is difficult to assess, in part because some of the plumes may not come from the CMB and in part because plumes account for only part of the core heat loss. The convective heat flux is given by

$$Q_{conv} = \rho C_p \overline{w_r \theta} \qquad [53]$$

where, as above, θ is the temperature perturbation with respect to the azimuthal temperature average. This may be broken down into two different components due to upwellings and downwellings, for which $\overline{w_r \theta}$ has the same sign. For our present discussion, this states that secular cooling is effected by both mantle plumes and downgoing slabs. In Rayleigh–Bénard convection with no internal heating, each component is equally important. In the Earth, convection is also driven by internal heating and secular cooling and this breaks the symmetry between upwelling and downwelling currents, at the expense of the former. In such a situation, heat transport at the CMB is dominated by the spreading of cold material from subducted slabs (Labrosse, 2002; Zhong, 2005; Mittelstaedt and Tackley, 2006). The contribution of hot spots therefore provides a lower bound to the total core heat loss. As explained below, an independent estimate of 13 ± 4 TW was derived by Lay *et al.* (2006) from the post-perovskite phase change and an estimate of thermal conductivity at the base of the mantle.

7.06.5.3 Other Sources: Tidal Heating, Crust–Mantle Differentiation

Earth's rotation is accelerating because of postglacial readjustments, and it is slowing down because of tidal interaction with the moon. The torque exerted on the Moon is due to the lag between the tidal potential and the tidal bulge which is 2.9° ahead of the potential. In the Earth–Moon system, angular momentum is conserved, but there is a net loss of the rotational and gravitational potential energy. This energy is converted into heat by frictional forces. With laser

ranging, the changes in the Earth–Moon distance have been measured accurately ($3.7\,\mathrm{cm\,yr^{-1}}$) and the slowing down of Earth's rotation due to tidal interaction with the Moon can be calculated exactly. The effect of the solar tidal potential on Earth rotation is ≈20% that of the Moon and it must be included in the calculations. The slowing down of Earth's rotation is $5.4 \times 10^{-22}\,\mathrm{rad\,s^{-1}}$ leading to $0.024\,\mathrm{ms\,yr^{-1}}$ increase in the length of the day. The energy loss has been calculated to be 3 TW, which must be accounted by dissipation in the oceans, in the solid earth, and in the Moon. It is commonly assumed that most of the tidal friction comes from dissipation in shallow seas because dissipation in the deep oceans was shown to be small (e.g., Jeffreys, 1962; Munk and MacDonald, 1960). Lambeck (1977) calculated that dissipation in the seas and oceans must account for 90–95% of the energy dissipation. The contribution of the solid Earth tide depends on the quality factor Q. For the values of Q in the mantle suggested by seismology, dissipation by the solid earth tide accounts for <0.1 TW (Zschau, 1986). Such a low value has now found confirmation from satellite observations of the lag between the solid earth tide (0.16°) and the lunar potential. This observation implies that the dissipation by the solid earth is 0.083 TW (Ray *et al.*, 1996).

Some gravitational potential energy is also released by the extraction of continental crust out of the mantle. A rough estimate of this energy loss is obtained by considering the potential energy of a differentiated Earth:

$$E_{gm} = -(3/5)GM_m^2/R_1 - GM_m M_c/R_1 \qquad [54]$$

where M_c is the mass of crust ($\approx 2.6 \times 10^{22}$ kg) and residual material with mass M_m is in a sphere of radius R_1. Comparing with E_g from eqn [3], we get $\Delta E_g \approx 10^{28}$ J. For a constant rate of crustal growth during 3 Gy, the contribution to the energy budget is small, ≈0.1 TW. If the crust differentiated in two or three short episodes, each episode may have added as much as ≈1 TW to the mantle budget. In contrast to the change of gravitational energy due to thermal contraction, this energy contributes to the bulk energy balance as compositional energy (see Braginsky and Roberts, 1995).

7.06.5.3.1 Summary

Various models for the BSE composition lead to results that differ significantly from one another. Uncertainties on the average uranium, thorium, and potassium abundances stem from the propagation of errors through a sequence of elemental ratios and from the correction procedure for depletion effects due to melting in mantle peridotites. A lower bound on the bulk mantle heat production may be derived from the average MORB mantle source. A large uncertainty remains on the heat flux from the core and better constraints will have to come from dynamo theory.

7.06.6 Secular Cooling: Constraints on Mantle Temperatures

In this section, we review evidence for secular cooling, starting with present-day evidence and working backwards in time. The total heat lost by the mantle is more than all the inputs. Our preferred values for the input and output of energy are 21 and 39 TW, respectively. The difference 18 TW must be accounted for by the secular cooling of the mantle. Assuming a constant value for the specific heat of $1250\,\mathrm{J\,kg^{-1}\,K^{-1}}$, the rate of cooling must be $3.8 \times 10^{-15}\,\mathrm{K\,s^{-1}}$ or $120\,\mathrm{K\,Gy^{-1}}$, with a range $50–190\,\mathrm{K\,Gy^{-1}}$.

7.06.6.1 The Present-Day Mantle Geotherm

The potential temperature of shallow oceanic mantle may be calculated from the composition of MORBs which have not been affected by fractional crystallization and also from heat flux and bathymetry data, as explained above. Such independent determinations are summarized in **Table 4** and are in very good agreement with one another. For temperatures at greater depth, one may use seismic discontinuities and the associated solid-state phase changes. This classical method requires specification of the mantle composition, which is usually taken to be pyrolite (Ringwood, 1962). Well-defined discontinuities at depths of 410 and 660 km have been linked to the olivine–wadsleyite transition and to the dissociation of spinel to perovskite and magnesowustite, the so-called 'post-spinel' transition (**Table 12**). Other seismic discontinuities have been identified, notably at a depth of about 500 km. Some of these are not detected everywhere and seem to have a regional character, and interpretation is still tentative to some extent. Recently, a new phase change relevant to the lowermost mantle has been discovered, from perovskite to post-perovskite (Murakami *et al.*, 2004; Oganov and Ono, 2004, *see also* Chapter 2.06).

Table 12 Anchor points for the mantle geotherm

Boundary	Depth (km)	Temperature (K)	Reference
MORB generation	50	1590–1750[a]	Kinzler and Grove (1992)
Olivine–Wadsleyite	410	1760 ± 45	Katsura *et al.* (2004)
Post-spinel	660	1870 ± 50	Katsura *et al.* (2003, 2004)
Core–mantle	2884	4080 ± 130	Alfé *et al.* (2002); Labrosse (2003), this paper

[a]indicates true range of temperatures in the shallow mantle.

The olivine–wadsleyite phase change has a large Clapeyron slope of 4 MPa K^{-1} and hence provides an accurate temperature estimate (Katsura *et al.*, 2004). Errors on temperature arise from the experimental data as well as from the slight differences in the exact depth of the seismic discontinuity. Accounting for both these errors, the temperature estimate at 410 km is 1760 ± 45 K for a pyrolitic upper mantle. Isentropic profiles (**Figure 10**) which pass through these (P, T) values correspond to potential temperatures in the range 1550–1650 K (Katsura *et al.*, 2004), in very good agreement with the independent estimates from the composition of MORBs and heat flux data (**Table 4**).

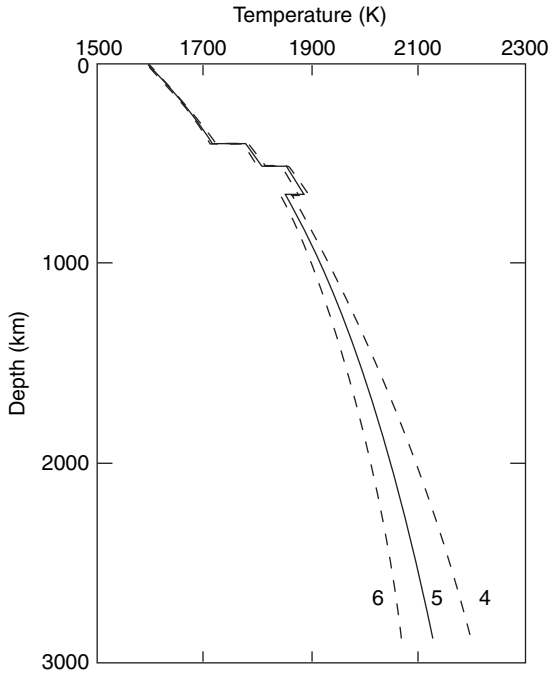

Figure 10 Isentropic temperature profiles in the mantle for different values of the Anderson–Grüneisen parameter, as labelled. From Katsura T, Yamada H, Nishikawa O, *et al.* (2004) Olivine-Wadsleyite transition in the system $(Mg,Fe)_2SiO_4$. *Journal of Geophysical Research* 109: B02209 (doi:10.1029/2003JB002438).

Recent laboratory studies have cast doubt on the post-spinel transition pressure (Irifune and Isshiki, 1998; Katsura *et al.*, 2003). Furthermore, this transition may have a very small Clapeyron slope (as small as -0.4 MPa K^{-1}, (Katsura *et al.*, 2003), implying that uncertainties on pressure lead to large errors on the transition temperature. For these reasons, one should treat temperature estimates for this transition with caution. Nevertheless, the uncertainty often quoted for this value is similar to that for the 410 km discontinuity, and the present-day 'best' value for the mantle temperature at a depth of 660 km is 1870 ± 50 K (Ito and Katsura, 1989; Katsura *et al.*, 2003, 2004).

The other major discontinuity, the CMB, is a chemical boundary and its temperature can be computed from the core side. Once again, the method relies on a phase change, in this case the solidification of iron at the inner-core boundary. Alfé *et al.* (2002) have recently determined that the melting temperature of pure Fe is in the range 6200–6350 K. Adding the effects of light elements (O, Si, S), the liquidus temperature at the inner-core boundary is lowered by 700 ± 100 K. The outer core can be assumed to be very close to isentropic (e.g., Braginsky and Roberts, 1995), and the variation in temperature can be linked to the variation in density by (e.g., Poirier, 2000)

$$\left(\frac{\partial T}{\partial \rho}\right)_S = \gamma \frac{T}{\rho} \qquad [55]$$

where γ is the Grüneisen parameter (*see* Chapter 7.02). According to the theoretical calculations of Vočadlo *et al.* (2003, *see also* Chapter 2.05), $\gamma = 1.5 \pm 0.01$ throughout the core. We may therefore assume that γ is constant and integrate eqn [55]:

$$T_{CMB} = T_{ICB}\left(\frac{\rho_{CMB}}{\rho_{ICB}}\right)^{\gamma} = 0.73\, T_{ICB} \qquad [56]$$

which relates the temperature at the CMB to that at the ICB and to density structure. Using $\gamma = 1.5$ and

density values from the preliminary reference Earth model (PREM) of Dziewonski and Anderson (1981, *see also* Chapter 1.01), we obtain a range of 3950–4210 K for the temperature at the top of the core. This does not account for uncertainties in the PREM density values and does not represent the full range of published values, but a full discussion of all the different estimates is outside the scope of this chapter.

The perovskite to post-perovskite phase change (Murakami *et al.*, 2004; Oganov and Ono, 2004, *see also* Chapter 2.03) provides a strong constraint on the temperature just above the CMB, if it takes place in the mantle. According to the latest experiments (Hirose *et al.*, 2006; Hirose, 2006), this phase change has a Clapeyron slope of $11.5 \pm 1.4\,\mathrm{MPa\,K^{-1}}$ and a temperature of 2400 K at 119 GPa. A key feature is that it occurs very near the boundary layer at the base of the mantle. Assuming an error function temperature profile in this boundary layer, Hernlund *et al.* (2005, *see also* Chapter 1.18) predicted that the phase change boundary should be crossed twice in cold regions of the mantle (**Figure 11**), and should not occur in hot regions, which seems to be consistent with seismic observations. As illustrated in **Figure 11**, the fact that the phase boundary is crossed twice implies that the temperature gradient at the base of the mantle is larger than that of the Clapeyron diagram. It also implies that the temperature at the CMB must be larger than the temperature of the phase change at the pressure of the CMB, which is in the range 3800–4200 K. This estimate is consistent with those obtained from the core side. Lateral variations of the depth of discontinuity that are deduced from seismological observations imply lateral temperature variations of ≈1500 K in the lowermost mantle (Hirose, 2006).

Paired seismic discontinuities have also been detected in hot regions near the CMB beneath the Pacific Ocean (Lay *et al.*, 2006). These can be reconciled with the dynamical model of Hernlund *et al.* (2005) if these regions are enriched in iron. Using a dynamical model for the boundary layer above the CMB, Lay *et al.* (2006) have estimated that the heat flux across the CMB is at least 13 ± 4 TW for a thermal conductivity value of $10\,\mathrm{W\,m^{-1}\,K^{-1}}$.

7.06.6.2 Temperature versus Time

One may use petrological constraints to investigate past temperatures of the mantle. Continental crustal material was different in the Archean than it is today. Basaltic lavas exhibit systematic compositional trends with time, including a secular decrease in average MgO content. MgO-rich ultramafic lavas named komatiites are common in the Archean and are almost absent from today's rock record. Early workers proposed that komatiites require the mantle source to be at least 300 K hotter than present (Green, 1975; Sleep, 1979) but they considered dry mantle only. The peridotite solidus depends strongly on water content, which in turn depends on the geological setting. If komatiites are generated by

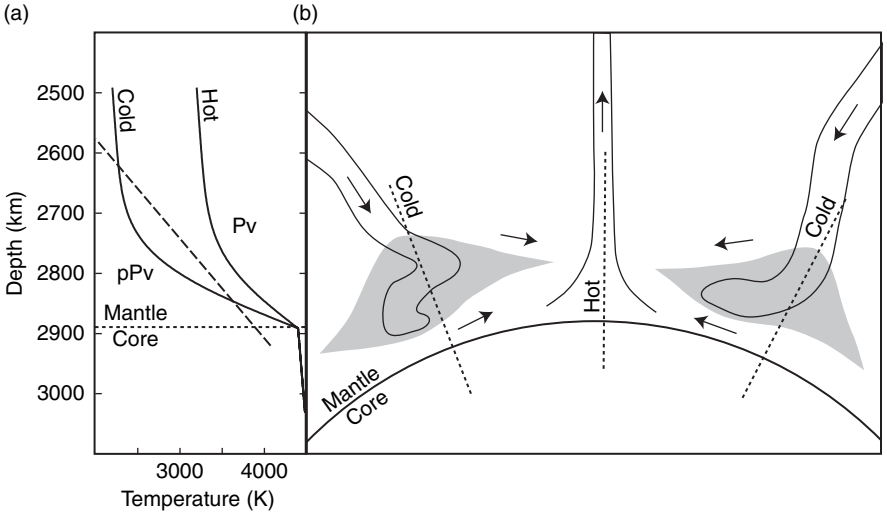

Figure 11 Sketch of post-perovskite lenses in cold regions of the lowermost mantle from Hernlund *et al.* (2005). (a) Schematic temperature profiles for 'cold' and 'hot' regions (plain curves) superimposed onto the phase boundary. (b) Sketch of thermal boundary layer at the base of the mantle with convective downwellings and upwellings.

mantle plumes, involving mantle that is essentially dry, that is, such that its water content is so small that it does not affect phase boundaries, one deduces that mantle plume temperatures have decreased by about 300 K in 3 Gy (Nisbet *et al.*, 1995). Jarvis and Campbell (1983) suggested that such hot mantle plumes did not require the Archean mantle to be more than 100 K hotter than present on average. According to an alternative hypothesis, komatiites are generated in a subduction environment, involving mantle hydrated by downgoing plates. In that case, one is led to conclude that this part of the mantle was only slightly hotter (≈100 K) in the Archean than it is today (Grove and Parman, 2004). In both cases, komatiites do not sample 'average' mantle and it is not clear how to incorporate these temperature estimates in models for the entire mantle.

Mid-ocean ridge tholeiites are better suited for studies of the mantle's average temperature because they can be sampled over very large areas. They are a compositionally heterogeneous group, however, which translates into a wide temperature range (≈200 K) (Klein and Langmuir, 1987; Kinzler and Grove, 1992). Abbott *et al.* (1994) calculated the liquidus temperature for Phanerozoic MORBs and Archean MORB-like greenstones and determined the maximum and minimum mantle potential temperatures versus time. Although the range of temperatures for each period is wide (≈200 K), the trend is well marked. Abbott *et al.* (1994) concluded that mantle temperatures decreased by ≈150 K since 3 Gy (137 K for the mean or 187 K for the maximum temperature recorded in each age bin), which is less than the range of mantle potential temperatures at a given time. Cooling of the mantle by $50\,\mathrm{K\,Gy^{-1}}$ represents ≈8 TW.

7.06.6.3 Early Earth

A full description of Earth's thermal evolution must include the initial conditions. Here, 'initial' refers to the time when the Earth had completed its main phase of core–mantle differentiation and the mantle had solidified to the point where its dynamics can be described as sub-solidus convection. Before reaching that point, a host of processes with different dynamics occurred. They may be separated into three categories: accretion, core formation, and magma ocean crystallization. The process of formation of the Earth brought together matter which was originally dispersed in the proto-solar nebula, thereby releasing gravitational energy. One may estimate the total energy released by taking the difference between the total gravitational energy before and after. The fate of this energy, however, depends on the way it is dissipated and transformed into another type of energy. The effect of core differentiation is quite different from that of accretion. Most of the processes involved remain speculative to some extent and we restrict our discussion to the points that are directly relevant to the early thermal structure. Several review articles (e.g., Stevenson, 1989; Wetherill, 1990) and two books (e.g., Newsom and Jones, 1990; Canup and Righter, 2000) deal with these issues in detail.

During accretion, the gravitational energy of impactors is first transformed into kinetic energy and then dissipated in the form of heat at the impact. One may define two limit-cases. If no energy is lost to space, the temperature of the whole Earth is raised by an amount equal to

$$\Delta T = \frac{-E_g}{MC_P} \sim 3.75 \times 10^5\,\mathrm{K} \qquad [57]$$

which would be sufficient to vaporize the whole planet. Most of the impact energy, however, was released at shallow levels and lost to space by radiation. Stevenson (1989) estimated that, if all the energy is made available for radiation, accretion would raise the temperature of the Earth by less than 70 K relative to that of the nebula. The actual evolution lies somewhere between these two limiting cases, involving partial dissipation of the impact energy within the planet and radiative heat transfer through the primordial atmosphere. One important factor is the size of the impactors. 'Small' impactors, which are much smaller than the target, account for the vast majority of impacts on Earth after the planetary embryo stage (Melosh and Ivanov, 1999). The depth of energy release increases with the size of the impactor and one key variable is the ratio between the time for energy transport to the surface and the time between two impacts. During accretion, evolution towards larger and fewer impactors has two competing effects: energy gets buried at greater depth while the time between two impacts increases, which enhances heat loss to the atmosphere. Assuming heat transport by diffusion, Stevenson (1989) concluded that typical accretion scenarios lead to significant energy retention within the planet. The extreme case is that of the giant impact thought to be at the origin of Moon formation. Calculations suggest that the whole-Earth temperature was raised

to as high as 7000 K (Cameron, 2001; Canup, 2004, *see also* Chapter 9.02). In such conditions, the whole Earth melted and parts of it were vaporized to form a thick atmosphere. The question of whether or not previous impacts were able to melt the Earth becomes irrelevant.

The formation of the core also has important energetic implications. Some gravitational energy is released by going from a uniform composition to a stratified core–mantle system. Kinetic energy plays no role in this process, in contrast to the accretionary sequence, and gravitational potential energy is directly dissipated by viscous heating in both the iron and silicate phases. Flasar and Birch (1973) estimated that this process would heat the whole Earth by about 1700 K. This estimate relies on the bulk difference in gravitational energy between the initial and final states and hence gives no information on where energy gets dissipated. We know now that iron-silicate differentiation occurred very early in the solar system and affected planetesimals (Kleine *et al.*, 2002). Clearly, core formation within planetesimals and in the Earth after the giant impact involve different dynamics. Models of the giant impact show that large parts of the cores of the two proto-planets merge without remixing with silicates (Canup, 2004). Emulsification of iron in the molten silicate is a possibility (Rubie *et al.*, 2003), because of the large viscous stresses involved.

Our current understanding of core formation suggests three mechanisms: iron droplets 'raining' through a magma ocean, diapirs generated by Rayleigh–Taylor instability at a rheological interface and interstitial flow across a solid permeable matrix (Stevenson, 1990; Rushmer *et al.*, 2000, *see also* Chapter 9.03. All three mechanisms may have been active at different times and have different implications for dissipation. For a Newtonian rheology, the amount of viscous heating is $\phi \sim \mu U^2/L^2$, where μ is the viscosity of the fluid phase, which may be silicate or iron, and U and L are the scales for velocity and length. In the case of an iron diapir, the velocity and length scales are the same for the metal and silicate phases, but the viscosity of the former is several orders of magnitudes smaller. Viscous heating is thus concentrated in the silicate phase and little heating of the iron phase results because heat diffusion is not efficient over the descent timescale. This would differentiate a core that is initially colder than the lower mantle. In the case of interstitial flow, the small size of iron veins makes heat diffusion very effective and thermal equilibration with the surrounding silicate phase is likely. In the case of iron droplets raining down through molten silicate, the droplet size is set by equilibrium between surface tension and viscous drag and is typically 1cm. Again, thermal equilibrium is likely and the core should initially be at the temperature of the lower mantle.

7.06.6.4 Magma Ocean Evolution

Both the giant impact and core-formation processes generated temperatures that were high enough for a magma ocean to include the whole silicate Earth. Cooling and crystallization of such a deep magma ocean involves heat transfer through the primordial atmosphere, convection, rotation, and crystal-melt separation. Available models have been aimed mostly at determining the extent of chemical stratification at the end of crystallization (Abe, 1997; Solomatov, 2000, *see also* Chapter 9.04). The pressure effect on the liquidus causes more crystallization at the bottom. The low viscosity of the melt and the size of Earth imply highly turbulent convective flows and rapid cooling, such that the lower parts of the magma ocean solidify in a few kiloyears. Two rheological transitions, from pure magma to slurry and from slurry to mush, affect the convective regime and the cooling rate. One important fact is that, in a convecting region, the isentropic temperature gradient is less than the gradients of liquidus and solidus.

Starting from a superheated magma ocean (i.e., at temperatures above the liquidus), the initial phase has a fully molten upper layer which becomes thinner as cooling proceeds. A first transition occurs when the fully molten layer vanishes. At this stage, the Earth is made of a partially crystallized magma ocean which may lie over already fully solidified mantle. The radial temperature profile is tied to the solidus which is steeper than the isentropic profile, which leads to convective overturn in the solid layer (Elkins-Tanton *et al.*, 2003). The two layers evolve at vastly different timescales because of their different rheologies. The bulk cooling rate is set by the heat loss through Earth's surface, which is controlled by the dynamics of the partially crystallized surficial magma ocean. In this second phase, heat transport occurs mostly by melt–solid separation and solidification proceeds from the bottom up. The fully solidified layer at the base of the magma ocean thickens rapidly and eventually becomes unstable. Convective overturn is slower than the cooling of the magma ocean and may be considered as a separate event which leads to decompression melting and

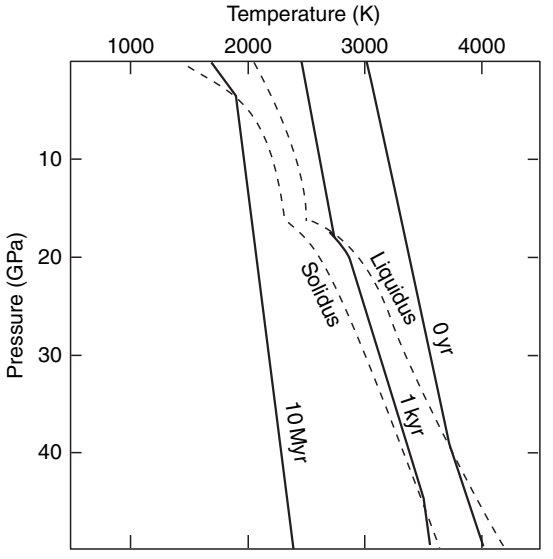

Figure 12 Three geotherms at different times in the early Earth. The timescale for the thermal evolution is set by heat loss at the upper boundary which decays rapidly with temperature. At about 10 My, the solid content in the partially molten upper mantle layer reaches the threshold value of 60%, which marks the cessation of liquid behavior. After that time, convection is in the subsolidus regime controlled by solid behavior which still prevails today. Adapted from Abe Y (1997) Thermal and chemical evolution of the terrestrial magma ocean. *Physics of the Earth and Planetary Interiors* 100: 27–39.

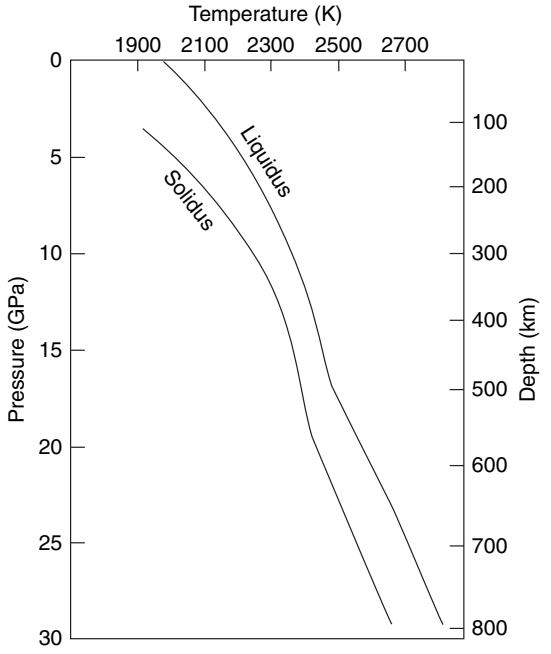

Figure 13 Solidus and liquidus for dry pyrolite as a function of pressure. Adapted from Litasov K and Ohtani E (2002) Phase relations and melt compositions in CMAS-pyrolite-H_2O system up to 25 GPa. *Physics of the Earth and Planetary Interiors* 134: 105–127.

the formation of a secondary magma ocean at the surface. The process of cooling and solidification of this magma ocean then repeats itself. This regime prevails until the shallow magma ocean reaches the rheological threshold between liquid and solid behavior, which probably occurs at a crystal fraction of about 60%. At this stage, the shallow partially crystallized layer becomes strongly coupled to the solid mantle below and cooling proceeds through bulk convection everywhere. According to Abe (1993, 1997), this was achieved in a few 10 My (**Figure 12**) and sets the initial conditions for secular cooling models of the solid Earth. From the most recent phase diagram (Herzberg and Zhang, 1996; Litasov and Ohtani, 2002), the final rheological transition corresponds to a potential temperature of about 1800 ± 100 K for a mantle composed of dry pyrolite (**Figure 13**).

Recent advances in geochemistry have confirmed the theoretical estimates of Abe (1997). Caro *et al.* (2003) have found evidence that pushes early crust formation as far back as 4.4 Gy. Others have claimed that liquid water was present on Earth's surface at 4.3 Gy (Mojzsis *et al.*, 2001). These studies cannot demonstrate that plate tectonics was already active at such early times, but provide some support for a solid upper mantle.

7.06.6.5 Average Secular Cooling Rate

Subsolidus convection began at a mantle potential temperature of about 1800 ± 100 K, which exceeds the present-day temperature by about 200 K. Even if the timing is not known precisely, this constrains the average cooling rate of the Earth to be about $50\ \mathrm{K\ Gy^{-1}}$. The analysis of Phanerozoic MORBs and Archean MORB-like greenstones due to Abbott *et al.* (1994) leads to the same estimate.

The present-day mantle potential temperature is fixed at 1600 K by a fit to heat flux and bathymetry data regardless of the water content of mantle rocks (McKenzie *et al.*, 2005). If the mantle contained significant amounts of water at the end of the magma ocean phase, however, the phase diagram must be shifted to lower temperatures. One consequence is that the starting potential temperature at the beginning of subsolidus convection was less than the

1800 K estimate given above. In this case, the average cooling rate must be even less than $50\,\mathrm{K\,Gy^{-1}}$.

7.06.6.6 Summary

At the end of accretion and core–mantle separation, a magma ocean probably extended through a large fraction of the silicate Earth. Crystallization of the magma ocean was achieved rapidly and led to a stratified mantle with a solid lower layer and a partially crystallized upper layer. At the start of solid-state mantle convection, upper-mantle temperatures were such that the surficial partially molten region had a solid fraction of about 60%. This sets the initial temperature of the solid Earth to a value which is about 200 K higher than the present.

7.06.7 Thermal Evolution Models

7.06.7.1 The Urey Ratio

The decay time of the bulk radiogenic heat production, which is such that heat production decreases by a factor e and which is the weighted average of the individual decay times of the four relevant isotopes (**Table 9**), is 3 Gy. Thus over the Earth's history, heat sources have decreased by a factor of about four. The efficiency of Earth's convective engine in evacuating heat generated by radioactive decay is commonly measured by the Urey ratio, *Ur*, which is the ratio of heat production over heat loss:

$$Ur = \frac{\int_V H\,\mathrm{d}V}{\int_A \mathbf{q}\cdot\mathbf{n}\,\mathrm{d}A} \qquad [58]$$

To calculate this ratio, we do not take continental heat sources into account because they are stored in the continental lithosphere and hence are not involved in mantle convection. Using the data of **Table 11**, we find that $Ur = 0.33$, with a total range of 0.21–0.49.

The heat budget of **Table 11** allows calculation of the present-day cooling rate. Secular variations of basalt compositions and consideration of initial thermal conditions provide constraints on the total temperature drop over Earth's history and hence on the average cooling rate. Thus, physical models are not needed to determine how the Earth has cooled down. Instead, the data allow a test of our understanding of mantle convection processes. Available constraints on the cooling rate can be turned into one for the rate of heat loss. The global heat balance reads as

$$M\langle C_p\rangle \frac{\mathrm{d}T}{\mathrm{d}t} = -Q + H \qquad [59]$$

where M is the mass of the Earth and $<C_p>$ an 'effective' heat capacity which accounts for the isentropic variation of temperature with depth. Integrating over the age of the Earth, one deduces that

$$\frac{\bar{Q} - \bar{H}}{Q - H} = \frac{(\mathrm{d}T/\mathrm{d}t)_{av}}{\mathrm{d}T/\mathrm{d}t} \qquad [60]$$

where $\bar{Q}$ and $\bar{H}$ are the time-averaged values of heat loss and heat production and $(\mathrm{d}T/\mathrm{d}t)_{\mathrm{av}}$ is the average cooling rate. The cooling rate has an average value of about $50\,\mathrm{K\,Gy^{-1}}$ and a larger present-day value (about $120\,\mathrm{K\,Gy^{-1}}$). Thus, the ratio in eqn [60] is less than 1 and probably as small as 0.4. This implies that the rate of heat loss varies less rapidly than that of heat production.

7.06.7.2 Parametrized Cooling Models

In steady-state well-mixed homogeneous convective layers with constant physical properties, the heat flux through the top boundary is a function of the Rayleigh number, which itself depends on the temperature difference across the layer (e.g., Schubert and Young, 1976; Sharpe and Peltier, 1978; Davies, 1980, *see also* Chapter 9.08). A very robust scaling law relates the dimensionless heat flux (i.e., the Nusselt number) to the Rayleigh number:

$$Nu = \frac{Q/A}{kT/D} = C_1 Ra^{\beta} \qquad [61]$$

where C_1 is a proportionality constant, Q/A the heat flux, T the temperature difference across the layer, D the layer thickness, and Ra the Rayleigh number:

$$Ra = \frac{g\alpha T D^3}{\kappa \nu_{\mathrm{M}}} \qquad [62]$$

where $\nu_M = \mu_M/\rho$ is the kinematic viscosity. This relationship can be turned into an equation for heat loss Q of the form:

$$Q = C_2 T^{1+\beta} \nu_{\mathrm{M}}^{-\beta} \qquad [63]$$

where the constants C_2 and β are obtained from boundary-layer theory as well as laboratory experiments (Howard, 1964; Turcotte and Oxburgh, 1967; Olson, 1987). This relationship is valid if, and only if, instability always occurs in the same conditions, for

example, when a Rayleigh number defined locally in the boundary layer exceeds a critical value. Typically, $\beta = 1/3$, such that heat loss is governed solely by local instabilities of the upper boundary layer. The value of constant C_2, but not that of exponent β, is set by the instability threshold and hence depends on the length of the convective cell (Olson, 1987; Grigné *et al.*, 2005). Cooling models of this kind have been termed 'parametrized' because they collapse all the physics of mantle convection into a single equation involving only temperature and two parameters, C_2 and β.

Further developments involved temperature-dependent physical properties. The key principle is that a hot layer evolves much more rapidly than a cold one because of the strong dependence of viscosity on temperature. One can approximate an Arrhenius law for viscosity by an equation of the form $\nu = \nu_0 (T/T_0)^{-n}$, with $n \sim 35$, which is valid for $T \sim T_0$ (Davies, 1980; Christensen, 1985). The thermal evolution equation then takes the following form:

$$M\langle C_p\rangle \frac{\mathrm{d}T}{\mathrm{d}t} = -Q_0 \left(\frac{T}{T_0}\right)^{1+\beta(1+n)} + H(t) \qquad [64]$$

where Q_0 is the heat loss at the reference potential temperature T_0. Temperature changes in the Earth are small compared to the absolute temperature (i.e., $\approx$200 K for a present-day temperature of $\approx$1600 K). One may thus linearize the above equation by considering the temperature variations around T_0:

$$T = T_0 + \Theta \quad \text{with} \quad \Theta \ll T_0 \qquad [65]$$

$$M\langle C_p\rangle \frac{\mathrm{d}\Theta}{\mathrm{d}t} = -Q_0 \left[1 + \frac{\Theta}{T_0}(1 + \beta + \beta n)\right] + H(t) \qquad [66]$$

The heat sources can be approximated as decreasing exponentially with time, $H(t) = H_0 \times \exp(-t/\tau_r)$, where $\tau_r \approx 3000$ My. The solution of eqn [66] is

$$\Theta = \Theta_0 \times \exp(-t/\tau_p) + \frac{Q_0 \tau_p}{M\langle C_p\rangle}\left(\exp(-t/\tau_p) - 1\right) + \frac{H_0 \tau_p \tau_r}{M\langle C_p\rangle(\tau_r - \tau_p)}\left(\exp(-t/\tau_r) - \exp(-t/\tau_p)\right) \qquad [67]$$

where the relaxation time constant τ_p is given by

$$\tau_p = \frac{M\langle C_p\rangle T_0}{(1 + \beta + \beta n) Q_0} \qquad [68]$$

Using standard values for the parameters and variables involved, $n = 35$, $\beta = 1/3$, $M = 6 \times 10^{24}$ kg, $Q_0 = 30$ TW, $T_0 = 1300$ K (the temperature jump across the boundary layer is the relevant parameter here) and $\langle C_p\rangle = 1200\,\mathrm{J\,kg^{-1}K^{-1}}$, this thermal adjustment timescale is about 800 My. From eqn [67], the Urey ratio as a function of time can be obtained. For $t \gg \tau_p$, the Urey ratio tends to a constant value $(\tau_r - \tau_p)/\tau_r \approx 0.75$. This is larger than observed.

A key point is that, after about 2 Gy, model predictions are not sensitive to the initial conditions, which has two implications. One is that failure of a model to reproduce the present-day Urey ratio cannot be blamed on the poorly known initial condition. The other implication is that 'backward' thermal calculations starting from the present become unreliable for old ages.

Parametrized models for whole-mantle convection lead to present-day values of the Urey ratio that are larger than 0.7, significantly more than observed. This reveals a fundamental flaw in the model setup. In order to meet the constraint of the Urey ratio, one must increase the adjustment time of mantle convection. One option is to appeal to a layered mantle (McKenzie and Richter, 1981). Another option is to make the bulk rate of heat loss less sensitive to temperature, which may be achieved by decreasing the value of exponent β in eqn [68]. According to Christensen (1984, 1985), this may be attributed to the temperature dependence of viscosity. For very large variations of viscosity, however, convection occurs in the stagnant lid regime (e.g., Ogawa *et al.*, 1991; Davaille and Jaupart, 1993; Solomatov and Moresi, 1997). In this case, plate tectonics is shut off, which is not a satisfactory solution. There may be an intermediate regime with subduction of the very viscous lid, such that $\beta = 0.293$ (Solomatov and Moresi, 1997), but this β-value is too large to meet the constraint of the Urey ratio. Another mechanism that has been invoked for decreasing the exponent β is the resistance to bending of the plate at subduction zones which, according to Conrad and Hager (1999), should lead to $\beta \sim 0$. Following a similar idea, Korenaga (2003) added the effect of temperature on the depth of melting, hence the thickness of the crust, as discussed by Sleep (2000). He proposed a negative value of β. Negative values of β would solve the problem at hand but there is no evidence that resistance to bending actually limits subduction on Earth.

This discussion shows that simple convection models cannot account for the observations. We now discuss how to properly account for the behavior of Earth's convective system. We discuss the relevance of heat loss 'parameterizations' to the true

Earth and evaluate whether the present-day heat balance is representative of secular cooling models which, by construction, deal only with long-term temperature changes.

7.06.7.3 The Peculiarities of Mantle Convection: Observations

The Earth's convecting mantle exhibits several features which make it very distinctive. One of them is the triangular age distribution of the seafloor, which occurs because subduction affects all ages with the same probability (**Figure 7**; Parsons, 1982). This is at odds with other convecting systems as well as with the parametrized schemes discussed above. We show in Appendix 8 the age distribution at the upper boundary of several convective systems. None of them resembles that of Earth, which illustrates current limitations in reproducing mantle convection processes.

A few other peculiar features of mantle convection are worth mentioning. Heat loss is unevenly distributed at the surface. The Pacific Ocean alone accounts for almost 50% of the oceanic total, and 34% of the global heat loss of the planet. This is due in part to the large area of this ocean and in part to its high spreading rate. Oceanic plates are transient, such that changes of oceanic heat loss may occur when a new ridge appears or when one gets subducted. For example, the heat flux out of the Atlantic Ocean is about 6 TW, 17% of the oceanic total (Sclater *et al.*, 1980). This ocean has almost no subduction and started opening only at 180 My. At that time, the generation of a new mid-ocean ridge led to an increase of the area of young seafloor at the expense of old seafloor from the other oceans, and hence to enhanced heat loss. The triangular age distribution may well be a consequence of this relatively recent plate reorganization. From the standpoint of the dynamics of convection, the most challenging features of mantle convection are perhaps the large variations of plate speeds and dimensions. With the small number of plates that are present, averaging values of spreading velocity and plate size may well be meaningless.

Earth's surface is partially covered by continents which have two effects on mantle convection. They do not allow large heat fluxes through them and generate boundaries with complicated shapes that constrain mantle flow. The controls they exert on secular cooling have been investigated by few authors (Lenardic *et al.*, 2005).

7.06.7.4 Convection with Plates

Here, we recapitulate the main physical controls on mantle convection. With rigid plates, several physical mechanisms are involved and it is convenient to use the dissipation equation [28].

For the Earth, the buoyancy flux is due almost entirely to subducting plates and their associated downwelling currents. For a plate going down with velocity U at a trench of length l, the buoyancy flux F_b is:

$$F_b = \rho\alpha g\overline{w_r\theta}\delta_T l = \frac{1}{2}\rho\alpha g U T_M \delta_T l \qquad [69]$$

where $\delta_T = \sqrt{\kappa\tau_m}$ is the thermal boundary-layer thickness. Here, $\delta_T l$ is the cross-sectional area of the plate that goes down into the mantle and the temperature profile through the plate is taken to be linear. Subducted material gets heated by radioactive sources and goes through mantle that is cooling down. Thus, the buoyancy flux is not conserved during descent. For a simple argument, we neglect these effects. In this case, if the plate remains vertical down to the CMB, the bulk buoyancy flux in eqn (28) is

$$\Phi_b = \int_V \rho\alpha g\overline{w_r\theta}\,\mathrm{d}V = \frac{1}{2}\rho\alpha g U T_M \delta_T l D \qquad [70]$$

where D is the mantle thickness.
Viscous dissipation may be written as

$$\phi_v \propto \sigma\frac{U}{\delta_v} \qquad [71]$$

where σ is the deviatoric stress and δ_v the thickness of the momentum boundary layer. For material with viscosity μ_M,

$$\sigma \propto \mu_M\frac{U}{\delta_v} \qquad [72]$$

which implies that $\phi_v \propto U^2$. For cell length L, balancing the total dissipation with the bulk buoyancy flux leads to

$$U \propto \frac{\rho g\alpha T_M \delta_T D}{\mu_M}\frac{\delta_v}{L} \qquad [73]$$

For large values of the Prandtl number, the momentum boundary layer is spread over large distances. For cellular convection, it extends throughout the convecting layer, such that $\delta_v \propto D$. In the Earth, however, convection is driven mostly by cooling from above, such that velocities are highest in downwellings and low in large-scale upward return flow. In

this case, viscous dissipation occurs mostly in the vicinity of downwellings, such that δ_v may not scale with the depth of the layer (Jarvis and McKenzie, 1980).

In the Earth, subduction involves cold and stiff plates, such that bending at subduction zones induces large amounts of dissipation (Conrad and Hager, 1999). Assuming that the plate behaves viscously, the rate of dissipation is

$$\phi_{\mathrm{P}} \propto \mu_{\mathrm{P}} \frac{\left(U\delta_{\mathrm{T}}\right)^2}{R_{\mathrm{p}}^2} \qquad [74]$$

where μ_{P} is the effective viscosity of the plate and R_{p} its radius of curvature. Note that this dissipation rate is also proportional to U^2, as for internal viscous dissipation. For an estimate of the bulk dissipation rate due to bending, one must specify the volume of plate that gets deformed. With this extra dissipation mechanism, one obtains another equation for velocity U.

Another equation is required to specify heat loss. For the sake of simplicity, we use a half-space cooling model because the predicted heat flux differs from observations at old ages only, and this difference represents a small fraction of the total: changing heat loss through seafloor older than 80 My by 30% (an overestimate) impacts the total heat loss value by only 6%. Thus, we assume that $q = kT_{\mathrm{M}}/\sqrt{\pi\kappa\tau}$. For a rectangular plate of length L and width l, heat loss Q_{P} is

$$Q_{\mathrm{P}} = \int_A q\,\mathrm{d}A = \int_0^{\tau_{\mathrm{m}}} qlU\,\mathrm{d}\tau = 2\frac{k}{\sqrt{\pi\kappa}} T_{\mathrm{M}} Ul\sqrt{\tau_{\mathrm{m}}} \qquad [75]$$

where τ_{m} is the maximum plate age. The rate of heat loss over the total area of the plate, $A_{\mathrm{P}} = Ll$, is

$$Q_{\mathrm{P}} = 2A_{\mathrm{P}} \frac{kT_{\mathrm{M}}}{\sqrt{\pi\kappa\tau_{\mathrm{m}}}} \qquad [76]$$

Note that this result was derived directly from [75] independently of eqn [73] for velocity U, that is, without involving dynamical constraints. All the dynamical information needed is in τ_{m}, which has not been determined yet.

All the key variables of convection, heat loss Q_{P}, velocity U, and plate length L, depend on τ_{m}. To obtain a closure equation for this variable, a widely used argument has been that the thermal boundary layer becomes unstable when a local Rayleigh number exceeds a threshold value such that

$$Ra_\delta = \frac{\rho g\alpha T_{\mathrm{M}}\delta_{\mathrm{T}}^3}{\kappa\mu_{\mathrm{P}}} = Ra_{\mathrm{c}} \qquad [77]$$

where Ra_{c} is some critical value. This leads to the 'parametrized' model equation with $\beta = 1/3$, which is not satisfactory. A key piece of physics is missing, which prevents us from specifying how τ_{m} changes when the mantle cools down. When the Earth was hotter, decompression melting proceeded to larger melt fractions and hence to larger amounts of depletion. This is demonstrated by secular changes of the composition of MORBs (Abbott *et al.*, 1994). Larger degrees of melting enhance dehydration of the residual solid and hence generate stiffer lithospheric plates. μ_{P}, the plate effective viscosity, increases with increasing temperature and hence was larger in the past than today (Korenaga, 2006). How this affects τ_{m} or L is not clear, however. One might imagine for example that higher intrinsic stiffness of lithospheric material gets compensated because subduction involves younger and hence thinner plates such that the total dissipation due to bending did not change much.

7.06.7.5 Cooling through the Ocean Floor

With the physical arguments developed above, one runs into two different types of difficulties when applying them to the Earth. Firstly, one must specify either the plate length L or the maximum plate age τ_{m}. Secondly, one must go from a single convection cell to several cells with different characteristics. Here, we derive several useful relationships that are independent of dynamical arguments.

A successful physical model must rely on accurate equations for the rate of heat loss and for the bulk buoyancy flux. Let us consider a thermal balance for the volume encompassing the thermal boundary layer below Earth's surface:

$$\int_{A^-} \rho C_p \overline{w_{\mathrm{r}}\theta}\,\mathrm{d}A = \int_{A^+} \mathbf{q}\cdot\mathbf{n}\,\mathrm{d}A \qquad [78]$$

where A^+ is the upper surface in contact with the hydrosphere and A^- lies at the base of the thermal boundary layer. This equation states that the subducting plates carry the energy deficit that has been accumulated by cooling to the sea. From this relation, we deduce that the bulk buoyancy flux is proportional to the rate of heat loss:

$$\Phi_{\mathrm{b}} = \frac{\alpha g}{C_p} QD \qquad [79]$$

Thus, accurate parametrizations of the buoyancy flux and of the rate of heat loss are equivalent.

We derive a general equation for heat loss on Earth. Because crustal radioactivity accounts for a large fraction of the continental heat flux, the basal heat flux into continents, out of the convecting

mantle, is very small. We consider that continental radioactivity plays no dynamic role and thus equate the heat loss of the Earth to that of the oceans. We shall again use the half-space cooling model which is sufficiently accurate. The distribution of sea floor age f in function of dimensionless age τ/τ_m is such that

$$\frac{dA}{d\tau} = C_A f\left(\frac{\tau}{\tau_m}\right) \quad [80]$$

Where C_A is the plate accretion rate and with $f(0) = 1$. Using the half-space expression [35], we obtain the total oceanic heat loss:

$$Q_{oc} = A_o \frac{kT_M}{\sqrt{\pi\kappa\tau_m}} \frac{\int_0^1 \frac{f(u)}{\sqrt{u}} du}{\int_0^1 f(u) du} = A_o \frac{kT_M}{\sqrt{\pi\kappa\tau_m}} \lambda(f) \quad [81]$$

Where A_o is the total ocean surface and $\lambda(f)$ a coefficient which depends on the dimensionless age distribution. This equation has the same form as eqn [76] derived above but it includes a new variable, the dimensionless age distribution. For the present-day triangular age distribution

$$Q_{oc} = \frac{8A_o}{3} \frac{kT_M}{\sqrt{\pi\kappa\tau_m}} \quad [82]$$

Even though we have not used any dynamical argument to derive the heat loss equation, we can relate changes of heat loss to changes of spreading rate. The total oceanic area is

$$A_o = C_A \tau_m \int_0^1 f(u) du \quad [83]$$

If we assume that the oceanic area and the age distribution remain constant, changes of heat loss imply changes of τ_m, which in turn imply changes of C_A, the rate of plate generation.

The oceanic heat loss can be equated with little error to the convective heat loss on Earth. Thus eqns [79], [81], and [83] provide the most compact description of the physical controls on cooling. They avoid the problem of defining an 'average' plate with average velocity and length. They say nothing, however, about the maximum plate age τ_m.

7.06.7.6 Vagaries of Seafloor Spreading

In eqn [81], one coefficient that can vary significantly over short time scales is $\lambda(f)$, which depends on the dimensionless distribution of seafloor ages. Cogné and Humler (2004) have attempted to calculate spreading rates in the past. The last 180 My have seen the closure of the Tethys Ocean and the subduction of several ridges in the paleo-Pacific Ocean (Engebretson *et al.*, 1984). Accounting for those, the total seafloor generation rate did not vary significantly over the last 180 My (**Figure 14**). Fluctuations in seafloor spreading may occur on a larger timescale. Subduction of young seafloor occurs mostly at the edge of continents and may be due to the complex geometry of the ocean–continent boundaries. With all continents assembled in a single landmass, the large continuous oceanic area imposes less constraints on spreading and subduction. In other words, the present-day distribution of subduction zones may be a transient feature associated with the breakup of Gondwana. The assembly and breakup of supercontinents occur over some characteristic time τ_W. Allègre and Jaupart (1985) have related this time to the 'mean free path' of continents at Earth's surface, such that continents sweep the whole surface of the Earth and necessarily run into one another. They obtained $\tau_W \approx 400$ My for present-day spreading rates and distribution of continents, which is less than the thermal adjustment time. τ_W varies as a function of continental area and drift velocity and has probably been larger in the past when continents accounted for a smaller fraction of Earth's surface. Geological data

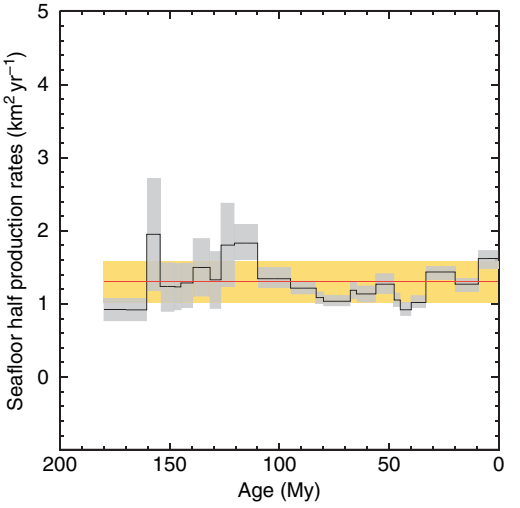

Figure 14 Variation of seafloor spreading rates over the last 180 My accounting for oceanic ridges that got subducted in the Pacific and Tethys Oceans. The black line is the half spreading rate and the gray area represent the uncertainty. The red line is the average value. Adapted from Cogné J-P and Humler E (2004) Temporal variation of oceanic spreading and crustal production rates during the last 180 My. *Earth and Planetary Science Letters* 227: 427–439.

support such an increase of τ_W (Hoffman, 1997). Note that this observation runs against the intuitive notion that plates moved faster in the past. If the rate of heat loss of the Earth depends on the distribution of continents, it oscillates on a timescale τ_W over a long-term decreasing trend. We now attempt to estimate how large these oscillations can be.

Convective systems that are not constrained by lateral boundaries lead to age distributions that are almost rectangular (see Appendix 8). In this case, subduction occurs at the same age everywhere and the parameter $\lambda(f) = 2$, which is 25% less than the value for the triangular distribution (8/3). This changes the estimated oceanic heat loss by about 8 TW, which amounts to about half of the difference between present heat loss and heat production in the mantle (**Table 11**). Assuming for the sake of argument that the life time of a supercontinent is as long as the Wilson cycle and that these cycles are accompanied by changes of the age distribution of seafloor, the time-averaged oceanic heat loss could be 12.5% (i.e., 4 TW) less than the estimate of **Table 11**. A similar result was obtained by Grigné *et al.* (2005) using numerical models with many interacting convection cells of variable wavelength.

We have so far assumed that the total area of oceans remains constant. Over a few tens of million years, changes of oceanic area that are not related to rigid plate tectonics may occur, however, due to zones of diffuse deformation. Such zones are found in both oceans and continents and presently account for ≈15% of Earth's surface (Gordon, 2000). In continents, extension occurs at the expense of oceans whereas shortening increases the oceanic area. These zones are usually very active and characterized by high heat flux, as in the Basin and Range Province, for example. Assuming that the average heat flux over such zones is equal to that in the Basin and Range (105 mW m^{-2}), the net effect on the global heat loss is small because this heat flux is approximately the average oceanic one.

The two types of short-lived transient phenomena that we have identified, changes of the age distribution of seafloor and diffuse deformation, may induce fluctuations of heat loss on the order 4 TW. This is not sufficient to explain the difference between the present and average values of the secular cooling rate.

Yet another type of transient may be due to enhanced or subdued hot-spot activity. Assessing the magnitude of the implied heat loss variations is difficult from the geological record and is best achieved through consideration of thermal boundary layers.

7.06.7.7 Heat Flow Out of the Core

The discussion above has made no distinction between mantle and core. Labrosse (2002) has argued that the integrated heat flux at the CMB is mostly due to the spreading of cold subducted material. If this is correct, the value of this heat flux varies in tandem with the surface heat flux. Let us sketch some implications of such a proposition.

One possibility is that the core cools at the same rate as the mantle. Such a slow variation is compatible with thermal evolution models of the Earth's core, provided that ohmic dissipation increased by a factor of four when the inner core started crystallizing (Labrosse, 2003). It is likely, however, that the core heat loss fluctuates over timescales that are short compared to the age of the Earth, much as the surface heat flux. The core loses heat to an unstable boundary layer which grows at the base of the mantle. Compared to the upper boundary layer of mantle convection, this layer involves a smaller heat flux. For the sake of discussion, let us estimate the energy contained in the D″ layer, taken here as the lower thermal boundary layer of the mantle. The temperature difference across this 200 km thick layer can be estimated to be about $\delta T = 1000$ K (e.g., Lay *et al.*, 1998). Assuming a linear temperature profile, the energy content of this layer is

$$U = \rho C_P 4\pi b^2 b \frac{\delta T}{2} \simeq 7.5 \times 10^{28}\,\mathrm{J} \qquad [84]$$

with $b = 3480$ km the radius of the CMB, $\rho \simeq 5 \times 10^3$ kg m^{-3} density, $h = 200$ km, and $C_P = 1000$ J kg^{-1} K^{-1}. This energy is transferred to the mantle when the boundary layer goes unstable. The time scale is that of conductive thickening of the layer, that is $h^2/\pi\kappa \simeq 400$ My for $\kappa = 10^{-6}$ m^2 s^{-1}. Dividing the total energy given by eqn [84] by this timescale predicts a heat flux variation of 5 TW. This accounts for a large fraction of the total heat flux across the CMB and has important implications for the dynamo.

Further changes of core heat loss may be due to variations of the mass flux of downwellings, which may occur due to plate reorganizations and supercontinent cycles.

7.06.7.8 Summary

Theoretical models for the cooling of the Earth rely on theory and measurements in convective systems that do not possess one key feature of

the present plate tectonic regime, which is that ocean floor of all ages gets subducted. The present imbalance between heat loss and heat production may be due in part to a particular convection phase with enhanced heat loss compared to the long-term evolution.

The main stumbling block in developing a realistic secular cooling model is our poor understanding of the subduction process. This hampers our ability to properly parametrize plate velocity and heat loss. Specifically, scaling arguments for mantle convection depend on only one parameter, τ_m, the maximum age of a plate at Earth's surface. Plate velocity U and plate length L, as well as the rate of heat loss depend on how this variable changes with time. Alternatively, past mantle temperature changes that are documented in a variety of ways provide powerful constraints for convection models. They imply that, in the past, the bulk rate of heat loss has changed less rapidly than heat production.

7.06.8 Conclusions

Studies of the thermal evolution of the Earth are as old as geophysics and remain central to geology, for they deal with the energy that drives all geological processes. The heat budget of the mantle can be established with a reasonable accuracy (≈20%) thanks to tremendous improvements in our knowledge of physical properties and data coverage. The Urey number is the ratio of heat production to heat loss, two imperfectly known quantities whose estimates are summarized in **Table 11**. Our current estimates for Urey number are in the range 0.2–0.5, which rules out early parametrized cooling models. This may be explained by the particular behavior of oceanic plates, which are subducted at all ages. This feature seems to be unique among convective systems of all kinds. It now appears that heat loss does not follow the decay of radiogenic heat production and that the time lag is on the order of the age of the Earth (Section 7.06.7.1).

The present mantle energy budget implies a secular cooling rate in the range of 50–190 K Gy^{-1}. Over long timescale, the average value for the cooling rate estimated from geological constraints appears to be at the very low end of this range (50 K Gy^{-1}). There is no reason to assume that the cooling rate has remained constant through time. Both geological data and physical constraints on the thermal structure of the early Earth indicate that the cooling rate increased as the planet got older (Section 7.06.7.6). Independent constraints on cooling rate come from considerations of early Earth evolution. Plate tectonics is a regime of mantle convection attainable only in a state of subsolidus rheology, that is with at most 40% melt. The most recent phase diagrams for the mantle (Zerr *et al.*, 1998; Litasov and Ohtani, 2002, *see* Chapter 2.18) indicate that this threshold is reached when the potential temperature is about 200 K higher than the present. If plate tectonics has been operating since the end of the magma ocean, the total amount of cooling is constrained and the average cooling rate cannot be more than about 50 K Gy^{-1}.

Appendix 1: Contraction of Earth due to Secular Cooling

The planet contracts as it cools down. This induces changes of gravity which themselves induce changes of pressure and density. Here, we derive an approximate solution for a homogeneous planet in order to demonstrate that the most important effect is that of temperature.

Assuming spherical symmetry, governing equations for a spherical planet are as follows:

$$\frac{1}{r^2}\frac{\mathrm{d}}{\mathrm{d}r}\left(r^2 g\right) = 4\pi G\rho \qquad [85]$$

$$\frac{\mathrm{d}P}{\mathrm{d}r} = -\rho g \qquad [86]$$

where G is the gravitational constant and P pressure, and where all variables depend on radial distance r only. From the equation of state, we deduce that

$$\frac{\mathrm{d}\rho}{\mathrm{d}r} = \frac{\mathrm{d}\rho}{\mathrm{d}P}\frac{\mathrm{d}P}{\mathrm{d}r} = \frac{\rho}{K_s}\frac{\mathrm{d}P}{\mathrm{d}r} \qquad [87]$$

$$= -\frac{\rho^2 g}{K_s} \qquad [88]$$

where K_s is the isentropic bulk modulus. For simplicity, the bulk modulus is assumed to be constant. In order to make the equations dimensionless, we use radius R as length-scale and density at the top (we shall define it more precisely later) ρ_T as density-scale. From those, we derive a gravity scale

$$[g] = G\rho_T R \qquad [89]$$

Equations can now be written using dimensionless variables:

$$\frac{1}{r^2}\frac{\mathrm{d}}{\mathrm{d}r}\left(r^2 g\right) = 4\pi\rho \qquad [90]$$

$$\frac{\mathrm{d}\rho}{\mathrm{d}r} = -\epsilon\rho^2 g \qquad [91]$$

where ϵ is a dimensionless number which provides a measure of the magnitude of density changes due to pressure:

$$\epsilon = \frac{\rho_T[g]R}{K_\mathrm{s}} = \frac{G\rho_\mathrm{T}^2 R^2}{K_\mathrm{s}} \qquad [92]$$

In this problem, we consider the cooling of the Earth's mantle, where the radial temperature profile is almost isentropic. We neglect the upper thermal boundary layer which does not contribute much to the total mass and energy. Thus, reference density ρ_T is the mantle density at the atmospheric pressure, that is, at the potential temperature of the isentropic radial profile. For what follows, the key point is that ρ_T does not depend on pressure, which varies in the planet interior during contraction. For $\rho_T = 3.3\times10^3\,\mathrm{kg\,m^{-3}}$, $\mathrm{R} = 6370\,\mathrm{km}$ and a value of 150 GPa for K_s, $\varepsilon \approx 0.2$. This is small and we expand all the variables in series of ϵ:

$$\rho = \rho_o + \epsilon\rho_1 + \cdots \qquad [93]$$

$$g = g_o + \epsilon g_1 + \cdots \qquad [94]$$

We find that

$$\rho_o = 1 \qquad [95]$$

$$\rho_1 = -\frac{4\pi}{6}\rho_o^3\left(r^2 - 1\right) \qquad [96]$$

$$g_o = \frac{4\pi}{3}\rho_o r \qquad [97]$$

$$g_1 = \frac{16\pi^2}{90}\rho_o^3 r\left(5 - 3r^2\right) \qquad [98]$$

We then calculate the mass of the planet to first order in ϵ:

$$M = \frac{4}{3}\pi\rho_\mathrm{T}R^3\left(1 + \frac{4\pi}{15}\epsilon\right) = \frac{4}{3}\pi\rho_\mathrm{T}R^3\left(1 + \frac{4\pi}{15}\frac{G\rho_\mathrm{T}^2R^2}{K_\mathrm{s}}\right) \qquad [99]$$

Writing that mass is conserved when ρ_T and R change, we obtain

$$\frac{\Delta R}{R} = -\frac{1}{3}\frac{\Delta\rho_\mathrm{T}}{\rho_\mathrm{T}}\left(1 + \frac{16\pi}{45}\frac{G\rho_\mathrm{T}^2R^2}{K_\mathrm{s}}\right) \qquad [100]$$

By definition, surface density ρ_T depends on temperature only, such that

$$\frac{\Delta\rho_\mathrm{T}}{\rho_\mathrm{T}} = -\alpha\Delta T \qquad [101]$$

where α is the thermal expansion coefficient. The end result is therefore

$$\frac{\Delta R}{R} = \frac{\alpha\Delta T}{3}\left(1 + \frac{16\pi}{45}\frac{G\rho_\mathrm{T}^2R^2}{K_\mathrm{s}}\right) \qquad [102]$$

This shows that contraction is enhanced by the change in gravity field and also that the correction to the temperature effect is small. An exact calculation involving a pressure-dependent bulk modulus would not alter this conclusion.

Appendix 2: Gravitational Energy Changes

Here, we present a demonstration for changes of the bulk gravitational energy which was made by Paul Roberts (personal communication). For a sphere of uniform density and radius R,

$$E_\mathrm{g} = -\frac{16\pi^2}{15}G\rho^2R^5 \qquad [103]$$

For a contracting object with moving material boundaries, it is convenient to employ Lagrangian variables. Because of mass conservation, the most convenient variable is the mass in a sphere of radius r:

$$M(r) = 4\pi\int_0^r \rho(r)r^2\,\mathrm{d}r = \int_0^r \rho(r)\mathrm{d}V \qquad [104]$$

Thus,

$$g(r) = \frac{-GM(r)}{r^2} \qquad [105]$$

The gravitational energy in a material volume bounded by spheres of radii r_1 and r_2 is

$$E_{12} = +\int_{r_1}^{r_2}\rho g r\,\mathrm{d}V = +\int_{M_1}^{M_2} rg\,\mathrm{d}M = +\int_{M_1}^{M_2}\frac{GM}{r}\mathrm{d}M \qquad [106]$$

The Lagrangian derivative is easily calculated using the variable M:

$$\frac{\mathrm{d}E_{12}}{\mathrm{d}t} = \int_{M_1}^{M_2}\frac{\mathrm{d}r}{\mathrm{d}t}\frac{GM}{r^2}\mathrm{d}M \qquad [107]$$

For this calculation, the velocity field is limited to contraction, such that $\mathrm{d}r/\mathrm{d}t = v_c$. Thus

$$\frac{\mathrm{d}E_{12}}{\mathrm{d}t} = \int_{M_1}^{M_2} v_c \frac{GM}{r^2}\mathrm{d}M = -\int_{r_1}^{r_2} \rho(\mathbf{v_c}\cdot\mathbf{g})\mathrm{d}V \qquad [108]$$

which is the integral form of eqn [17] in the main text.

Appendix 3: Viscous Dissipation

Here, we derive an equation for viscous dissipation which, by definition, involves deviatoric stresses and hence departures from hydrostatic equilibrium in the momentum equation. For convection in the solid Earth, inertial terms can be neglected in the momentum balance, with the consequence that changes of kinetic energy are also negligible in the mechanical energy balance [10]. Subtracting the hydrostatic balance [14] from the momentum balance, we get

$$0 = -\nabla(\delta p) - \nabla\cdot\boldsymbol{\sigma} + \delta\rho\mathbf{g} \qquad [109]$$

where δ_p and δ_ρ are deviations from the azimuthal averages of pressure and density, respectively, and where we have neglected perturbations to the gravity field, which only appear in second-order terms. Introducing the temperature perturbation, θ, the density perturbation is obtained by a Taylor expansion about the mean:

$$\delta\rho = \left(\frac{\partial\rho}{\partial p}\right)_a \delta p + \left(\frac{\partial\rho}{\partial T}\right)_a \theta \qquad [110]$$

where derivatives are taken along the azimuthally averaged density profile. Introducing the thermal expansion coefficient, this can be recast as

$$\delta\rho = \frac{\partial\bar{\rho}/\partial r}{\partial\bar{p}/\partial r}\delta p - \bar{\rho}\alpha\theta \qquad [111]$$

Substituting for the density perturbation in eqn [109] and using the hydrostatic expression for $\partial\bar{\rho}/\partial r$ (eqn [14] of the main text), we get

$$0 = -\nabla(\delta p) - \frac{\partial\bar{\rho}/\partial r}{\bar{\rho}g}\delta p\mathbf{g} - \nabla\cdot\boldsymbol{\sigma} - \bar{\rho}\alpha\theta\mathbf{g} \qquad [112]$$

This can be recast as

$$0 = -\bar{\rho}\nabla\left(\frac{\delta p}{\bar{\rho}}\right) - \nabla\cdot\boldsymbol{\sigma} - \bar{\rho}\alpha\theta\mathbf{g} \qquad [113]$$

From this, we deduce a modified form of the mechanical energy balance:

$$0 = -\bar{\rho}\mathbf{w}\cdot\nabla\left(\frac{\delta p}{\bar{\rho}}\right) - \mathbf{w}\cdot\nabla\cdot\boldsymbol{\sigma} - \bar{\rho}\alpha\theta\mathbf{w}\cdot\mathbf{g} \qquad [114]$$

Integrating this equation over the planet volume yields three separate integrals which are evaluated separately. The first term on the right-hand side yields

$$\begin{aligned}\int_V \bar{\rho}\mathbf{w}\cdot\nabla\left(\frac{\delta p}{\bar{\rho}}\right)\mathrm{d}V &= \int_V \nabla\cdot(\delta p\mathbf{w})\mathrm{d}V - \int_V \frac{\delta p}{\bar{\rho}}\nabla\cdot(\bar{\rho}\mathbf{w})\mathrm{d}V \\ &= \int_A \delta p\,\mathbf{w}\cdot\mathbf{dA} - \int_V \frac{\delta p}{\bar{\rho}}\nabla\cdot(\bar{\rho}\mathbf{w})\mathrm{d}V\end{aligned} \qquad [115]$$

where the first term on the right is zero because the pressure perturbation δp must vanish at Earth's surface where pressure is held constant. From the continuity equation in the anelastic approximation, $\nabla\cdot(\bar{\rho}\mathbf{w}) = 0$ (Braginsky and Roberts, 1995). The second term on the right of the mechanical energy balance [114] yields

$$\begin{aligned}\int_V \mathbf{w}\cdot\nabla\cdot\boldsymbol{\sigma}\,\mathrm{d}V &= \int_V (\mathbf{w}\cdot\nabla\cdot\boldsymbol{\sigma} - \nabla\cdot[\boldsymbol{\sigma}\cdot\mathbf{w}])\mathrm{d}V \\ &\quad + \int_V \nabla\cdot[\boldsymbol{\sigma}\cdot\mathbf{w}]\mathrm{d}V \\ &= \int_V \phi\,\mathrm{d}V + \int_A \mathbf{w}\cdot[\boldsymbol{\sigma}\cdot\mathbf{d}A]\end{aligned} \qquad [116]$$

The last term on the right of this equation is the work of shear stresses at Earth's surface, which is negligible. Using these results, the mechanical energy equation may be reduced to

$$-\int_V \rho\alpha g\overline{w_r\theta}\,\mathrm{d}V + \int_V \bar{\phi}\,\mathrm{d}V = 0 \qquad [117]$$

This equation states that viscous dissipation is balanced by the bulk buoyancy flux and explains why it does not enter the bulk energy balance.

Appendix 4: Half-Space Cooling Model with Temperature-Dependent Properties

The general form of the 1-D heat equation is

$$\rho C_p\frac{\partial T}{\partial\tau} = \frac{\partial}{\partial z}\left(k\frac{\partial T}{\partial z}\right) \qquad [118]$$

where all properties depend on temperature T. In this section, the temperature for the half-space is initially T_M and temperature is set to zero at the surface: $T(z = 0, \tau) = 0$.

For constant physical properties, the temperature for the half-space is given by Carslaw and Jaeger (1959):

$$T(z,\,t) = T_{\mathrm{M}}\mathrm{erf}\left(\frac{z}{2\sqrt{\kappa\tau}}\right) \qquad [119]$$

and the surface heat flux is

$$q(0,\,t) = \frac{kT_{\mathrm{M}}}{\sqrt{\pi\kappa\tau}} \qquad [120]$$

For temperature-dependent properties, Carslaw and Jaeger (1959) introduce the following variable:

$$\theta = \frac{1}{k_0}\int_0^T k\,\mathrm{d}T \qquad [121]$$

where k_0 is thermal conductivity at the reference temperature $T = 0$. The heat equation becomes

$$\frac{1}{\kappa}\frac{\partial\theta}{\partial\tau} = \frac{\partial^2\theta}{\partial z^2} \qquad [122]$$

where κ is the temperature-dependent thermal diffusivity. For the boundary and initial conditions of interest here, this equation can be written in terms of a similarity variable η:

$$\theta(z,\,t) = \Theta(\eta),\ \text{with}\ \eta = z\tau^{-1/2} \qquad [123]$$

$$-\frac{\eta}{2\kappa}\Theta' = \Theta'' \qquad [124]$$

with the following boundary conditions:

$$\Theta(0) = 0,\quad \Theta(\infty) = \Theta_{\mathrm{M}},\quad \Theta'(\infty) = \Theta''(\infty) = 0 \qquad [125]$$

The surface heat flux is thus

$$q = k\frac{\partial T}{\partial z}_{z=0} = k_0\tau^{-1/2}\Theta'(0) \qquad [126]$$

which is of the form $C_Q\,\tau^{-1/2}$ regardless of the specific functional form of ρ, C_{p}, and k. This beautiful result was pointed out first by Lister (1977).

Appendix 5: Plate Models for the Oceanic Lithosphere

For a plate of thickness L initially at temperature T_{M}, with $T(z = 0,\,\tau) = 0$ and $T(z = L,\,\tau) = T_{\mathrm{M}}$, the temperature for $0 < z < L$ is given by

$$\tau(z,\,\tau) = T_{\mathrm{M}} \times\left(\frac{z}{L} + \sum_{n=1}^{\infty}\frac{2}{n\pi}\sin\left(\frac{n\pi z}{L}\right)\exp\left(\frac{-n^2\pi^2\kappa\tau}{L^2}\right)\right) \qquad [127]$$

and the surface heat flux is given by

$$q(0,\,t) = \frac{kT_{\mathrm{M}}}{L}\left(1 + 2\sum_{n=1}^{\infty}\exp\left(\frac{-n^2\pi^2\kappa\tau}{L^2}\right)\right) \qquad [128]$$

which diverges at $\tau = 0$. For $\tau \ll L^2/\kappa$, the heat flux

$$q(0,\,\tau) \approx \frac{kT_{\mathrm{M}}}{\sqrt{\pi\kappa\tau}} \qquad [129]$$

With fixed heat flux at the base, $Q\,(L,\,\tau) = kT_{\mathrm{M}}/L$, the temperature of the plate is given by

$$T(z,\,\tau) = \frac{T_{\mathrm{M}}z}{L} - \frac{4T_{\mathrm{M}}}{\pi}\sum_{n=0}^{\infty}\frac{(-1)^n}{(2n+1)} \times\cos\left(\frac{(2n+1)\pi(z-L)}{2L}\right) \times\exp\left(\frac{-(2n+1)^2\pi^2\kappa\tau}{4L^2}\right) + \frac{8T_{\mathrm{M}}}{\pi^2}\sum_{n=0}^{\infty}\frac{(-1)^n}{(2n+1)^2} \times\sin\left(\frac{(2n+1)\pi z}{2L}\right)\exp\left(\frac{-(2n+1)^2\pi^2\kappa\tau}{4L^2}\right) \qquad [130]$$

and the surface heat flux is given by

$$\frac{q(0,\,t)}{(kT_{\mathrm{M}}/L)} = 1 + 2\sum_{n=0}^{\infty}\exp\left(\frac{-(2n+1)^2\pi^2\kappa\tau}{4L^2}\right) + \frac{4}{\pi}\sum_{n=0}^{\infty}\frac{(-)^n}{(2n+1)}\exp\left(\frac{-(2n+1)^2\pi^2\kappa\tau}{4L^2}\right) \qquad [131]$$

The surface heat flux for these three different boundary conditions are compared in **Figure 15**, with the

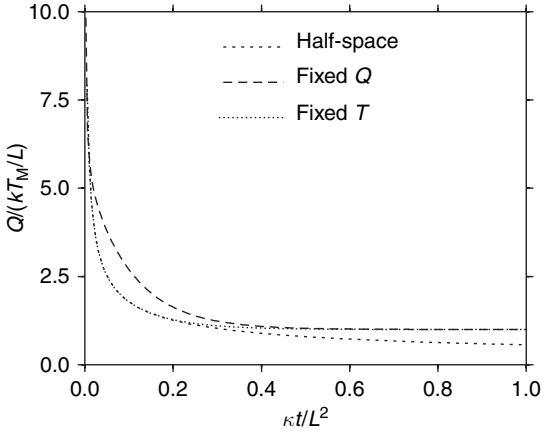

Figure 15 Normalized heat flux as a function of reduced time for different cooling models for the oceanic lithosphere. Length-scale L^* is equal to L, the plate thickness, in the fixed temperature model and to $L/2$ in the fixed flux model. In the half-space model, L^* cancels out. See Appendix 5.

same length scale L for the half-space and the constant-temperature boundary condition and $L/2$ for the heat flux boundary condition.

Appendix 6: Differences Between Estimates of the Energy Budget

Table 13 compares our construction of the mantle energy budget with those proposed by Stacey (1992) and Davies (1999). Although the total energy budget is almost identical, there are major differences in the breakdown of the budget between different items. These differences originate in the various assumptions made as well as in the objectives that are sought. Our estimate uses a slightly different total oceanic area which reflects our better knowledge of continental margins. It also includes the contribution of hot spots, which is not accounted for by bulk lithosphere cooling. Finally, it allows for a small amount of radioelements in the subcontinental lithospheric mantle and takes advantage of our improved constraints on crustal heat production.

For Stacey (1992), the total heat production (27 TW) is significantly higher than the value of 20 TW for BSE, and almost equal to that of the non-depleted chondritic model of Birch (1965). It seems that Stacey has added the crustal heat production to BSE. The core heat loss is low because it is assumed identical to the heat carried by hot spots. Stacey assumed that all the gravitational energy released by thermal contraction (2.1 TW) goes to heat.

In Davies (1999), the secular cooling of the mantle is assumed to be fixed by petrological data and the lower mantle heat production is the variable that is adjusted to balance the budget when all the other variables are fixed. Core cooling is also assumed identical to the total heat flux from hot spots. Upper mantle heat production is known to be low (from samples of the mantle carried to the surface). Lower mantle is assumed to be a mixture between a depleted chondritic composition, which would give 11 TW, and a MORB-like component, which would yield 27 TW. The ratio of those two components is adjusted to balance the budget. (Note that depleted mantle should give only 3 TW, and the MORB-like component seems to have the same heat production as that of chondrites).

The global energy budget of the Earth was one of the arguments used by Kellogg *et al.* (1999) to propose that the lowermost mantle forms a distinct reservoir with chondritic concentration in radioelements, the 'abyssal layer'. The heat production in the depleted MORB mantle (i.e., the source of depleted MORBs) is $\approx 0.6\ \mathrm{pW\ kg^{-1}}$. Assuming that this is representative of the whole mantle, the total mantle heat production would only be 2.5 TW, that is, much less than the 14 TW obtained by removing the crustal heat production from BSE. (Note that Kellogg *et al.* (1999) used 31 TW for the total heat production in a 'chondritic' Earth).

Appendix 7: Average Thermal Structure and Temperature Changes in Upwellings and Downwellings

The reference vertical temperature profile is often called 'adiabatic', which is misleading. Here, we recapitulate the definitions and introduce two different

Table 13 Various estimates of the global budget (TW)

	Stacey (1992)	Davies (1999)[a]	This study
Total heat loss	42	41	46
Continental heat production	8	5	7
Upper mantle		1.3	
Lower mantle		11–27	
Mantle heat production	19	12–28[b]	13
Latent heat – core differentiation	1.2	<1	
Mantle differentiation	0.6	0.3	0.3
Gravitational (Thermal contraction)	2.1		
Tidal dissipation		0.1	0.1
Core heat loss	3	5	8
Mantle cooling	10	9	18
Present Urey ratio	0.64	0.3–0.68	0.21–0.49

[a]Mantle cooling is fixed.
[b]Lower mantle heat production is variable and calculated to fit the mantle cooling rate.

reference temperature profiles. The equation for the entropy per unit mass, s, is

$$\rho T\frac{\mathrm{D}s}{\mathrm{D}t}=\rho C_p\frac{\mathrm{D}T}{\mathrm{D}t}-\alpha T\frac{\mathrm{D}p}{\mathrm{D}t} \quad [132]$$

$$=-\nabla\cdot\mathbf{q}+\phi+H \quad [133]$$

Note that this shows that entropy is not conserved due to irreversible dissipation and radioactive decay. Density changes due to temperature have a small impact on pressure and dynamic pressure variations are small compared to the hydrostatic pressure. Thus,

$$\frac{\mathrm{D}p}{\mathrm{D}t}\approx-\rho gw \quad [134]$$

where w is the radial velocity component.
From these equations, we may deduce the isentropic temperature profile, such that $\mathrm{D}s/\mathrm{D}t=0$. In the interior of the convecting system, far from the upper and lower boundaries, the dominant velocity component is vertical. Assuming steady-state and using eqn [132]:

$$\rho C_p w\frac{\mathrm{d}T_\mathrm{S}}{\mathrm{d}r}=-\alpha T_\mathrm{S}\rho gw \quad [135]$$

where T_S stands for the isentropic temperature profile. Thus,

$$\frac{\mathrm{d}T_\mathrm{S}}{\mathrm{d}r}=-\frac{\alpha g}{C_p}T_\mathrm{S} \quad [136]$$

This is close to the vertical profile of the azimuthally averaged temperature in a steady-state well-mixed convective system with no internal heat production and negligible viscous dissipation.

The isentropic temperature gradient derived above provides a convenient 'reference' profile which illustrates the role of compressibility. However, it is a poor approximation for the temperature path followed by a rising (or sinking) mantle parcel. We may consider for simplicity that such a parcel does not exchange heat with its surroundings, which is a good approximation for the broad return flow away from subduction zones. In this case, we set $\mathbf{q}=0$, use the same approximation as before for pressure and obtain

$$\rho C_p\frac{\mathrm{D}T}{\mathrm{D}t}\approx\rho C_p\left(\frac{\partial T}{\partial t}+w\frac{\partial T}{\partial r}\right)=-(\alpha T)\rho gw+H+\phi \quad [137]$$

The material parcel's temperature changes due to radiogenic heat production and dissipation as well as due to the work of pressure forces. This may be recast as follows:

$$\frac{\partial T}{\partial r}=-\frac{\alpha g}{C_p}T+\frac{1}{w}\left(\frac{\phi+H}{\rho C_p}-\frac{\partial T}{\partial t}\right) \quad [138]$$

where one should note that secular cooling acts in the same direction as internal heat production. The radial temperature gradient from eqn [138] differs from the isentropic value by about 30%. Here, we see the importance of knowing precisely the secular cooling rate $\partial T/\partial t$.

Appendix 8: Seafloor Age Distribution as Seen from Models of Mantle Convection

We present here a few examples of temperature fields obtained in numerical models of convection and compute the seafloor age distribution they would provide for comparison with that of Earth today. In all cases presented, convection is set by imposing a destabilizing temperature difference ΔT between top and bottom and a uniform internal heating rate per unit volume H. This defines two dimensionless parameters (e.g., Sotin and Labrosse, 1999), the Rayleigh number Ra and the dimensionless internal heating rate H^*:

$$Ra=\frac{g\alpha\Delta TD^3}{\kappa\nu_0}\;;\;H^*=\frac{HD^2}{k\Delta T} \quad [139]$$

where D is the thickness of the system and ν_0 is the dynamic viscosity at some reference point. The other symbols are the same as in the rest of the chapter. A third dimensionless number is the Prandtl number $Pr=\nu_0/\kappa$, which is of order 10^{23} in the mantle and is accordingly set to infinity. The viscosity of mantle material is known to vary with temperature, pressure, mineral phase, etc. To reproduce the plate tectonics regime of mantle convection, a complex rheological law must be used (*see* Chapters 7.01 and 7.02). This introduces yet another set of parameters. For example, the pseudoplastic rheology used by Tackley (2000) is defined by an effective viscosity

$$\eta_\mathrm{eff}=\min\left[\eta(T),\frac{\sigma_\mathrm{y}}{2\dot{\varepsilon}}\right] \quad [140]$$

where σ_y is a yield stress and $\dot{\varepsilon}=\sqrt{\dot{\varepsilon}_{i,j}\dot{\varepsilon}_{i,j}}/2$ the second invariant of the strain-rate tensor. Viscosity is temperature dependent:

$$\eta(T) = \exp\left[\frac{23.03}{T+1} - \frac{23.03}{2}\right] \quad [141]$$

This specific rheological law was used to obtain the results of **Figure 3** Grigné *et al.*, 2005).

In numerical models of mantle convection, determining the age of each point at the surface requires extensive calculations with markers. To alleviate this difficulty, we use the fact that the surface heat flux is due to conductive cooling and define a pseudoage as follows:

$$q \propto \frac{1}{\sqrt{\tau}} \quad [142]$$

We thus use heat flux values to determine the age distribution.

The first configuration tested is that of isoviscous Rayleigh–Bénard convection with internal heating. Using a snapshot from Labrosse (2002), we get a distribution of pseudoages that is peaked at low values and exhibits a roughly exponential tail at large ages (**Figure 16**). This reflects that, with a large amount of internal heating, convective flow is dominated by strong cold plumes and passive return flow in most of the interior. There are weak hot plumes in the lower part of the domain but they do not contribute much to the heat flux, in a manner reminiscent of that on Earth. The distribution of surface heat flux is due to the distributed return flow.

A somewhat more realistic model relying on the pseudoplastic rheology has been developed by Grigné *et al.* (2005) and a snapshot is shown in **Figure 3**. The

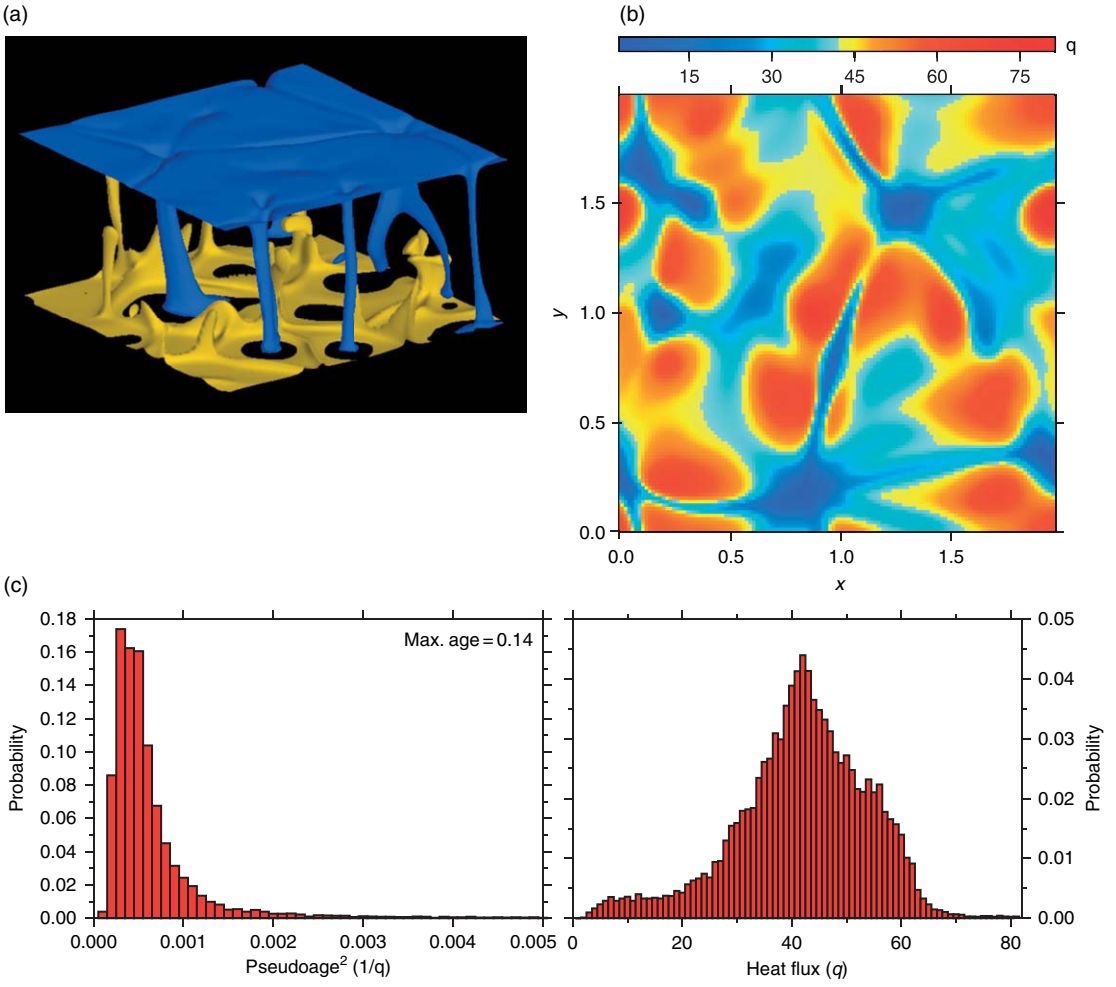

Figure 16 Snapshot of temperature (a), surface heat flux (b), and the corresponding pseudoage distribution (c) in a convection system with a Rayleigh number $Ra = 10^7$ and an internal heating rate $H = 20$. Note that the age distribution is far from that of the Earth's oceans, which is triangular. From the model of Labrosse (2002). See Appendix 8 for details.

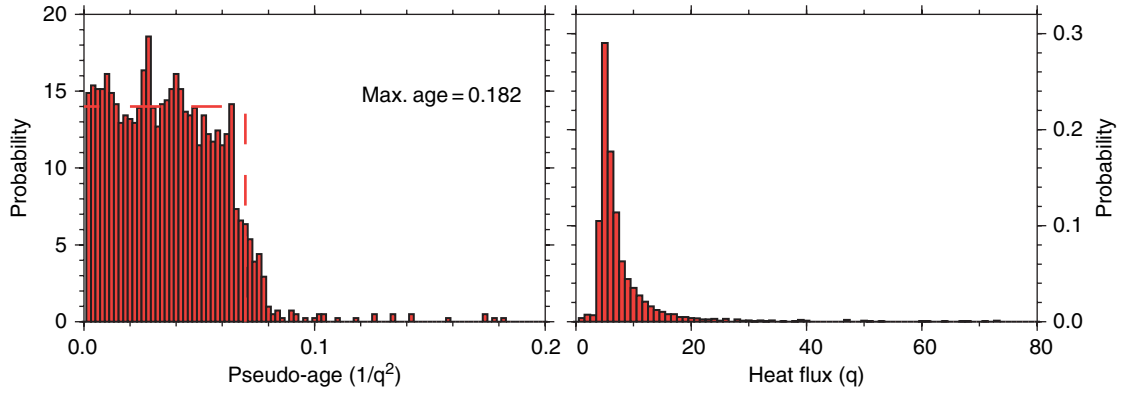

Figure 17 Distribution of surface heat flux (q, right) and pseudoage ($1/q^2$) for a model with plate-like behavior, corresponding to **Figure 3**. The age distribution is close to a rectangular one (dashed line). See Appendix 8 for details. From Grigné C, Labrosse S, and Tackley PJ (2005) Convective heat transfer as a function of wavelength: Implications for the cooling of the Earth. *Journal of Geophysical Research* 110(B03): 409 (doi:10.1029/2004JB003376).

distribution of surface heat flux and pseudoage for this model is given in **Figure 17**. The plate-like behavior is such that the distribution of heat flux is peaked at low values and the pseudoage distribution is approximately rectangular, reflecting the fact that all plates have similar sizes and velocities.

References

Abbott D, Burgess L, Longhi J, and Smith WHF (1994) An empirical thermal history of the Earth's upper mantle. *Journal of Geophysical Research* 99: 13835–13850.

Abe Y (1993) Physical state of the very early Earth. *Lithos* 30: 223–235.

Abe Y (1997) Thermal and chemical evolution of the terrestrial magma ocean. *Physics of the Earth and Planetary Interiors* 100: 27–39.

Alfé D, Gillan MJ, and Price GD (2002) *Ab initio* chemical potentials of solid and liquid solutions and the chemistry of the Earth's core. *Journal of Chemical Physics* 116: 7127–7136.

Allègre CJ and Jaupart C (1985) Continental tectonics and continental kinetics. *Earth and Planetary Science Letters* 74: 171–186.

Ashwal LD, Morgan P, Kelley SA, and Percival J (1987) Heat production in an Archean crustal profile and implications for heat flow and mobilization of heat producing elements. *Earth and Planetary Science Letters* 85: 439–450.

Birch F (1965) Speculations on the thermal history of the Earth. *Bulletin of the Geological Society of America* 76: 133–154.

Birch F, Roy RF, and Decker ER (1968) Heat flow and thermal history in New England and New York. In: An-Zen E (ed.) *Studies of Appalachian Geology*, pp. 437–451. New York: Wiley-Interscience.

Bird RB, Stewart WE, and Lightfoot EN (1960) *Transport Phenomena*. New York: Wiley.

Bodell JM and Chapman DS (1982) Heat flow in the North Central Colorado plateau. *Journal of Geophysical Research* 87: 2869–2884.

Bonneville A, Von Herzen RP, and Lucazeau F (1997) Heat flow over Reunion hot spot track: Additional evidence for thermal rejuvenation of oceanic lithosphere. *Journal of Geophysical Research* 102: 22731–22748.

Brady RJ, Ducea MN, Kidder SB, and Saleeby JB (2006) The distribution of radiogenic heat production as a function of depth in the Sierra Nevada batholith, California. *Lithos* 86: 229–244.

Braginsky SI and Roberts PH (1995) Equations governing convection in Earth's core and the geodynamo. *Geophysical and Astrophysical Fluid Dynamics* 79: 1–97.

Breuer D and Spohn T (1993) Cooling of the Earth, Urey ratios, and the problem of potassium in the core. *Geophysical Research Letters* 20: 1655–1658.

Cameron AGW (2001) From interstellar gas to the Earth–Moon system. *Meteoritics and Planetary Science* 36: 9–22.

Canup RM (2004) Simulations of a late lunar-forming impact. *Icarus* 168: 433–456.

Canup RM and Righter K (eds.) (2000) *Origin of the Earth and Moon*. Tucson, AZ: The University of Arizona Press.

Carlson RL and Johnson HP (1994) On modeling the thermal evolution of the oceanic upper mantle: An assessment of the cooling plate model. *Journal of Geophysical Research* 99: 3201–3214.

Caro G, Bourdon B, Birck J-L, and Moorbath S (2003) ^{146}Sm–^{142}Nd evidence from Isua metamorphosed sediments for early differentiation of the Earth's mantle. *Nature* 423: 428–432 doi:10.1038/nature01668.

Carslaw HS and Jaeger JC (1959) *Conduction of Heat in Solids* 2nd edn. Oxford (UK): Clarendon Press.

Cermak V and Bodri L (1986) Two-dimensional temperature modelling along five East-European geotraverses. *Journal of Geodynamics* 5: 133–163.

Chapman DS and Pollack HN (1974) 'Cold spot' in West Africa: Anchoring the African plate. *Nature* 250: 477–478.

Christensen UR (1984) Heat transport by variable viscosity convection and implications for the Earth's thermal evolution. *Physics of the Earth and Planetary Interiors* 35: 264–282.

Christensen UR (1985) Thermal evolution models for the Earth. *Journal of Geophysical Research* 90: 2995–3007.

Christensen UR and Tilgner A (2004) Power requirement of the geodynamo from ohmic losses in numerical and laboratory dynamos. *Nature* 429: 169–171.

Clauser C, Giese P, Huenges E, *et al.* (1997) The thermal regime of the crystalline continental crust: Implications from the KTB. *Journal of Geophysical Research* 102: 18417–18441.

Cogley JG (1984) Continental margins and the extent and number of continents. *Reviews Geophysics and Space Physics* 22: 101–122.

Cogné J-P and Humler E (2004) Temporal variation of oceanic spreading and crustal production rates during the last 180 My. *Earth and Planetary Science Letters* 227: 427–439.

Conrad CP and Hager BH (1999) The thermal evolution of an Earth with strong subduction zones. *Geophysical Research Letters* 26: 3041–3044.

Crane K and O'Connell S (1983) The distribution and implications of the heat flow from the Gregory rift in Kenya. *Tectonophysics* 94: 253–272.

Cull JP (1991) Heat flow and regional geophysics in Australia. In: Cermak V and Rybach L (eds.) *Terrestrial Heat Flow and the Lithosphere Structure*, pp. 486–500. Berlin: Springer Verlag.

Davaille A and Jaupart C (1993) Transient high-Rayleigh-number thermal convection with large viscosity variations. *Journal of Fluid Mechanics* 253: 141–166.

Davies GF (1980) Thermal histories of convective Earth models and constraints on radiogenic heat production in the Earth. *Journal of Geophysical Research* 85: 2517–2530.

Davies GF (1980) Review of oceanic and global heat flow estimates. *Reviews of Geophysics and Space Physics* 18: 718–722.

Davies GF (1988) Ocean bathymetry and mantle convection, Part 1: large-scale flow and hotspots. *Journal of Geophysical Research* 93: 10467–10480.

Davies GF (1999) *Dynamic Earth: Plates, Plumes, and Mantle Convection*. Cambridge: Cambridge University Press.

Davis EE, Chapman DS, Wang K, *et al.* (1999) Regional heat flow variations across the sedimented Juan de Fuca ridge eastern flank: Constraints on lithospheric cooling and lateral hydrothermal heat transport. *Journal of Geophysical Research* 104: 17675–17688.

Davis EE and Elderfield H (2004) *Hydrogeology of the oceanic lithosphere*. Cambridge: Cambridge University Press.

Donnelly KE, Goldstein SL, Langmuir CH, and Spiegelman M (2004) Origin of enriched ocean ridge basalts and implications for mantle dynamics. *Earth and Planetary Science Letters* 226: 347–366.

Duchkov AD (1991) Review of Siberian heat flow data. In: Cermak V and Rybach L (eds.) *Terrestrial Heat Flow and the Lithosphere Structure*, pp. 426–443. Berlin: Springer-Verlag.

Dziewonski AM and Anderson DL (1981) Preliminary reference Earth model. *Physics of the Earth and Planetary Interiors* 25: 297–356.

Elkins-Tanton LT, Parmentier EM, and Hess PC (2003) Magma ocean fractional crystallization and cumulate overturn in terrestrial planets: Implications for Mars. *Meteoritics and Planetary Science* 38: 1753–1771.

Engebretson DC, Cox A, and Gordon RG (1984) Relative motions between oceanic plates of the Pacific basin. *Journal of Geophysical Research* 89: 10291–10310.

England PC, Oxburg ER, and Richardson SW (1980) Heat refraction in and around granites in north–east England. *Geophysical Journal of the Royal Astronomical Society* 62: 439–455.

Erickson AJ, Von Herzen RP, Sclater JG, Girdler RW, Marshall BV, and Hyndman R (1975) Geothermal measurements in deep-sea drill holes. *Journal of Geophysical Research* 80: 2515–2528.

Flasar FM and Birch F (1973) Energetics of core formation: A correction. *Journal of Geophysical Research* 78: 6101–6103.

Fountain DM and Salisbury MH (1981) Exposed cross-sections through the continental crust: Implications for crustal structure, petrology, and evolution. *Earth and Planetary Science Letters* 56: 263–277.

Fountain DM, Salisbury MH, and Furlong KP (1987) Heat production and thermal conductivity of rocks from the Pikwitonei–Sachigo continental cross-section, central Manitoba: Implications for the thermal structure of Archean crust. *Canadian Journal of Earth Sciences* 24: 1583–1594.

Fournier RO (1989) Geochemistry and dynamics of the Yellowstone National Park hydrothermal system. *Annual Review of Earth and Planetary Sciences* 17: 13–53.

Francheteau J, Jaupart C, Jie SX, *et al.* (1984) High heat flow in southern Tibet. *Nature* 307: 32–36.

Gordon RG (2000) Diffuse oceanic plate boundaries: Strain rates, vertically averaged rheology, and comparisons with narrow plate boundaries and stable plate interiors. In: Richards MA, Gordon RG, and van der Hilst RD (eds.) *Geophysical Monograph Series* 121: *The History and Dynamics of global plate Motions*, pp. 143–159. Washington, DC: American Geophysical Union.

Green DH (1975) Genesis of Archean peridotitic magmas and constraints on Archean geothermal gradients and tectonics. *Geology* 3: 15–18.

Grigné C, Labrosse S, and Tackley PJ (2005) Convective heat transfer as a function of wavelength: Implications for the cooling of the Earth. *Journal of Geophysical Research* 110(B03): 409 (doi:10.1029/2004JB003376).

Grove TL and Parman SW (2004) Thermal evolution of the Earth as recorded by komatiites. *Earth and Planetary Science Letters* 219: 173–187.

Gubbins D and Roberts PH (1987) Magnetohydrodynamics of the Earth's core. In: Jacobs JA (ed.) *Geomagnetism*, vol. 2, pp. 1–183. London: Academic.

Guillou L, Mareschal JC, Jaupart C, Gariépy C, Bienfait G, and Lapointe R (1994) Heat flow and gravity structure of the Abitibi belt, Superior Province, Canada. *Earth and Planetary Science Letters* 122: 447–460.

Guillou-Frottier L, Mareschal J-C, Jaupart C, Gariepy C, Lapointe R, and Bienfait G (1995) Heat flow variations in the Grenville Province, Canada. *Earth and Planetary Science Letters* 136: 447–460.

Gupta ML, Sharma SR, and Sundar A (1991) Heat flow and heat generation in the Archean Dharwar craton and implication for the southern Indian Shield geotherm. *Tectonophys* 194: 107–122.

Harris RN and Chapman DS (2004) Deep-seated oceanic heat flow, heat deficits and hydrothermal circulation. In: Davis E and Elderfield H (eds.) *Hydrogeology of the Oceanic Lithosphere*, pp. 311–336. Cambridge: Cambridge University Press.

Hart SR and Zindler A (1986) In search of a bulk-Earth composition. *Chemical Geology* 57: 247–267.

Henry SG and Pollack HN (1988) Terrestrial heat flow above the Andean subduction zone in Bolivia and Peru. *Journal of Geophysical Research* 93: 15153–15162.

Hernlund JW, Thomas C, and Tackley PJ (2005) Phase boundary double crossing and the structure of Earth's deep mantle. *Nature* 434: 882–886 (doi:10.1038/nature03472).

Herzberg C and Zhang J (1996) Melting experiments on anhydrous peridotite KLB-1: Compositions of magmas in the upper mantle and transition zone. *Journal of Geophysical Research* 101: 8271–8296.

Hirose K (2006) Postperovskite phase transition and its geophysical implications. *Reviews of Geophysics* 44: RG3001 (doi:10.1029/2005RG000186).

Hirose K, Sinmyo R, Sata N, and Ohishi Y (2006) Determination of post-perovskite phase transition boundary in $MgSiO_3$ using Au and MgO pressure standards. *Geophysical Research Letters* 33: L01310 (doi:10.1029/2005GL024468).

Hoffman PF (1997) Tectonic geology of North America. In: van der Pluijm B and Marshak S (eds.) *Earth Structure: An*

Introduction to Structural Geology and Tectonics, pp. 459–464. New York: McGraw Hill.

Howard LN (1964) Convection at high Rayleigh number. In: Gortler H (ed.) *Proceedings of the Eleventh International Congress of Applied Mechanics*, pp. 1109–1115. New York: Springer-Verlag.

Hu S, He L, and Wang J (2000) Heat flow in the continental area of China: A new data set. *Earth and Planetary Science Letters* 179: 407–419.

Hulot G, Eymin C, Langlais B, Mandea M, and Olsen N (2002) Small-scale structure of the geodynamo inferred from Oersted and Magsat satellite data. *Nature* 416: 620–623.

Humler E, Langmuir C, and Daux V (1999) Depth versus age: New perspectives from the chemical compositions of ancient crust. *Earth and Planetary Science Letters* 173: 7–23.

Irifune T and Isshiki M (1998) Iron partitioning in a pyrolite mantle and the nature of the 410-km seismic discontinuity. *Nature* 392: 702–705.

Ito E and Katsura T (1989) A temperature profile of the mantle transition zone. *Geophysical Research Letters* 16: 425–428.

Jacobs J and Allan DW (1956) The thermal history of the Earth. *Nature* 177: 155–157.

Jacobs JA (1961). *Some Aspects of the Thermal History of the Earth*, 267p, The Earth Today, 1961.

Jarvis GT and Campbell IH (1983) Archean komatiites and geotherms – solution to an apparent contradiction. *Geophysical Research Letters* 10: 1133–1136.

Jarvis GT and McKenzie DP (1980) Convection in a compressible fluid with infinite Prandtl number. *Journal of Fluid Mechanics* 96: 515–583.

Jaupart C (1983) Horizontal heat transfer due to radioactivity contrasts: Causes and consequences of the linear heat flow-heat production relationship. *Geophysical Journal of the Royal Astronomical Society* 75: 411–435.

Jaupart C and Mareschal J-C (1999) The thermal structure of continental roots. *Lithos* 48: 93–114.

Jaupart C and Mareschal JC (2003) Constraints on crustal heat production from heat flow data. In: Rudnick RL (ed.) *Treatise on Geochemistry, The Crust*, vol. 3, pp. 65–84. New York: Permagon.

Jaupart C, Mann JR, and Simmons G (1982) A detailed study of the distribution of heat flow and radioactivity in New Hampshire (USA). *Earth and Planetary Science Letters* 59: 267–287.

Jaupart C, Francheteau J, and Shen X-J (1985) On the thermal structure of the southern Tibetan crust. *Geophysical Journal of the Royal Astronomical Society* 81: 131–155.

Javoy M (1999) Chemical Earth models. *Comptes Rendus de l'Académie des Sciences* 329: 537–555.

Jeffreys H (1962) *The Earth: Its Origin, History, and Physical Constitution,* 5th edn. Cambridge, UK: Cambridge University Press.

Joeleht TH and Kukkonen IT (1998) Thermal properties of granulite facies rocks in the Precambrian basement of Finland and Estonia. *Tectonophysics* 291: 195–203.

Jones MQW (1988) Heat flow in the Witwatersrand Basin and environs and its significance for the South African shield geotherm and lithosphere thickness. *Journal of Geophysical Research* 93: 3243–3260.

Katsura T, Yamada H, Shinmei T, *et al.* (2003) Post-spinel transition in Mg_2SiO_4 determined by *in-situ* X-ray diffractometry. *Physics of the Earth and Planetary Interiors* 136: 11–24.

Katsura T, Yamada H, Nishikawa O, *et al.* (2004) Olivine-Wadsleyite transition in the system $(Mg,Fe)SiO_4$. *Journal of Geophysical Research* 109: B02209 (doi:10.1029/2003JB002438).

Kellogg LH, Hager BH, and van der Hilst RD (1999) Compositional stratification in the deep mantle. *Science* 283: 1881–1884.

Ketcham RA (1996) Distribution of heat-producing elements in the upper and middle crust of southern and west central Arizona: Evidence from the core complexes. *Journal of Geophysical Research* 101: 13611–13632.

Kinzler RJ and Grove TL (1992) Primary magmas of mid-ocean ridge basalts. Part 2: Applications. *Journal of Geophysical Research* 97: 6907–6926.

Klein EM and Langmuir CH (1987) Global correlations of ocean ridge basalt chemistry with axial depth and crustal thickness. *Journal of Geophysical Research* 92: 8089–8115.

Kleine T, Münker C, Mezger K, and Palme H (2002) Rapid accretion and early core formation on asteroids and the terrestrial planets from Hf-W chronometry. *Nature* 418: 952–955.

Korenaga J (2003) Energetics of mantle convection and the fate of fossil heat. *Geophysical Research Letters* 30, doi:10.1029/2003GL016982.

Korenaga J (2006) Archean geodynamics and the thermal evolution of the Earth. In: Benn K, Mareschal JC, and Condie KC (eds.) *Geophysical Monograph Series*: *Archean Geodynamics and Environments*, vol. 164, pp. 7–32. Washington, DC: American Geophysical Union.

Kremenentsky AA, Milanovsky SY, and Ovchinnikov LN (1989) A heat generation model for the continental crust based on deep drilling in the Baltic shield. *Tectonophysics* 159: 231–246.

Kukkonen IT and Peltonen P (1999) Xenolith-controlled geotherm for the central Fennoscandian shield: Implications for lithosphere–asthenosphere relations. *Tectonophysics* 304: 301–315.

Labrosse S (2002) Hotspots, mantle plumes and core heat loss. *Earth and Planetary Science Letters* 199: 147–156.

Labrosse S (2003) Thermal and magnetic evolution of the Earth's core. *Physics of the Earth and Planetary Interiors* 140: 127–143.

Labrosse S (2005a) Heat flow across the core–mantle boundary. In: Gubbins D and Herrero-Bervera E (eds.) *Encyclopedia of Geomagnetism and Paleomagnetism*. New York: Springer.

Labrosse S (2005b) Energy source for the geodynamo. In: Gubbins D and Herrero-Bervera E (eds.) *Encyclopedia of Geomagnetism and Paleomagnetism*. New York: Springer.

Labrosse S, Poirier J-P, and Le Mouël J-L (1997) On cooling of the Earth's core. *Physics of the Earth and Planetary Interiors* 99: 1–17.

Lachenbruch AH (1970) Crustal temperature and heat production: Implications of the linear heat flow heat production relationship. *Journal of Geophysical Research* 73: 3292–3300.

Lachenbruch AH and Sass JH (1978) Models of an extending lithosphere and heat flow in the Basin and Range province. *Memoirs of the Geological Society of America* 152: 209–258.

Lambeck K (1977) Tidal dissipation in the oceans: Astronomical, geophysical, and oceanographic consequences. *Philosophical Transactions of the Royal Society of London Series A* 287: 545–594.

Langmuir CH, Goldstein SL, Donnelly K, and Su YK (2005) Origins of enriched and depleted mantle reservoirs. In: *Eos Transactions*, Fall Meeting Supplement, vol. 86, p. 1, American Geophysical Union, Abstract V23D–02.

Langseth MG, Le Pichon X, and Ewing M (1966) Crustal structure of the mid-ocean ridges, 5, heat flow through the Atlantic Ocean floor and convection currents. *Journal of Geophysical Research* 71: 5321–5355.

Lapwood ER (1952) The effect of contraction in the cooling of a gravitating sphere, with special reference to the Earth. *Monthly Notices of the Royal Astronomical Society Geophysics* (supplement 6): 402–407.

Lay T, Hernlund J, Garnero EJ, and Thorne MS (2006) A Post-Perovskite lens and D'' heat flux beneath the central Pacific. *Science* 314: 1272–1276.

Lay T, Williams Q, and Garnero EJ (1998) The core–mantle boundary layer and deep Earth dynamics. *Nature* 392: 461–468 (doi:10.1038/33083).

Lenardic A, Moresi L-N, Jellinek M, and Manga M (2005) Continental insulation, mantle cooling, and the surface area of oceans and continents. *Earth and Planetary Science Letters* 234: 317–333.

Lister CRB (1977) Estimators for heat flow and deep rock properties based on boundary layer theory. *Tectonophysics* 41: 157–171.

Lister CRB, Sclater JG, Davis EE, Villinger H, and Nagahira S (1990) Heat flow maintained in ocean basins of great age: Investigations in the north equatorial west Pacific. *Geophysical Journal International* 102: 603–630.

Lister JR (2003) Expressions for the dissipation driven by convection in the Earth's core. *Physics of the Earth and Planetary Interiors* 140: 145–158.

Lister JR and Buffett BA (1995) The strength and efficiency of thermal and compositional convection in the geodynamo. *Physics of the Earth and Planetary Interiors* 91: 17–30.

Litasov K and Ohtani E (2002) Phase relations and melt compositions in CMAS-pyrolite-H_2O system up to 25 GPa. *Physics of the Earth and Planetary Interiors* 134: 105–127.

Lyubetskaya T and Korenaga J (2007) Chemical composition of Earth's primitive mantle and its variance. Part 1: Method and results. *Journal of Geophysical Research* 112: B03211 (doi:10.1029/2005JB004223).

MacDonald GJF (1959) Calculations on the thermal history of the Earth. *Journal of Geophysical Research* 64: 1967–2000.

Mareschal JC and Jaupart C (2004) Variations of surface heat flow and lithospheric thermal structure beneath the North American craton. *Earth and Planetary Science Letters* 223: 65–77.

Mareschal JC, Jaupart C, Cheng LZ, *et al.* (1999) Heat flow in the trans-Hudson Orogen of the Canadian Shield: Implications for proterozoic continental growth. *Journal of Geophysical Research* 104: 29007–29024.

Mareschal JC, Jaupart C, Gariépy C, *et al.* (2000) Heat flow and deep thermal structure near the southeastern edge of the Canadian Shield. *Canadian Journal of Earth Sciences* 37: 399–414.

Mareschal JC, Poirier A, Rolandone F, *et al.* (2000) Low mantle heat flow at the edge of the North American continent Voisey Bay, Labrador. *Geophysical Research Letters* 27: 823–826.

Mareschal JC, Jaupart C, Rolandone F, *et al.* (2005) Heat flow, thermal regime, and rheology of the lithosphere in the Trans–Hudson Orogen. *Canadian Journal of Earth Sciences* 42: 517–532.

McDonough WF and Sun SS (1995) The composition of the Earth. *Chemical Geology* 120: 223–253.

McKenzie D and Bickle MJ (1988) The volume and composition of melt generated by extension of the lithosphere. *Journal of Petrology* 29: 625–679.

McKenzie DP and Richter FM (1981) Parameterized thermal convection in a layered region and the thermal history of the Earth. *Journal of Geophysical Research* 86: 11667–11680.

McKenzie DP and Weiss N (1975) Speculations on the thermal and tectonic history of the Earth. *Geophysical Journal of the Royal Astronomical Society* 42: 131–174.

McKenzie DP, Jackson J, and Priestley K (2005) Thermal structure of oceanic and continental lithosphere. *Earth and Planetary Science Letters* 233: 337–349.

Melosh HJ and Ivanov BA (1999) Impact crater collapse. *Annual Review of Earth and Planetary Sciences* 27: 385–415.

Mittlestaedt E and Tackley PJ (2006) Plume heat flow is much lower than CMB heat flow. *Earth and Planetary Science Letters* 241: 202–210.

Mojzsis SJ, Harrison TM, and Pidgeon RT (2001) Oxygen-isotope evidence from ancient zircons for liquid water at the Earth's surface 4,300 Myr ago. *Nature* 409: 178–181.

Morgan P (1983) Constraints on rift thermal processes from heat flow and uplift. *Tectonophysics* 94: 277–298.

Morgan P (1985) Crustal radiogenic heat production and the selective survival of ancient continental crust. *Journal of Geophysical Research* (Supplement 90): C561–C570.

Müller RD, Roest WR, Royer J-Y, Gahagan LM, and Sclater JG (1997) Digital isochrons of the world's ocean floor. *Journal of Geophysical Research* 102: 3211–3214.

Munk WH and MacDonald GJF (1960) *The Rotation of the Earth*. Cambridge, UK: Cambridge University Press.

Murakami M, Hirose K, Kawamura K, Sata N, and Ohishi Y (2004) Post-perovskite phase transition in $MgSiO_3$. *Science* 304: 855–858.

Newsom HE and Jones JH (eds.) (1990) *Origin of the Earth*. Oxford: Oxford University Press.

Nicolaysen LO, Hart RJ, and Gale NH (1981) The Vredefort radioelement profile extended to supracrustal rocks at Carletonville, with implications for continental heat flow. *Journal of Geophysical Research* 86: 10653–10661.

Nisbet EG, Cheadle MJ, Arndt NT, and Bickle MJ (1995) Constraining the potential temperature of the Archean mantle: A review of the evidence from komatiites. *Lithos* 30: 291–307.

Nyblade AA (1997) Heat flow across the east African Plateau. *Geophysical Research Letters* 24: 2083–2086.

Oganov AR and Ono S (2004) Theoretical and experimental evidence for a post-perovskite phase of $MgSiO_3$ in Earth's D'' layer. *Nature* 430: 445–448.

Ogawa M, Schubert G, and Zebib A (1991) Numerical simulations of three-dimensional thermal convection in a fluid with strongly temperature dependent viscosity. *Journal of Fluid Mechanics* 233: 299–328.

Olson PA (1987) A comparison of heat transfer laws for mantle convection at very high Rayleigh numbers. *Physics of the Earth and Planetary Interiors* 48: 153–160.

Palme H and O'Neill HSC (2003) Cosmochemical estimates of mantle composition. In: Carlson RW (ed.) *Treatise on Geochemistry*, Vol 2: Mantle and Core, pp. 1–38. Amsterdam: Elsevier.

Pari G and Peltier WR (1995) The heat flow constraint on mantle tomography-based convection models: Towards a geodynamically self-consistent inference of mantle viscosity. *Journal of Geophysical Research* 100: 12731–12752.

Parsons B (1982) Causes and consequences of the relation between area and age of the ocean floor. *Journal of Geophysical Research* 87: 289–302.

Parsons B and Sclater JG (1977) An analysis of the variation of the ocean floor bathymetry and heat flow with age. *Journal of Geophysical Research* 82: 803–827.

Peltier WR and Jarvis GT (1982) Whole mantle convection and the thermal evolution of the Earth. *Physics of the Earth and Planetary Interiors* 29: 281–304.

Perry HKC, Jaupart C, Mareschal JC, and Bienfait G (2006) Crustal heat production in the Superior Province, Canadian Shield, and in North America inferred from heat flow data. *Journal of Geophysical Research* 111: B04401 (doi:10.1029/2005JB003893).

Pinet C and Jaupart C (1987) The vertical distribution of radiogenic heat production in the Precambrian crust of Norway and Sweden: Geothermal implications. *Geophysical Research Letters* 14: 260–263.

Pinet C, Jaupart C, Mareschal JC, Gariépy C, Bienfait G, and Lapointe R (1991) Heat flow and structure of the lithosphere in the Eastern Canadian shield. *Journal of Geophysical Research* 96: 19941–19963.

Poirier J-P (2000) *Introduction to the Physics of the Earth's Interior, 2 edn, Cambridge: Cambridge University Press.*

Pollack HN and Chapman DS (1977a) On the regional variations of heat flow, geotherms, and lithospheric thickness. *Tectonophysics* 38: 279–296.

Pollack HN and Chapman DS (1977b) Mantle heat flow. *Earth and Planetary Science Letters* 34: 174–184.

Pollack HN, Hurter SJ, and Johnston JR (1993) Heat flow from the Earth's interior: Analysis of the global data set. *Reviews of Geophysics* 31: 267–280.

Poort J and Klerkx J (2004) Absence of a regional surface thermal high in the Baikal rift; new insights from detailed contouring of heat flow anomalies. *Tectonophysics* 383: 217–241.

Ray RD, Eanes RJ, and Chao BF (1996) Detection of tidal dissipation in the solid Earth by satellite tracking and altimetry. *Nature* 381: 595–597.

Ringwood AE (1962) A model for the upper mantle. *Journal of Geophysical Research* 67: 857–867.

Roberts PH, Jones CA, and Calderwood AR (2003) Energy fluxes and ohmic dissipation in the Earth's core. In: Jones CA, Soward AM, and Zhang K (eds.) *Earth's Core and Lower Mantle*, pp. 100–129. London: Taylor & Francis.

Rolandone F, Jaupart C, Mareschal JC, *et al.* (2002) Surface heat flow, crustal temperatures and mantle heat flow in the Proterozoic Trans-Hudson Orogen, Canadian Shield. *Journal of Geophysical Research* 107: 2314 (doi:10.1029/2001JB000,698).

Rowley DB (2002) Rate of plate creation and destruction; 180 Ma to present. *Geological Society of America Bulletin* 114: 927–933.

Roy RF, Decker ER, Blackwell DD, and Birch F (1968) Heat Flow in the United States. *Journal of Geophysical Research* 73: 5207–5221.

Roy S and Rao RUM (2000) Heat flow in the Indian shield. *Journal of Geophysical Research* 105: 25587–25604.

Royer J, Müller R, Gahagan L, *et al.* (1992) A global isochron chart. *Technical Report* 117, University of Texas Institute for Geophysics, Austin, 1992.

Rubie DC, Melosh HJ, Reid JE, Liebske C, and Righter K (2003) Mechanisms of metal-silicate equilibration in the terrestrial magma ocean. *Earth and Planetary Science Letters* 205: 239–255.

Rudnick RL and Fountain DM (1995) Nature and composition of the continental crust: A lower crustal perspective. *Reviews of Geophysics* 33: 267–309.

Rudnick RL and Gao S (2003) Composition of the continental crust. In: Rudnick RL (ed.) *Treatise on Geochemistry, The Crust*, vol. 3, pp. 1–64. New York: Permagon.

Rudnick RL and Nyblade AA (1999) The thickness of Archean lithosphere: Constraints from xenolith thermobarometry and surface heat flow. In: Fei Y, Bertka CM, and Mysen BO (eds.) *Mantle Petrology: Field Observations and high pressure Experimentation: A Tribute to Francis R. (Joe) Boyd*, pp. 3–11. Houston, TX: Geochemical Society.

Rudnick RL, McDonough WF, and O'Connell RJ (1998) Thermal structure, thickness and composition of continental lithosphere. *Chemical Geology* 145: 395–411.

Rushmer T, Minarik WG, and Taylor GJ (2000) Physical processes of core formation. In: Canup RM and Drake K (eds.) *Origin of the Earth and Moon*, pp. 227–243. Tucson, AZ: The University of Arizona Press.

Russell JK, Dipple GM, and Kopylova MG (2001) Heat production and heat flow in the mantle lithosphere, Slave Craton, Canada. *Physics of the Earth and Planetary Interiors* 123: 27–44.

Rybach L (1988) Determination of heat production rate. In: Haenel R, Rybach L, and Stegena L (eds.) *Handbook of Terrestrial Heat-Flow Density Determinations*, pp. 125–142. Amsterdam: Kluwer.

Schubert G, Stevenson D, and Cassen P (1980) Whole planet cooling and the radiogenic heat source contents of the Earth and Moon. *Journal of Geophysical Research* 85: 2531–2538.

Schubert G, Turcotte DL, and Olson P (2001) *Mantle Convection in the Earth and Planets*. Cambridge, UK: Cambridge University Press.

Schubert G and Young RE (1976) Cooling the Earth by whole mantle subsolidus convection: A constraint on the viscosity of the lower mantle. *Tectonophysics* 35: 201–214.

Sclater JG and Francheteau J (1970) Implications of terrestrial heat flow observations on current tectonic and geochemical models of crust and upper mantle of Earth. *Geophysical Journal of the Royal Astronomical Society* 20: 509–542.

Sclater JG, Crowe J, and Anderson RN (1976) On the reliability of oceanic heat flow averages. *Journal of Geophysical Research* 81: 2997–3006.

Sclater JG, Jaupart C, and Galson D (1980) The heat flow through oceanic and continental crust and the heat loss of the Earth. *Reviews of Geophysics and Space Physics* 18: 269–312.

Sharpe HN and Peltier WR (1978) Parameterized mantle convection and the Earth's thermal history. *Geophysical Research Letters* 5: 737–740.

Sleep NH (1971) Thermal effects of the formation of Atlantic continental margins by continental breakup. *Geophysical Journal of the Royal Astronomical Society* 24: 325–350.

Sleep NH (1979) Thermal history and degasing of the Earth: Some simple calculations. *Journal of Geology* 87: 671–686.

Sleep NH (1990) Hotspots and mantle plumes: Some phenomenology. *Journal of Geophysical Research* 95: 6715–6736.

Sleep NH (2000) Evolution of the mode of convection within terrestrial planets. *Journal of Geophysical Research* 105: 17563–17578.

Solomatov VS (2000) Fluid dynamics of a terrestrial magma ocean. In: Canup RM and Righter K (eds.) *Origin of the Earth and Moon*, pp. 323–338. Tucson, AZ: The University of Arizona Press.

Solomatov VS and Moresi LN (1997) Three regimes of mantle convection with non-newtonian viscosity and stagnant lid convection on the terrestrial planets. *Geophysical Research Letters* 24: 1907–1910.

Sotin C and Labrosse S (1999) Three-dimensional thermal convection of an isoviscous, infinite–Prandtl–number fluid heated from within and from below: Applications to heat transfer in planetary mantles. *Physics of the Earth and Planetary Interiors* 112: 171–190.

Stacey FD (1992) *Physics of the Earth, 2nd edn.,* Brisbane, Qld: Brookfield Press.

Stein CA and Stein S (1992) A model for the global variation in oceanic depth and heat flow with lithospheric age. *Nature* 359: 123–129.

Stevenson DJ (1989) Formation and early evolution of the Earth. In: Peltier W (ed.) *Mantle Convection*, pp. 817–873. NY: Gordon and Breach.

Stevenson DJ (1990) Fluid dynamics of core formation. In: Newsom HE and Jones JH (eds.) *Origin of the Earth*, pp. 231–249. New York: Oxford University Press.

Su YJ (2000) Mid-ocean ridge basalt trace element systematics: Constraints from database management, ICPMS analysis, global data compilation and petrologic modeling. Unpub. Ph.D. thesis, Columbia University, New York, 1, 569p, 2000.

Swanberg CA, Chessman MD, Simmons G, Smithson SB, Gronlie G, and Heier KS (1974) Heat-flow heat-generation studies in Norway. *Tectonophysics* 23: 31–48.

Tackley PJ (2000) Self-consistent generation of tectonic plates in time-dependent, three-dimensional mantle convection simulations. Part 1: pseudoplastic yielding. *Geochemistry Geophysics Geosystems* 1, doi:10.1029/2000GC000036.

Thomson W (Lord Kelvin) (1862) On the secular cooling of the Earth. *Transactions of the Royal Society of Edinburgh* 23: 295–311.

Turcotte DL and Oxburgh ER (1967) Finite amplitude convective cells and continental drift. *Journal of Fluid Mechanics* 28: 29–42.

Vasseur G and Singh RN (1986) Effects of random horizontal variations in radiogenic heat source distribution on its relationship with heat flow. *Journal of Geophysical Research* 91: 10397–10404.

Vogt P and Ostenso N (1967) Steady state crustal spreading. *Nature* 215: 810–817.

von Herzen RP (1959) Heat flow values from the southwestern Pacific. *Nature* 183: 882–883.

Vosteen HD, Rath V, Clauser C, and Lammerer B (2003) The thermal regime of the Eastern Alps from inverse analyses along the TRANSALP profile. *Physics and Chemistry of the Earth* 28: 393–405.

Vočadlo L, Alfè D, Gillan MJ, and Price GD (2003) The properties of iron under core conditions from first principles calculations. *Physics of the Earth and Planetary Interiors* 140: 101–125.

Wasserburg G, McDonald GJF, Hoyle F, and Fowler (1964) Relative contributions of uranium, thorium, and potassium to heat production in the Earth. *Science* 143: 465–467.

Wetherill GW (1990) Formation of the Earth. *Annual Review of Earth and Planetary Sciences* 18: 205–256.

Williams DL and von Herzen RP (1974) Heat loss from the Earth: New estimate. *Geology* 2: 327–328.

Workman RK and Hart SR (2005) Major and trace element composition of the depleted MORB mantle (DMM). *Earth and Planetary Science Letters* 231: 53–72.

Zerr A, Diegeler A, and Boehler R (1998) Solidus of Earth's deep mantle. *Nature* 281: 243–246.

Zhong SJ (2005) Dynamics of thermal plumes in three-dimensional isoviscous thermal convection. *Geophysical Journal International* 162: 289–300.

Zschau J (1986) Constraints from the Chandler wobble period. In: Anderson AJ and Cazenave A (eds.) *Space Geodesy and Geodynamics*, pp. 315–344. New York: Academic Press.